

CHEMIA

**STUDIA
UNIVERSITATIS BABEȘ-BOLYAI
CHEMIA**

2/2018

EDITORIAL BOARD OF STUDIA UNIVERSITATIS BABEȘ-BOLYAI CHEMIA

ONORARY EDITOR:

IONEL HAIDUC - Member of the Romanian Academy

EDITOR-IN-CHIEF:

LUMINIȚA SILAGHI-DUMITRESCU

EXECUTIVE EDITOR:

CASTELIA CRISTEA

EDITORIAL BOARD:

PAUL ȘERBAN AGACHI, Babeș-Bolyai University, Cluj-Napoca, Romania

LIVAIN BREAU, UQAM University of Quebec, Montreal, Canada

HANS JOACHIM BREUNIG, Institute of Inorganic and Physical Chemistry,
University of Bremen, Bremen, Germany

MIRCEA DIUDEA, Babeș-Bolyai University, Cluj-Napoca, Romania

JEAN ESCUDIE, HFA, Paul Sabatier University, Toulouse, France

ION GROSU, Babeș-Bolyai University, Cluj-Napoca, Romania

EVAMARIE HEY-HAWKINS, University of Leipzig, Leipzig, Germany

FLORIN DAN IRIMIE, Babeș-Bolyai University, Cluj-Napoca, Romania

FERENC KILAR, University of Pecs, Pecs, Hungary

BRUCE KING, University of Georgia, Athens, Georgia, USA

ANTONIO LAGUNA, Department of Inorganic Chemistry, ICMA, University of
Zaragoza, Zaragoza, Spain

JURGEN LIEBSCHER, Humboldt University, Berlin, Germany

KIERAN MOLLOY, University of Bath, Bath, UK

IONEL CĂȚĂLIN POPESCU, Babeș-Bolyai University, Cluj-Napoca, Romania

CRISTIAN SILVESTRU, Babeș-Bolyai University, Cluj-Napoca, Romania

<http://chem.ubbcluj.ro/~studiachemia/>; studiachemia@chem.ubbcluj.ro

http://www.studia.ubbcluj.ro/serii/chemia/index_en.html

YEAR
MONTH
ISSUE

Volume 63 (LXIII) 2018
JUNE
2

S T U D I A

UNIVERSITATIS BABEȘ–BOLYAI

CHEMIA

2

ISSUE DOI:10.24193/subbchem.2018.2

STUDIA UBB EDITORIAL OFFICE: B.P. Hasdeu no. 51, 400371 Cluj-Napoca, Romania,
Phone + 40 264 405352

CUPRINS – CONTENT – SOMMAIRE – INHALT

BEATA SZEFLER, PRZEMYSŁAW CZELEŃ, MIRCEA V. DIUDEA, Docking of Indolizine Derivatives on Cube Rhombellane Functional- ized Homeomorphs	7
THOMAS DIPPONG, ALEXANDRA AVRAM, FIRUTA GOGA, QSPR Analysis of a Set of Liquid Crystals in the Benzylideneaniline Class According to their Transition Temperature	19
NAHID SOHREVARDI, FARHOUSH KIANI, FARDAD KOOHYAR, Theoretical Calculation of Thermodynamic Properties and Diffusion Coefficients for Pure Ethanol, Pure Water and Binary Mixture of (Ethanol + Water) as Function of Temperature by Molecular Dynamic Simulation.....	31
FLAVIA POP, Effect of Microwave Heating on Quality and Fatty Acids Composition of Vegetable Oils	43

ADINA GHIRIŞAN, SIMION DRĂGAN, CONSTANTIN COŢA, NICOLAE CIOICA, ELENA-MIHAELA NAGY, VASILE MICLĂUŞ, The Influence of Temperature and Dolomite Addition on the Drying Kinetics of Sugar Beet Pulp (<i>Beta Vulgaris L.</i>).....	53
CARMEN NICULĂESCU, LOREDANA OLAR, RĂZVAN STEFAN, MIHAI TODICA AND CORNEL-VIOREL POP, XRD and IR Investigations of Some Commercial Polystyrene Samples Thermally Degraded	63
DIANA SUCALĂ, CODRUŢA SAROSI, CĂTĂLIN POPA, ILEANA COJOCARU, MARIOARA MOLDOVAN, AUREL GEORGE MOHAN, <i>In Vitro</i> Behaviour of New Experimental Adhesive Systems.....	71
ADRIANA MIHAELA CHIRILĂ BĂBĂU, VALER MICLE, IOANA MONICA SUR, Characterization of Soils in the Almasu Mare Area through the Determination of Lead Concentrations	83
ALEXANDRA DREANCĂ, RADU A POPESCU, AMALIA NEAGU, GEORGE ENACRACHI, IULIA CIMPOEŞ, NICODIM FIŢ, MARIOARA MOLDOVAN, LAURA SILAGHI DUMITRESCU, ANCA JURJ, IOANA BERINDAN-NEAGOE, IOAN MARCUS, <i>In Vitro</i> Testing of a Polylactic Polymer Synthesized from Whey.....	93
NOÉMI DEAK, RALUCA SEPTELEAN, IONUT-TUDOR MORARU, SONIA MALLETT-LADEIRA, DAVID MADEC, GABRIELA NEMES, Palladium and Ruthenium Derivatives Stabilised by Bis-Sulfone Ligand	105
BALÁZS BRÉM, QUENTIN COLANGE, EMESE GAL, DAN PORUMB, CASTELIA CRISTEA, LUIZA GĂINĂ, TAMÁS LOVÁSZ, LUMINIŢA SILAGHI-DUMITRESCU, (Phenothiazinyl)Vinyl-Indolium Cationic Dyes	117
MIHAIL MANOLACHE, TIBERIA IOANA POP, ANCA CRISTINA BABEŞ, IULIA-ALEXANDRA FARCAŞ, MARIA LAURA MUNCACIU, ANAMARIA CĂLUGĂR, EMESE GAL, Volatile Composition of Some Red Wines from Romania Assessed by GC-MS	125
TABITA-TEODORA LISANDRU, ANDREA BUNEA, ADRIAN FÜSTÖS, ADELINA DUMITRAŞ, CLAUDIU-IOAN BUNEA, VALENTIN SEBASTIAN DAN, EMESE GÁL, VIOREL MITRE, Chromatographic Analysis of Carotenoids and Anthocyanins in Sweet Cherry Autumn Leaves Used in Ornamental Landscapes.....	143
CLAUDIA-CRINA TOMA, BOGDAN TITA, NELI-KINGA OLAH, GIANCARLO STATTI, Investigation of Thermal Behavior of <i>Nigellae Sativae Semen</i> from Different Types of Extracts.....	157
ALEXANDRA FARCAŞ, TITUS A. BEU, Complexation of DNA with Cationic Polymers.....	165

Studia Universitatis Babes-Bolyai Chemia has been selected for coverage in Thomson Reuters products and custom information services. Beginning with V. 53 (1) 2008, this publication is indexed and abstracted in the following:

- Science Citation Index Expanded (also known as SciSearch®)
- Chemistry Citation Index®
- Journal Citation Reports/Science Edition

DOCKING OF INDOLIZINE DERIVATIVES ON CUBE RHOMBELLANE FUNCTIONALIZED HOMEOMORPHS

BEATA SZEFLER^{a*}, PRZEMYSŁAW CZELEŃ^a,
MIRCEA V. DIUDEA^b

ABSTRACT. Indolizines represent a class of heteroaromatic compounds (of pharmacological importance) containing two condensed (5- and 6-membered) rings bridged by a nitrogen atom, showing a variety of biological activities. An attempt was made to deposit indolizines on the cube rhombellane homeomorphs surface as possible nano-drug complexes, since rhombellane homeomorphs may be bound in a protein as the active pocket and further may be used in personalized medicine. In the present study, a molecular docking analysis of two indolizine derivatives on some cube rhombellane homeomorphs was carried out for the first time.

Keywords: *binding energy, indolizine, molecular docking, nanostructure, cube rhombellane homeomorph.*

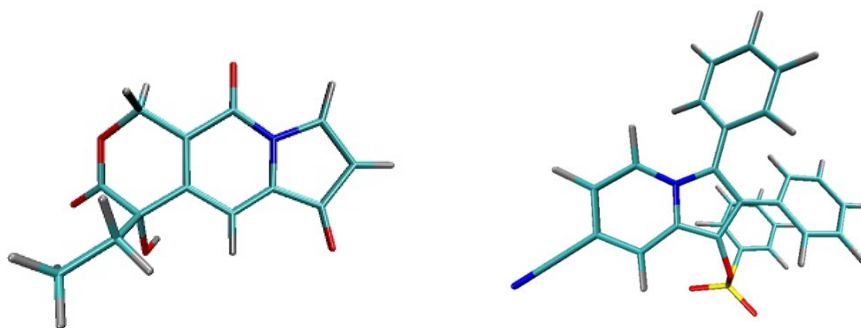
INTRODUCTION

In recent years, interest in modern methods of drug delivery using nanostructures has increased; drug delivery is becoming an important aspect of medicine, as more potent and specific drugs are being developed – particularly with the increased understanding of disease pathways generated by the Human Genome Project. Novel materials and formulations are enabling the site-specific targeting and controlled release of traditional pharmaceuticals, recombinant proteins, vaccines and nucleic acids. Nano-scale drug-delivery systems can be devised to tune release kinetics, to regulate biodistribution and bioavailability, to minimize toxic side effects, thus enhancing the therapeutic efficiency of a given drug [1-5].

^a *Department of Physical Chemistry, Faculty of Pharmacy, Collegium Medicum, Nicolaus Copernicus University, Kurpińskiego 5, 85-096, Bydgoszcz, Poland.*

^b *Department of Chemistry, Faculty of Chemistry and Chemical Engineering, Babes-Bolyai University, 400028 Cluj-Napoca, Romania.*

Indolizine derivatives are heteroaromatic compounds of pharmacological importance with two condensed (5- and 6-membered) rings bridged by a nitrogen atom (Figure 1). They can inhibit enzyme activity and act as calcium entry blockers in cardiovascular activity, also they show antimicrobial, antioxidant, anti-inflammatory, tuberculostatic, antihistaminic or antitumoral properties [6,7]. In nature they have been isolated from animals, insects, plants, marine organisms, and microbes [8]. Synthesis of indolizines involve 1,3-dipolar cycloadditions, cyclization reactions, etc. [9].



Ligand 1 (CID=359849)

Ligand 2 (CID=491916)

Figure 1. Structure of studied ligands: Ligand 1 (Lig1) with PDB Code 359849 (left) and Ligand 2 (Lig2) with PDB Code 491916 (right).

The choice of indolizine ligands was guided by our earlier studies [10-12] and the use of these Indolizine derivatives as inhibitors for enzymes Beta lactamase and Nicotinamide phosphoribosyltransferase; the two ligands are: Lig1, CID=359849 and Lig2, CID=491916 (PubChem, [13]).

CUBE RHOMBELLANE HOMEOMORPHS

Rhombellanes are structures with all strong rings being rhombs/squares; they have been proposed by Diudea in 2017 [14]. [1,1,1]Propellane is an organic molecule, first synthesized in 1982 [15]; by *IUPAC* rules, it is named tricyclo[1.1.1.0^{1,3}]pentane, a hydrocarbon with formula C₅H₆, containing only triangles; its reduced form, C₅H₈, eventually named bicyclo[1.1.1]pentane, has only quadrilateral rings; it can be represented as K_{2,3} - the complete bipartite graph. The two bridge carbon atoms can be functionalized, e.g., by bromine or COOH, or even by repeating the K_{2,3} motif, as in the polymer called staffane [16]. A rhombellane was defined by Diudea [17] as a structure having:

- All strong rings are squares/rhombs;
- Vertex classes consist of all non-connected vertices;
- Omega polynomial has a single term: $1X^n|E|$;
- Line graph of the parent graph has a Hamiltonian circuit;
- It contains at least one $K_{2,3}$ subgraph.

Rhombellanes are designed by the “rhombellation” procedure; it starts with diagonalizing each face of an all-rhomb map Rh_0 by a joint point (called “rbl-point”); then, add new vertices opposite to the parent vertices and join each of them with the rbl-vertices lying in the proximity of each parent vertex, thus local Rh-cells being formed. The process can continue, considering the envelope Rh_n as “ Rh_0 ” for Rh_{n+1} , in this way shell by shell being added to the precedent structure. Since the two diagonals of a rhomb may be topologically different, each generation may consist of two isomers. Construction of the cube-rhombellane (**1**) is illustrated in Figure 2, left. Each square face forms a $K_{2,3}$ rhombellane by joining the opposite corners with homeomorphic diagonals; these diagonals are joint together in an adamantane motif (in red); $K_{2,3}$ and adamantane are both “tiles”, not polyhedra.

A homeomorph of a graph contains on each parent edge one (or more) point(s) of degree two, see for example, the cube homeomorph (**2**) in Figure 2 (middle). The structure (**3**), which is the homeomorph of (**1**) has seventy points/atoms, as illustrated in Figure 1 (right); the vertex connectivity in (**3**) is 6; 3 and 2, respectively.

To synthesize (**3**) as a molecule, one may start from 1,2,3,4,5,6-Hexahydroxy-cyclohexane, that may form an ether (**4**) (Figure 3), which is a (hyper) homeomorph of the cube (**2**) and the “core” of $rbl(C)$ -homeomorph (**3**); the vertices of connectivity 6 will be just the hexahydroxy-cyclohexane while the three-connected points may be 1,3,5-trihydroxy-cyclohexane or its derivatives (e.g., hexahydroxy- cyclohexane, 1,3,5-trihydroxy-benzene, etc.).

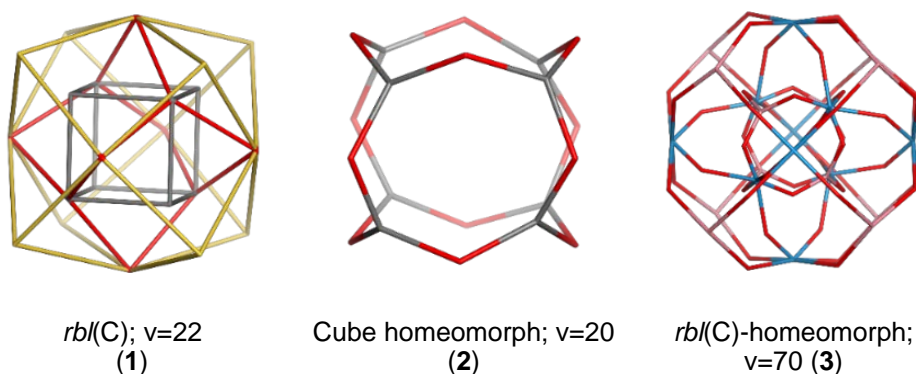


Figure 2. Cube-rhombellane and related structures (v =no. vertices/atoms).

Note that silsesquioxanes are synthesized molecules having a core homeomorph of the cube (**2**) [18,19].

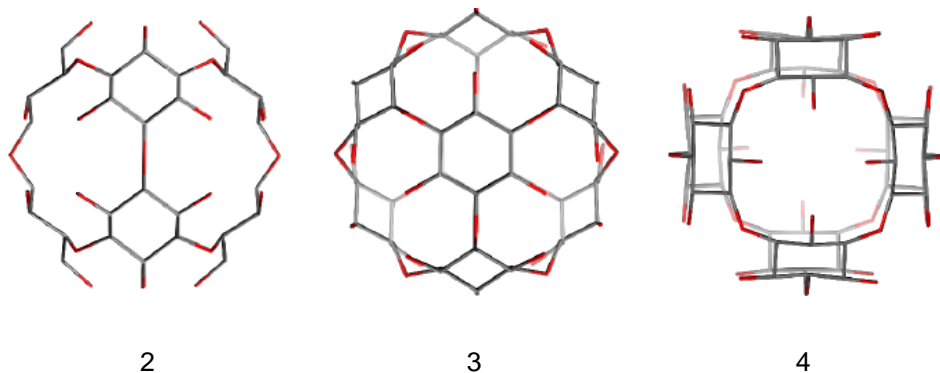


Figure 3. Cube-rbl (ether) core (**4**), $v=156$; in 2-, 3- and 4-fold symmetry, respectively.

ADA-MOTIF AND FUNCTIONALIZED RHOMBELLANES.

Cube-rbl homeomorphs comprise a hyper-adamantane motif, ADA-rbl (**5**) (Figure 4, left); including a Cube-rbl-core and completing the external shell (by adding 8 tri-connected units), one obtains complete the Cube-rbl-amide (**6**)/ester(**7**) structures (Figure 4, middle and right). Specification of the herein discussed Diudea's structures [20] is given in Table 1.

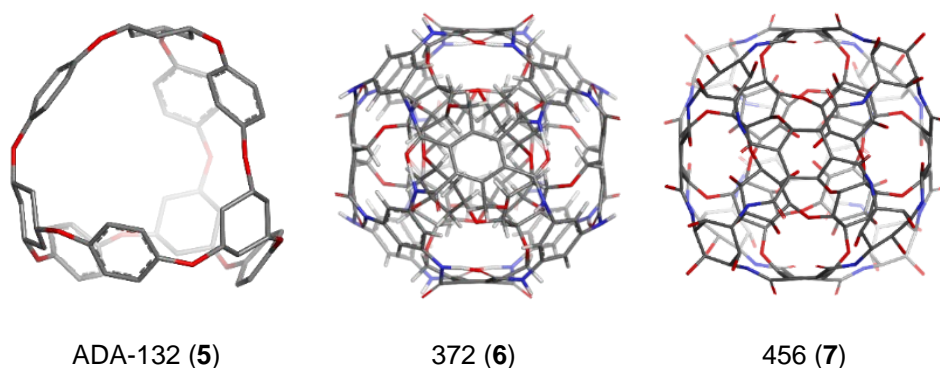


Figure 4. ADA-rbl intermediate and Cube rhombellane homeomorphs (functionalized).

Table 1. Cube rhombellane homeomorph derivatives: v=no. vertices/atoms; elemental composition, structure and type.

v	C	N	O	H	Structure	Type I	Type II	Type III
144	48	12	0	84	Core	Ether	6(6)6(3)	in-in; in-ex; ex-ex
156	48	12	12	84	Core	Ether	6(6)6(6)	in-in; in-ex; ex-ex
132	60	0	12	60	ADA-rbl	Ether	6(3);B(2)	-
360	168	0	84	108	C-rbl	Ester	6(6);6(6)	B(3)
372	168	24	48	132	C-rbl	Amide	6(6);6(3)	B(3)
396	192	0	72	132	C-rbl	Ester	6(6);B(3)	B(3)M
420	192	24	48	156	C-rbl	Amide	6(6);B(3)	B(3)M
444	192	24	48	180	C-rbl	Amide	6(6);6(3)	B(3)M
456	156	24	84	192	C-rbl	Amide	6(6);6(6)	B(3)M

Name of Cube rhombellane homeomorphs: Rbl(C)-(6(6),x(y))-B(3)z-ester/amide

METHOD

In the docking procedure, the molecules were loaded and stored as pdb-files, after assigning hydrogen bonds [21], using the AutoDockVina software [22]. The investigated ligands were loaded and their torsions along the rotatable bonds were assigned, then the files were saved as "ligand.pdbqt". The grid menu was next toggled [23]; after loading "pdbqt", the map files were selected directly with setting up the grid points, for the search of ligand-rbl interactions, separately for each structure. The docking parameter files were completed by using the Lamarckian genetic algorithm [24]. As a reference structure the fullerene C₆₀, the most referred structure in Nanoscience was considered.

RESULTS AND DISCUSSION

The results are presented in the following tables and figures. Rhombellane structures are given by their atom number.

Table 2. Binding affinity of ligand Lig1, CID=359849, with the active site of Rbl-nano-structures (first column) during nine conformations.

Cube Rbl	1	2	3	4	5	6	7	8	9	Docked energy (kcal/mol)
144_ex_ex	-2.8	-2.8	-2.8	-2.8	-2.8	-2.8	-2.8	-2.8	-2.8	-2.8
144_in_ex	-3	-3	-3	-3	-3	-3	-3	-3	-3	-3
156_ex_ex	-3.1	-3.1	-3.1	-3.1	-3.1	-3.1	-3.1	-3.1	-3.1	-3.1
156_in_ex	-3.3	-3.3	-3.3	-3.3	-3.3	-3.3	-3.2	-3.2	-3.2	-3.3
360	-4.7	-4.7	-4.7	-4.7	-4.7	-4.7	-4.7	-4.6	-4.6	-4.7
372	-4.6	-4.6	-4.6	-4.6	-4.6	-4.6	-4.6	-4.5	-4.5	-4.6
396	-4.1	-4.1	-4.1	-4.1	-4.1	-4.1	-4.1	-4.1	-4.1	-4.1
420	-3.9	-3.9	-3.9	-3.9	-3.9	-3.9	-3.9	-3.9	-3.9	-3.9
444	-4	-4	-3.9	-3.9	-3.9	-3.9	-3.9	-3.9	-3.9	-4
456	-4.1	-4	-4	-4	-4	-4	-4	-4	-4	-4.1
ADA_132	-3.2	-3.2	-3.2	-3.2	-3.2	-3.2	-3.2	-3.2	-3.2	-3.2
C ₆₀	-4.3	-4.3	-4.3	-4.3	-4.3	-4.3	-4.3	-4.3	-4.3	-4.3

The most of binding affinity values for all complexes Ligand 1 (CID=359849) – Rhombellane are lower compared with the value exhibited by the complex Ligand 1 – C₆₀ (-4.3 kcal/mol - Table 2) and lower compared with complexes Ligand 2 – Rhombellane (Table 3).

Only 360 and 372 structures form stronger complexes with Ligand 1 compared to C₆₀ (-4.7 and -4.6 Kcal/mol, respectively).

The best affinity Ligand 2 (CID=491916) to Cube-rhombellanes is showed in case of 396 affinity value -5.4 kcal/mol - Table 3). A little lower value was recorded for 372 and 360 structures (-5 and -4.9 kcal/mol, respectively). The energy of interaction between Lig 2 and C₆₀ is -4.9 kcal/mol. In general, the values of binding affinity are higher for the Lig2 than Lig1. (compare Table 2 with Table 3).

Table 3. Binding affinity of ligand Lig2, CID=491916, with the active site of Rbl-nano-structures (first column) during nine conformations.

Cube Rbl	1	2	3	4	5	6	7	8	9	Docked energy (kcal/mol)
144_ex_ex	-2.9	-2.9	-2.9	-2.9	-2.9	-2.9	-2.9	-2.9	-2.9	-2.9
144_in_ex	-3.5	-3.5	-3.5	-3.5	-3.5	-3.5	-3.5	-3.5	-3.4	-3.5
156_ex_ex	-3.5	-3.5	-3.5	-3.5	-3.5	-3.5	-3.5	-3.5	-3.5	-3.5
156_in_ex	-3.8	-3.8	-3.8	-3.8	-3.8	-3.8	-3.8	-3.8	-3.8	-3.8
360	-4.9	-4.8	-4.8	-4.8	-4.8	-4.8	-4.8	-4.7	-4.7	-4.9
372	-5	-4.9	-4.9	-4.9	-4.9	-4.9	-4.9	-4.9	-4.8	-5
396	-5.4	-5.4	-5.4	-5.4	-5.4	-5.4	-5.4	-5.3	-5.3	-5.4
420	-4.6	-4.6	-4.6	-4.6	-4.6	-4.5	-4.5	-4.5	-4.5	-4.6
444	-4.8	-4.8	-4.8	-4.7	-4.6	-4.6	-4.6	-4.6	-4.6	-4.8
456	-4.8	-4.8	-4.8	-4.8	-4.7	-4.7	-4.6	-4.6	-4.6	-4.8
ADA_132	-4	-4	-4	-4	-3.9	-3.9	-3.9	-3.9	-3.9	-4
C ₆₀	-4.9	-4.9	-4.9	-4.9	-4.9	-4.9	-4.9	-4.9	-4.9	-4.9

Percentage deviations of the affinity values of the ligands Lig1 and Lig2 were estimated for the tested Rbl-structures in relation to the affinity value obtained for the fullerene C₆₀. The highest positive percentage deviations from the affinity of Lig1 and Lig2 to fullerene C₆₀ were obtained for those Rbl-structures showing the highest binding values (Table 4, column 4 and 5 – in boldface).

Two last columns show the equilibrium K value of the bonds, calculated by:

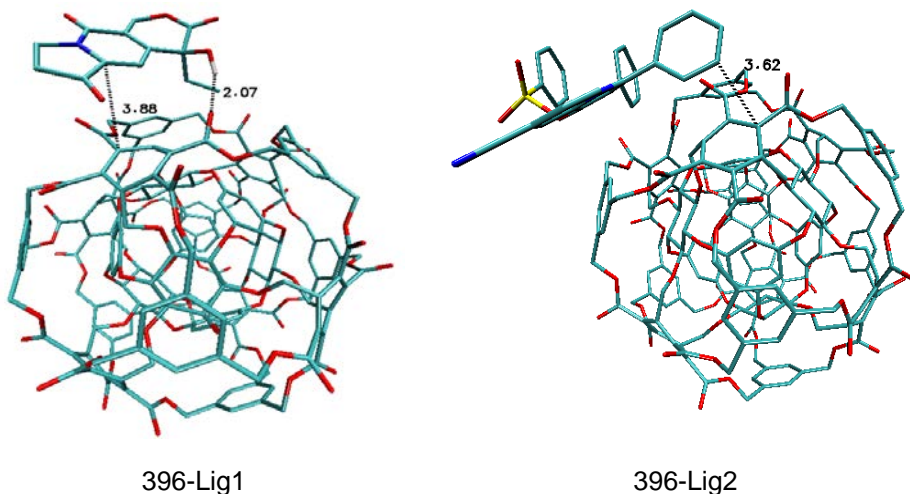
$$K_B = \exp\left(\frac{-\Delta G_B}{RT}\right),$$

where: K_b is binding constant, R- gas constant (J/mol*K), T - temperature 298 K, - ΔG_b binding affinity (J/mol). The higher the K value the more the reaction proceeds towards the formation of the complex.

Detailed analysis of structural properties after docking showed that the affinity of the ligands to the Rhombellanes surface are correlated with the quality of hydrogen bonds formed between them and stacking interactions between aromatic rings of ligands and aromatic rings of Rhombellanes.

Table 4. The best binding affinity of ligands: Lig1 and Lig2, the percentage difference in binding affinity relative to ligand-fullerene C₆₀ (namely affinity), K – constant binding balance.

Cube Rbl	The best binding affinity (kcal/mol)		% difference in binding affinity relative to ligand-fullerene C ₆₀		K – constant binding balance	
	Lig1	Lig2	Lig1	Lig2	Lig1	Lig2
144_ex_ex	-2.8	-2.9	-34.9	-40.8	111.4	131.8
144_in_ex	-3	-3.5	69.8	71.4	156.0	361.9
156_ex_ex	-3.1	-3.5	-27.9	-28.6	184.6	361.9
156_in_ex	-3.3	-3.8	-23.3	-22.4	258.5	599.7
360	-4.7	-4.9	9.3	0.0	2728.3	3820.3
372	-4.6	-5.0	7.0	2.0	2305.6	4520.7
396	-4.1	-5.4	-4.7	10.2	993.7	8863.8
420	-3.9	-4.6	-9.3	-6.1	709.7	2305.6
444	-4.0	-4.8	-7.0	-2.0	839.8	3228.5
456	-4.1	-4.8	-4.7	-2.0	993.7	3228.5
ADA_132	-3.2	-4.0	-25.6	-18.4	218.4	839.8
C ₆₀	-4.3	-4.9	0.0	0.0	1391.5	3820.3

**Figure 5.** Interactions found in the complexes of Rhl-396 and ligands Lig1 (left) and Lig2 (right) after the docking procedure.

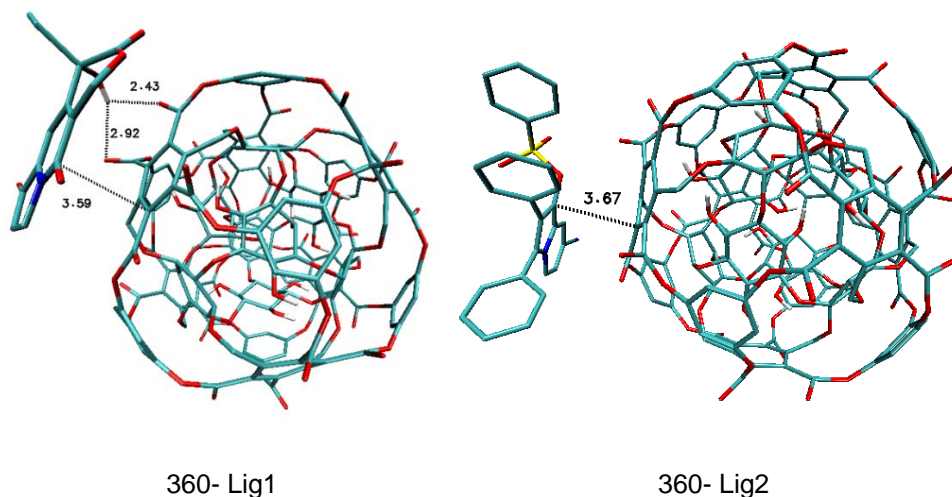


Figure 7. Interactions found in the complexes of RhI-360 and ligands Lig1 (left) and Lig2 (right) after the docking procedure.

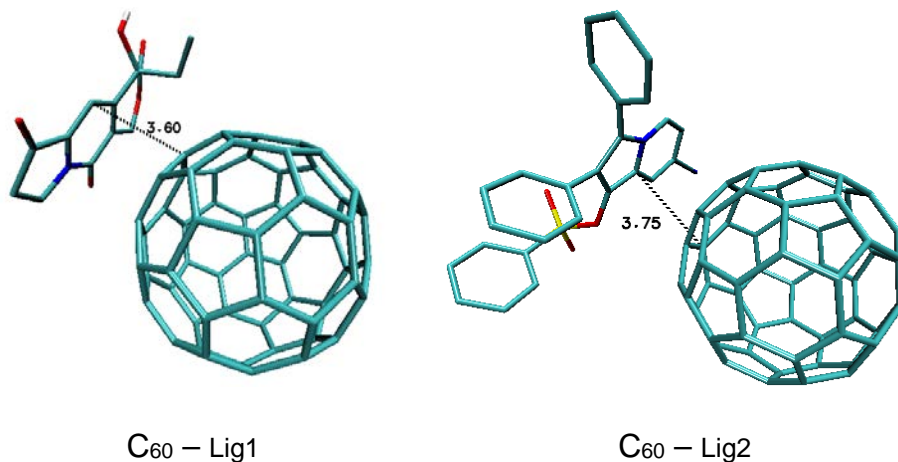


Figure 8. Interactions found in the complexes of fullerene C₆₀ and ligands Lig1 (left) and Lig2 (right) after the docking procedure.

CONCLUSIONS

An attempt was made to deposit the indolizine ligands on the Cube Rhombellane homeomorphs surface as a proposal of a new nano-drug.

The most of binding affinity values for all complexes Ligand 1 (CID=359849) – Rhombellane are lower compared with the corresponding values for the complex Ligand 1 – C₆₀ (-4.3 kcal/mol, Table 2) and lower compared with those for the complexes Ligand 2 – Rhombellane (Table 3). Only Rbl-360 and Rbl-372 structures form stronger complexes with Lig1 compared to C₆₀. The best affinity was shown in case of Rbl-360 (-4.7 kcal/mol). Only a little low value was shown by the complex Lig2 – Rbl-372(-4.6 kcal/mol); the reference complex Lig1-C₆₀ energy has -4.3 kcal/mol. The best affinity was recorded for the complex Lig2 – Rbl-396 (-5.4 kcal/mol), followed by the complexes Lig2-Rbl-372 and Lig2-Rbl-360 (-5 and -4.9 kcal/mol, respectively). The energy of interaction between Lig 2 and C₆₀ is -4.9 kcal/mol. Different order of affinity values can be observed among the complexed made by the two ligands with the Rhombellanes.

Percentage deviations of the affinity value of the ligands Lig1 and Lig2 were estimated for the data obtained on the tested Rhombellanes, in relation with the affinity value obtained for the fullerene C₆₀. The highest positive percentage deviations were obtained for Lig-Rbl complexes showing the highest binding energy values.

Detailed analysis of structural properties after docking showed that the values of affinity of the studied indolizine ligands to the Rhombellanes surface are correlated with the strength/length of hydrogen bonds formed between them, first of all caused by the stacking interactions between aromatic rings of ligands and aromatic rings of Rhombellanes.

ACKNOWLEDGEMENTS

This research was supported by PL-Grid Infrastructure (<http://www.plgrid.pl/en>)

REFERENCES

1. Q. Long, Y. Xiel, Y. Huang et al., *Journal Biomedical Nanotechnology*, **2013**, *9*, 965.
2. M. Benezra, O. Penate-Medina, P.B. Zanzonico, et al. *Journal of Clinical Investigation*, **2011**, *121*, 2768.
3. H. Ali-Boucetta, K. T. Al-Jamal, D. McCarthy et al., *Chemical Communications*, **2008**, *28*, 459.
4. S. Sánchez-Paradinas, M. Pérez-Andrés, M.J. Almendral-Parra, et al., *Journal of Inorganic Biochemistry*, **2014**, *131*, 8.

5. M. P. Evstigneev, A. S. Buchelnikov, D. P. Voronin, Y. V. Rubin, L. F. Belous, Y. I. Prylutsky, U. Ritter, *Chem. Phys. Chem.*, **2013**, *14*, 568.
6. G. S. Singh, E. E. Mmatli, *European Journal of Medicinal Chemistry*, **2011**, *46*, 5237.
7. S. S. Juang, M. Chang, L. F. Wang, J. L. Han, C. H. Ong, *Tetrahedron*, **2005**, *61*, 1693.
8. T. Przewloka, S. Chen, Z. Xia, H. Li, S. Zhang, D. Chimmanamada, E. Kostik, D. James, K. Koya, L. Sun, *Tetrahedron Lett.*, **2007**, *48*, 5739.
9. I. V. Seregin, A. W. Schammel, V. Gevorgyan, *Tetrahedron*, **2008**, *64*, 6876.
10. B. Szefler, T. E. Harsa, A. M. Harsa, *Studia UBB Chemia*, **2015**, *60*, 201.
11. B. Szefler, P. Czeleń, M. V. Diudea, *Current Computer-Aided Drug Design*, **2017**, *13*, 22.
12. B. Szefler, P. Czeleń, *Journal. Molecular Modeling*, **2017**, *23*, 208.
13. PubChem database, accessed 10. 10. 2014.
14. M. V. Diudea, Intl. Conf. "Bio-Nano-Math-Chem", **2017**, Cluj, Romania.
15. K. B. Wiberg, F. H. Walker, [1.1.1]Propellane, *Journal of American Chemical Society*, **1982**, *104*, 5239.
16. P. Kazynsky, J. Michl, *Journal of American Chemical Society*, **1988**, *110*, 5225.
17. M. V. Diudea, *Iranian Journal of Mathematical Chemistry*, **2018**, *9*, 1.
18. D. R. Do Carmo, L. L. Paim, N. L. Dias Filho, N. R. Stradiotto, *Applied Surface Science*, **2007**, *253*, 3683.
19. D. R. Do Carmo, U. O. Bicalho, T. F. Silveira, N. L. Dias Filho, L. L. Paim, *Journal of Chemistry*, **2013**, *2*, 1.
20. M. V. Diudea, *International Journal of Chemical Modeling*, **2018**, *9*, 2, 000.
21. O. Trott, A. J. Olson, *Journal Computer Chemistry*, **2010**, *31*, 455.
22. B. K. Shoichet, I. D. Kuntz, D. L. Bodian, *Journal Computer Chemistry*, **2004**, *13*, 380.
23. K. Dhananjayan, K. Kalathil, A. Sumathy, P. Sivanandy, *Der Pharma Chemica*, **2014**, *6*, 378.
24. R. Abagyan, M. Totrov, *Current Opinion in Chemical Biology*, **2001**, *5*, 375.

QSPR ANALYSIS OF A SET OF LIQUID CRYSTALS IN THE BENZYLIDENEANILINE CLASS ACCORDING TO THEIR TRANSITION TEMPERATURE

THOMAS DIPPONG^a, ALEXANDRA AVRAM^b, FIRUTA GOGA^{b*}

ABSTRACT The present paper focuses on the connection amongst the structure of 25 liquid crystals in the benzylideneaniline class and some of their physico-chemical properties. Simple and multiple correlations between transition temperatures and 34 calculated molecular descriptors (25 topological indices and 12 Van der Waals parameters), for each compound, were made. Simple and multiple correlations amongst topological indices and Van der Waals parameters, respectively, observing the variations taking place, are presented.

Keywords: *liquid crystals, benzylideneaniline, topological indices, Van de Waals parameters*

INTRODUCTION

The microstructure of liquid crystals is complex and very variable. Some organic substances pass from crystalline, solid to isotropic, liquid states, not directly, but through a phase [1,2]. The mechanical and symmetrical properties of these phases are intermediate to the properties of liquids and crystals [3,4]. Because of this, these substances are called liquid crystals or liquid anisotropic crystals. Anisotropic liquids are characterized by a molecular order, which can be translational, rotational, or combinations of the two. The translational order is conditioned by the non-spherical or elongated shape of the molecules that make up the mesophase [5]. The molecular structure is a defining criterion in the categorization of mesophases as anisotropic liquids or liquid crystals [6].

^a *Technical University of Cluj-Napoca, Faculty of Sciences North University Center at Baia Mare, Department of Chemistry and Biology, 76 Victoriei Street, 430122 Baia Mare, Romania*

^b *Babeş-Bolyai University, Faculty of Chemistry and Chemical Engineering, 11 Arany Janos Street., RO-400028, Cluj-Napoca, Romania*

* *Corresponding author: fgoga@chem.ubbcluj.ro*

According to Friedel [7,8], three types, or groups of liquid crystals are distinguished: smectic, nematic and cholesteric, as well as discotic liquid crystals called columnar. The liquid crystals belonging to each of these groups are distinguished by their physical properties, primarily optical ones. These differences arise as a result of a difference in structure.

In smectic liquid crystals, molecules, elongated in the form of sticks, are arranged parallel to their length and form layers of equal thickness, close to the length of the molecules [9]. These layers are organized one above the other at equal distances. Molecular layers in typical smectics are mobile, moving slightly parallel to one another. The transition temperature in the mesomorphic state is quite high. This temperature must be of such value as to destroy the bond between the molecules placed at close distances. Distance between layers can be measured by X-ray diffraction [10].

In cholesteric liquid crystals, the molecules have an orientational ordering of the molecules of the long axis and the center of mass unordered formation, similar to the nematic, but in contrast to this the structure of the balance [11]. Cholesterol derivatives are part of this category, hence the name of the group of liquid crystals. In cholesteric liquid crystals molecules are arranged in layers, as in smectics, but the long axes are parallel to the layers' planes. The layers in the cholesteric liquid crystals are thin, monomolecular. The direction of the long axis orientation of the molecules in each layer is terminated with respect to the previous one, which leads to the formation of a spiral molecular structure [9,11]. Most cholesteric fluids are cholesterol derivatives, cholesteryl acetate, cholesteryl nitrate.

The nematic phase is characterized by long-range orientation [12], which means that long axes of molecules tend to move along the preferential axis. The nematic mesomorphic structure is characterized in that the orientation of the axes of the molecules in such crystals is parallel but does not form layers [13].

Liquid column crystals are different from previous shapes, the molecules are not elongated or discoidal in shape and the arrangement involves an overlapping of the discs in the columns [14]. This mesophase is characterized by a packet of columns and molecules. The columns are wrapped together along the two surface crystalline dimensions. Arranging the molecules in columns leads to the formation of new mesophases [15,16].

In technology, thin-film nematic crystals change their transmission properties for natural or polarized light when an electric field is applied [17,18]. It can be used for alphanumeric and analog display, image conversion, and matrix screens for image playback. In medicine, the use of cholesterol-based liquid crystals in skin thermography and diagnosis derives from the special optical properties of thin films of these substances that indicate

rapidly and directly through their color [19]. In chemistry, nematic and cholesteric liquid crystals are very good solvents for organic molecules. They can be incorporated into liquid crystals in concentrations that do not damage the internal order of the liquid crystals. They are used for spectroscopic investigations of the anisotropic properties of molecules. Liquid crystals are used as solvents in ultraviolet-visible spectroscopy, magnetic resonance imaging, electronic spin resonance to obtain information on the length of solute molecule bonds [20,16].

The present paper focuses on the connection amongst the structure of 25 liquid crystals in the benzylideneaniline class, molecules that fall into the nematic liquid crystals, and some of their physico-chemical properties. The polymers and coordination compounds in the benzylideneaniline class (with π conjugate systems) are important optical functional compounds and have been applied extensively in the fields of liquid crystal materials [22]. Thus, we calculated and tested 34 molecular descriptors, of which 25 topological indices and 12 Van der Waals parameters.

RESULTS AND DISCUSSION

The values of the R correlation coefficient that resulted from Pearson's linear correlation test, between the transition temperature and each of the 35 molecular descriptors are shown in Table 1. Relatively low correlations, both in regards to Van der Waals parameters – transition temperatures, and, topological indices – transition temperatures, in the case of liquid crystals in the benzylideneaniline compounds class, are noted.

The obtained coefficients, lower than $R^2=0.4$, lead to weak correlations, almost insignificant when compared to previous studies (column liquid crystals), where correlations higher than 0.8, with the same topological indices or Van der Waals parameters, were obtained.

The tracked Van der Waals parameters were: Van der Waals Molecular Volume (V^W), van der Waals surface (S^W), Van der Waals ratio (V^W/S^W), volume of the sphere (V^{SF}), volume of the ellipsoid (V^{EL}), the ellipsoid semi-axes (EX, EY, EZ), the ratio between the volume of the sphere and the Van der Waals volume (GL_1), the ratio between the volume of the sphere and that of the ellipsoid (GL_2), the degree of volume globularity (GLOB, the ratio between the Van der Waals volume and that of the sphere) [23]. The used topological indices were as follows: Wiener (W), polarity (P), Gordon-Scantlebury Index (N_2), Zagreb (M_1 si M_2), Randić ($^1\chi, ^2\chi, ^3\chi$), Balaban (J_2, J_3), Balaban and Randić index with the covalent radii (J^{rc}, χ^{rc}), Mulliken's electronegativities (J^{el}, χ^{el}) and by Van der Waals radii (J^{Rw}, χ^{Rw}), Kier and

Hall Indices ($\chi^{D^{el}}$, JD^{el} were calculated for Mulliken's electronegativities, the indices $\chi^{D^{rc}}$ and JD^{rc} for the covalent radii, and, respectively, the indices $\chi^{D^{Rw}}$, JD^{Rw} for van der Waals radii) [23].

Table 1. Statistical parameters of the mono-variable regressions equations

Van der Wals parameters			Topological indices		
Independent variable	Statistical parameter		Independent variable	Statistical parameters	
	R ²	F		R ²	F
V ^W	0.442	7.72	W	0.354	6.55
S ^W	0.446	7.89	P	0.402	7.63
V ^W /S ^W	0.205	3.39	N ₂	0.431	7.60
V ^{SF}	0.350	6.03	M ₁	0.446	7.90
S ^{SF}	0.501	9.14	M ₂	0.436	7.70
V ^{EL}	0.415	7.94	¹ χ	0.411	7.92
Ex	0.400	16.94	² χ	0.321	6.09
EY	0.206	4.39	³ χ	0.394	6.64
Ez	0.108	1.20	χ ^{rc}	0.407	7.11
GL ₁	0.312	5.22	χ ^{el}	0.402	7.65
GL ₂	0.215	4.08	χ ^{Rw}	0.401	7.20
GLOB	0.508	12.5	χ ^{D^{rc}}	0.391	6.55
			χ ^{D^{el}}	0.396	7.23
			χ ^{D^{Rw}}	0.386	7.39
			J ₂	0.324	5.47
			J ₃	0.222	4.00
			J ^{rc}	0.055	0.13
			J ^{el}	0.068	0.12
			J ^{Rw}	0.006	0.001
			JD ^{rc}	0.112	1.15
			JD ^{el}	0.009	0.002
			JD ^{Rw}	0.008	0.002

As an example, ,the best' simple linear correlations between temperature and E_x, and, transition temperature and globularity (GLOB), are rendered as a graph, where: R² – coefficient of determination SE – standard error, MSE – Mean Square error.

$$T_z = - 70.06 + 15.05 EX \quad (1)$$

$$R^2 = 0.400 \quad SE = 33.34 \quad F = 16.94 \quad MSE = 146.14$$

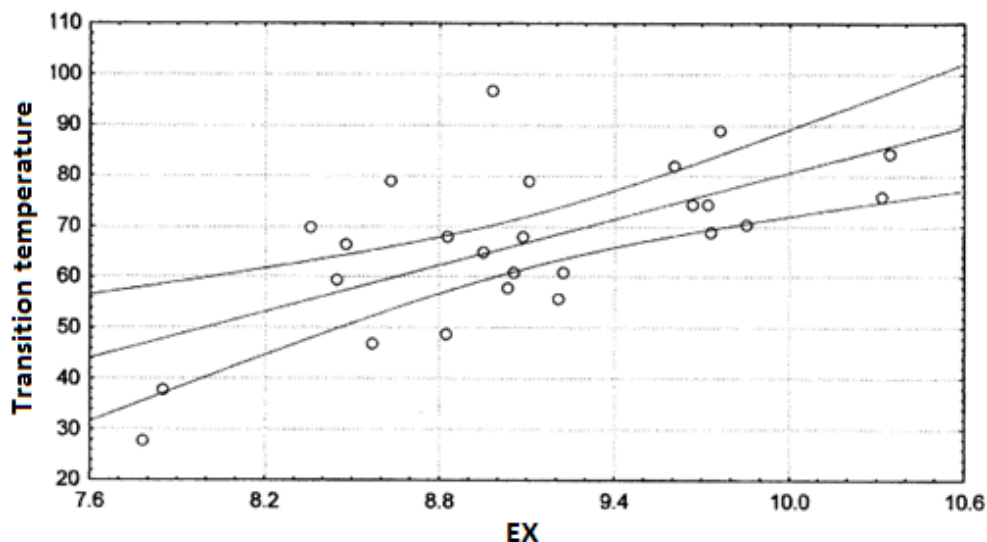


Figure 1. Correlation between the transition temperature and Ex

$$T_z = 167.16 - 384.23 \text{ GLOB} \quad (2)$$

$$R^2 = 0.508 \quad SE = 28.49 \quad F = 12.5 \quad MSE = 164.4$$

Eliminating the values located outside the confidence interval (the two curves), even if, the statistical parameters would improve, is not recommended, as, the application generality of the obtained result would diminish.

As can be seen, the correlation between the transition temperature and the Van der Waals ratio (V^W/S^W) presents very weak correlations, even lower than those between separates of the Van der Waals volume ($R^2=0.442$) and Van der Waals surface ($R^2=0.446$), the vapor dispersion being a lot higher.

$$T_z = 5.45 + 0.17 V^W \quad (3)$$

$$R^2 = 0.442 \quad SE = 22.25 \quad F = 7.73 \quad MSE = 189.9$$

$$T_z = 2.30 + 0.227 S^W \quad (4)$$

$$R^2 = 0.446 \quad SE = 23.13 \quad F = 7.89 \quad MSE = 188.9$$

$$T_z = 872.99 - 1011.61 V^W/S^W \quad (5)$$

$$R^2 = 0.205 \quad SE = 22.1123 \quad F = 3.39 \quad MSE = 221.11$$

In case of correlating the surface of the S^{SF} sferoid, a better correlation can be obtained ($R^2=0.501$), but weaker than in the case of globularity ($R^2=0.508$).

$$T_z = 29.018 - 0.034 S^{SF} \quad (6)$$

$$R^2 = 0.501 \quad SE = 12.82 \quad F = 9.10 \quad MSE = 181.81$$

In these calculations we find the multiple correlation coefficient R^2 (which for a good correlation should tend to the value of 1, F (the Fisher test value) which, for the statistical significance of correlations, is desired to be as high as possible. S is the explained variance, a statistical indicator commonly used in the study of structure-property relationships as it shows what percentage of the property being analyzed is explained by the variables used in a correlation.

In the case of correlations of transition temperatures with topological indices, low correlation coefficients are also obtained, usually between 0.3-0.45, $^2\chi$, presenting the best correlation of this class of compounds.

$$T_z = 12.776 + 6.872 ^2\chi \quad (7)$$

$$R^2 = 0.321 \quad SE = 22.07 \quad F = 6.09 \quad MSE = 200.59$$

Other correlations with over 0.5 were obtained in the case of the correlation between the transition temperature and Gordon (N_2), M_1 , M_2 and J_3 .

$$T_z = -21.420 + 3.420 N_2 \quad (8)$$

$$R^2 = 0.431 \quad SE = 32.11 \quad F = 7.60 \quad MSE = 190.69$$

$$T_z = -25.752 + 0.948 M_1 \quad (9)$$

$$R^2 = 0.446 \quad SE = 33.05 \quad F = 7.90 \quad MSE = 188.88$$

$$T_z = -33.689 + 0.932 M_2 \quad (10)$$

$$R^2 = 0.436 \quad SE = 36.32 \quad F = 7.70 \quad MSE = 190.11$$

$$T_z = 68.023 - 0.119 J_3 \quad (11)$$

$$R^2 = 0.222 \quad SE = 3.00 \quad F = 4.00 \quad MSE = 216.14$$

Several multilinear correlations have been made, trying to find those descriptors that are not interleaved and, thus, increase the correlation coefficient. The best result was obtained by the multilinear correlation of the

transition temperature with the topological indices and Van der Waals parameters. Thus, by correlating the transition temperature and ${}^2\chi$, ${}^3\chi$, J^{el} , JD^{rc} , N_2 (equation 12), a R^2 of 0.720 is obtained, compared to very low coefficients obtained separately.

$$T_z = -782.42 + 144.9 {}^2\chi - 177.8 {}^3\chi + 10185.4 J^{el} - 1119.2 JD^{rc} - 13.37 N_2 \quad (12)$$

$$R^2 = 0.720 \quad SE = 15.86 \quad F = 10.49 \quad MSE = 100.31$$

Taking into account the method of calculating the topological indices, we find that the ${}^2\chi$ și J^{el} ones are favorable to the increase of the transition temperature, therefore, there is a flexibility component [Kier and Hall [24]] and a favorable electronic one (J^{el} is the index J calculated for atomic electronegativity). In the case of the above set, the ${}^2\chi$ și ${}^3\chi$ indices are intercorrelated.

Only by correlating the transition temperature with the randic and balaban indices, does the R^2 correlation coefficient decrease.

$$T_z = -1722 + 86.91 \chi^{el} + 407022 J^{Rw} - 225149 J^{rc} - 936228 J^{el} \quad (13)$$

$$R^2 = 0.704 \quad SE = 12.63 \quad F = 6.72 \quad MSE = 108.45$$

As randic indices encode information about the size and branching of molecules, it is interesting to see what happens if the mentioned indices are replaced by the van der Waals report, thus, obtaining function 14.

$$T_z = -7196 + 8997 V^W/S^W - 1270 J_2 - 184124 J_3 - 225.7 J^{el} \quad (14)$$

$$R^2 = 0.615 \quad SE = 15.34 \quad F = 4.41 \quad MSE = 121.29$$

There is a decrease in the correlation coefficient at 0.615, which denotes an inverse effect from that of the column liquid crystals, where there was an increase in the correlation coefficient following the involvement of the Van der Waals report [23].

A main purpose of QSPR is to detect a mathematical link between the surveyed property and the molecular descriptors derived from the structure of the molecule [25].

Opposed to columnar liquid crystals [23], liquid crystals from the benzylideneaniline group present weaker mathematical models. It can be concluded that the linear chemical structure of these compounds is not that stable when compared to the branched one of columnar liquid crystals.

CONCLUSIONS

The information obtained from the molecules of the benzylideneanilide liquid crystals is insufficient, as the property taken into account also depends on other factors not covered by the considered molecular descriptors. These molecules fall into the nematic liquid crystals, which have the main characteristic of orienting themselves along a straight line called a steering axis, being formed by relatively long molecules without distinct branches. This is also evident from the fact that the best correlation is given by the Ex transition ($R^2 = 0.40$), a ratio that can be assimilated in a first approximation with a length. It is assumed that other parameters such as the average angle of the molecules with the reference axis, the degree of ordering and a series of parameters describing the intermolecular interactions of physical nature (electrostatic) taking into account the polarity of the compounds can be considered. Although the correlation between the transition temperature and Van der Waals parameters, respectively topological indices, give lower correlation coefficients than with column liquid crystals. If multiple correlations are achieved, higher correlation coefficients are obtained. This study is very important as it takes a new, unique approach in regards to the structure of liquid crystals in the benzylideneaniline class and the correlation degree between transition temperature, topological indices and Van der Waals parameters, respectively. An improvement upon mathematical models as a result of multiple regressions between transition temperature – topological indices – Van der Waals parameters can also be observed.

EXPERIMENTAL SECTION

The used method of determining the liquid crystal transition temperature allows a highlight of the type of texture, the type of phase, and the transition temperature of the liquid crystal samples using the polarizing microscope. Study cells contain nematic crystals (4-cyano-phenyl-4-pentylbenzoate). Each cell is made of glass walls on which a transparent conductive layer of In_2O_3 has been deposited. Measurements require the use of a heating device and a one for stabilizing and measuring the temperature. As heating device, an aluminum electric furnace having dimensions of $5 \times 6 \text{ cm}^2$ and 1 cm thickness, was used. Heating of the furnace is made by means of an electrical resistance, the heating current being controlled by the temperature stabilizer. The furnace is provided with a seat for fixing the sample. The temperature transducer that fits through a furnace inlet and has its ends connected to the temperature-determining device is fixed on the cell. The

furnace has outputs for supplying the electrical resistance, allowing the application of an electric field to the samples. Both the furnace and lid are equipped with windows for visualising samples and optical measurements. After the sample has been placed inside, the furnace is connected to the microscope and heated to 70-80°C.

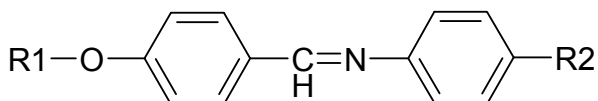


Figure 4. General structure of the benzylideneaniline class

Table 2. The most important representatives of the benzylideneaniline class

Comp.	R1	R2	T _{transition}
t01	CH ₃	CH ₃	38
t02	C ₂ H ₅	CH ₃	79
t03	C ₃ H ₇	CH ₃	49
t04	C ₄ H ₉	CH ₃	68
t05	C ₅ H ₁₁	CH ₃	58
t06	CH ₃	C ₂ H ₅	28
t07	C ₂ H ₅	C ₂ H ₅	70
t08	C ₃ H ₇	C ₂ H ₅	66,5
t09	C ₄ H ₉	C ₂ H ₅	65
t10	C ₅ H ₁₁	C ₂ H ₅	61
t11	CH ₃	C ₃ H ₇	59,5
t12	C ₂ H ₅	C ₃ H ₇	97
t13	C ₃ H ₇	C ₃ H ₇	68
t14	C ₄ H ₉	C ₃ H ₇	82
t15	C ₅ H ₁₁	C ₃ H ₇	74,5
t16	CH ₃	C ₄ H ₉	47
t17	C ₂ H ₅	C ₄ H ₉	79
t18	C ₃ H ₇	C ₄ H ₉	56
t19	C ₄ H ₉	C ₄ H ₉	74,5
t20	C ₅ H ₁₁	C ₄ H ₉	69
t21	CH ₃	C ₅ H ₁₁	61
t22	C ₂ H ₅	C ₅ H ₁₁	89
t23	C ₃ H ₇	C ₅ H ₁₁	70,5
t24	C ₄ H ₉	C ₅ H ₁₁	84,5
t25	C ₅ H ₁₁	C ₅ H ₁₁	76

When this temperature is reached, the heating system is decoupled and monitored during sample cooling: the temperature at which the crystal transitions from the liquid state to the mesophase (transition temperature), the transition temperature F , the solid state and the type of texture that occurs in this phase.

The results of the simple linear correlations of the transition temperatures with the calculated molecular descriptors are presented in the following tables, the first column being the independent variable (topological index or Van der Waals parameter), the second, the R correlation coefficient (which, for good correlation, must tend to the value of 1) and, in the third column, is the Fisher test value for the statistical significance of the correlations, which is desirable to be as high as possible. All formulas were drawn in the Hyperchem program, then optimized by molecular modeling, calculating free energies. In order to refine the calculations, an ab initio calculation was chosen, as, in the ab initio variants, the different energy components of the molecules, including the electron-based component, can be calculated. Topological indices and Van der Waals parameters were calculated using the formulas mentioned above. Linear and multiple correlations were performed with Statistics 7.0 and OriginPro8.

Table 3. Topological indices for benzylideneanilines

Nr	W	P	N2	M1	M2	$^1\chi$	$^2\chi$	$^3\chi$	J	J2	J3
b1	616	40	21	82	91	8.28	6.42	3.85	1.59	0.23	0.0251
b2	733	43	22	86	95	8.78	6.80	4.22	1.57	0.21	0.0227
b3	872	45	23	90	99	9.28	7.15	4.49	1.55	0.20	0.02
b4	1030	46	24	94	103	9.78	7.51	4.58	1.53	0.18	0.017
b5	1208	48	25	98	107	10.28	7.86	4.83	1.50	0.17	0.0149
b6	729	42	23	86	96	8.81	6.59	3.97	1.58	0.22	0.0225
b7	864	44	24	90	100	9.31	6.97	4.18	1.57	0.20	0.0199
b8	1018	46	25	94	104	9.81	7.32	4.45	1.55	0.19	0.0176
b9	1192	48	26	98	108	10.31	7.68	4.70	1.53	0.18	0.0155
b10	1387	50	27	102	112	10.81	8.03	4.95	1.50	0.16	0.0138
b11	864	44	24	90	100	11.31	6.97	4.18	1.57	0.20	0.0201
b12	1014	46	25	94	104	9.81	7.35	4.38	1.55	0.19	0.0179
b13	1184	48	26	98	108	10.31	7.70	4.65	1.54	0.18	0.0159
b14	1375	50	27	102	112	10.81	8.06	4.90	1.52	0.17	0.0142
b15	1588	52	28	106	116	11.31	8.41	5.15	1.50	0.16	0.0127
b16	1018	46	25	94	104	11.81	7.32	4.45	1.55	0.19	0.018
b17	1184	48	26	98	108	10.31	7.70	4.65	1.54	0.18	0.0161
b18	1317	50	27	102	112	10.81	8.06	4.92	1.52	0.17	0.0144
b19	1580	52	28	106	116	11.31	8.41	5.17	1.51	0.16	0.0129
b20	1812	54	29	110	120	11.81	8.76	5.42	1.49	0.15	0.0116
b21	1192	48	26	90	108	10.31	7.68	4.70	1.53	0.18	0.016
b22	1375	50	27	102	112	10.81	8.06	4.90	1.52	0.17	0.0145
b23	1580	52	28	106	116	11.31	8.41	5.17	1.51	0.16	0.013
b24	1808	54	29	110	120	11.81	10.38	5.42	1.49	0.15	0.0118
b25	2060	56	30	114	124	12.31	10.97	5.67	1.48	0.14	0.0106

Table 4. Van der Waals parameters for benzylideneanilines

	S ^W	V ^W	V ^{SF}	S ^{SF}	V ^{EL}	E _x	E _y	E _z	GLOB	GL1	V ^W /S ^W
b1	215.2	266.4	2024.7	774.0	645.1	7.8	6.7	2.9	0.31	0.32	0.81
b2	232.6	289.0	2692.7	936.0	695.1	8.6	6.6	2.9	0.28	0.26	0.81
b3	250.0	310.7	2875.0	977.8	761.2	8.8	7.1	2.9	0.27	0.26	0.80
b4	267.1	333.1	2881.8	979.3	923.0	8.8	8.6	2.9	0.27	0.32	0.80
b5	283.3	355.7	321.7	1053.4	1005.5	9.0	9.1	2.9	0.26	3.13	0.79
b6	233.4	290.9	1973.3	760.8	928.3	7.8	7.3	3.9	0.31	0.47	0.80
b7	249.4	312.8	2443.9	877.4	1055.5	8.4	7.8	3.9	0.29	0.43	0.79
b8	267.0	334.9	2552.9	903.3	1169.1	8.5	8.5	3.9	0.28	0.46	0.79
b9	283.5	356.7	3073.5	1022.3	1266.5	8.9	9.0	3.7	0.26	0.41	0.79
b10	300.5	378.5	3735.6	1164.3	1392.6	9.0	9.6	3.8	0.25	0.37	0.79
b11	250.2	313.0	2522.8	896.2	1069.9	8.4	7.8	3.9	0.28	0.42	0.8
b12	267.4	334.9	3032.3	1013.1	1189.1	8.9	8.4	3.8	0.27	0.39	0.79
b13	283.5	356.8	3138.9	1036.7	1299.9	9.1	8.9	3.8	0.26	0.41	0.79
b14	301.5	378.9	3710.6	1159.1	1459.3	9.6	9.5	3.8	0.25	0.39	0.79
b15	318.1	401.3	4347.2	1288.1	1576.5	9.6	18.1	3.8	0.24	0.36	0.79
b16	266.8	334.9	2633.3	922.1	1269.4	8.6	8.3	4.2	0.28	0.48	0.79
b17	285.7	356.8	3161.2	1841.7	1419.8	9.1	8.8	4.2	0.26	0.45	0.8
b18	300.4	378.9	3478.0	1110.1	1522.4	9.2	9.4	4.2	0.25	0.44	0.79
b19	318.6	400.8	4164.3	1251.7	1705.5	9.7	9.9	4.2	0.24	0.41	0.79
b20	333.9	422.	4925.6	1399.9	1780	9.7	10.5	4.1	0.23	0.36	0.79
b21	282.6	356.9	3281.5	1067.9	1463.4	9.2	8.6	4.4	0.26	0.45	0.79
b22	301.6	379.1	3894.9	1197.1	1631.0	9.7	9.1	4.4	0.24	0.42	0.79
b23	316.6	400.3	4006.2	1219.8	1176.5	9.8	9.8	4.4	0.24	0.29	0.79
b24	334.1	423.6	4696.9	1356.3	1936.2	10.	10.4	4.3	0.23	0.41	0.79
b25	352.6	445.7	5531.3	1512.5	2002.7	10.3	10.9	4.2	0.22	0.36	0.79

REFERENCES

1. A. Dequidt, P. Oswald, *The European Physical Journal E*, **2007**, *24*, 157.
2. Y. Chen, F. Peng, T. Yamaguchi, X. Song, S-T. Wu, *Crystals*, **2013**, *3*, 483.
3. C.-F. Dascalu, B.C. Zelinschi, D. Ortansa Dorohoi, *Annals of ,Dunarea de jos' University of Galati*, Fascicle II, **2011**, *46*.
4. S. Ermakov, A. Beletskii, O. Eismont, V. Nikolaev, *Liquid Crystals in Biotribology (Biological and Medical Physics, Biomedical Engineering)*, Springer International Publishing, **2016**, Chapter 2: Brief review of liquid crystals.
5. S. Chandrasekhar, B.K. Sadashiva, K.A. Suresh, *Pramana*, **1977**, *9*, 471.
6. G.H. Brown, *Journal of Chemical Education*, **1983**, *60*, 900.
7. S. Chandrasekhar, "Liquid Crystals", Cambridge University Press, **1992**.

8. D. Demus, J.W.G. Goodby, G.W. Gray, H.W. Spiess, "Handbook of Liquid Crystals", Wiley-VCH, **1998**.
9. D. Andrienko, *Journal of Molecular Liquids*, **2018**, in press, <https://doi.org/10.1016/j.molliq.2018.01.175>.
10. A. Alvarez fernandez, P.H.J. Kouwer, *International Journal of Molecular Sciences*, **2016**, *17*, 731.
11. M.R. Alcantara, E.G. Fernandes, *Journal of Physiscs*, **2002**, *2*, 32.
12. S. Yilmaz, H. Melik, F. Angay, M. Emek, A. Yildirim, *Journal of Modern Physics*, **2011**, *2*, 248.
13. H. Ozbek, S. Ustunel, E. Kutlu, M.C. Cetinkaya, *Journal of Molecular Liquids*, **2014**, *199*, 275.
14. H. Bock, *Columnar Liquid Crystals*, **2001**, 355.
15. A. Shulty, S. Diele, S. Laschat, "Novel columnar tetraphenylethenes", Technische Universitat Braunschweig, **1998**.
16. E. Westphal, M. Prehm, I.H. Bechtold, C Tschierskeb, H, Gallardo, *Journal of Materials Chemistry C*, **2013**, *1*, 8011.
17. L.A. Bulavin, L.N. Lisetski, S.S. Minenko, A.N. Samoilov, V.V. Klepko, S.I. Bohvan, N.I. Lebovka, *Journal of Molecular Liquids*, **2017**, in press, <https://doi.org/10.1016/j.molliq.2017.12.078>.
18. S.M. Kelly, M. O'Neill, *Handbook of Advanced Electronic and Photonic Materials and Devices*, edited by H.S. Nalwa, Volume 7: Liquid Crystals, Display and Laser Materials, Chapter 1, Academic Press, **2000**.
19. I. Abdulhalim, R. Moses, R. Sharon, *Acta Physica Polonica A*, **2007**, *112*, 715.
20. B. Stevansson, A.Marini, H. Zimmermann, A. Maliniak, *Journal of Physical Chemistry B*, **2011**, *115*, 7561.
21. E. Westphal, M. Prehm, I.H. Bechtold, C Tschierskeb, H, Gallardo *Journal of Materials Chemistry C*, **2013**, *1*, 8011.
22. L. Wang, C. Cao, C. Cao, *Journal of Physical Organic Chemistry*, **2014**, *27*, <https://doi.org/10.1002/poc.3341>.
23. Z. Berinde, T. Dippong, C. Butean, *Studia UBB Chemia*, **2016**, *61*, 51.
24. L.B. Kier, L.H. Hall, "Molecular Connectivity in Chemistry and Drug Research", Acad. Press, **1976**.
25. J.H. Al-Fahemi, *Liquid Crystals*, **2014**, *41*, 1575.

THEORETICAL CALCULATION OF THERMODYNAMIC PROPERTIES AND DIFFUSION COEFFICIENTS FOR PURE ETHANOL, PURE WATER AND BINARY MIXTURE OF (ETHANOL + WATER) AS FUNCTION OF TEMPERATURE BY MOLECULAR DYNAMIC SIMULATION

NAHID SOHREVARDI^a, FARHOUSH KIANI^{a*}, FARDAD KOOHYAR^{b,c*}

ABSTRACT. In this research work, we presented the results of theoretical calculations for the change of thermodynamic properties such as enthalpy ΔH , entropy ΔS , heat capacity ΔC_p , and Gibbs free energy ΔG , for pure water, pure ethanol and interaction of mixture (50% water + 50% ethanol) and binary mixture of (water + ethanol) under thermal equilibrium condition at $T = (273.15, 283.15, 293.15, 298.15, 305.15, 311.15, 320.15, 333.15)$ K and at atmospheric pressure. This theoretical calculation was done using Molecular Dynamic (MD) simulation.

The results show that the values of ΔH and ΔS increase and also value of ΔC_p decreases by temperature growth. The obtained value of change of Gibbs free energy for interaction of mixture (50% water + 50% ethanol) shows that this interaction is possible at $T = (298.15, 311.15, 320.15, 333.15)$ K. Also, it showed that the self-diffusion coefficient and the mutual diffusion coefficients increase by increasing temperature.

Key words: *water, ethanol, mixture, interaction, thermodynamic properties, temperature, MD simulation.*

^a Department of Chemistry, Faculty of Science, Ayatollah Amoli Branch, Islamic Azad University, Amol, Iran

^b Division of Computational Physics, Institute for Computational Science, Ton Duc Thang University, Ho Chi Minh City, Vietnam

^c Faculty of Applied Sciences, Ton Duc Thang University, Ho Chi Minh City, Vietnam

* Corresponding authors: fardadkoohyar@tdt.edu.vn; Farhoush_kiani@yahoo.com

INTRODUCTION

Among various components that have been added to water, monohydric alcohols offer most favorable conditions for such studies owing to the amphiphilic nature of alcohol molecules. Alcohols strongly interact with water molecules through hydrogen bonds. The force of this interaction depends on the number and steric arrangement of their alkyl groups, also through hydrophobic effects. Some methods have been applied to the analyses of single atom materials [1], water [2-6] and more complex structured materials. Properties of ethanol, in liquid form, are usually experimentally known with high accuracy, and their calculation is most often straightforward. Heat capacity is a basic thermodynamic property, which could be used to characterize a liquid. It is directly linked with temperature derivatives of other basic thermodynamic functions and is therefore indispensable for calculation of differences in these functions between different temperatures. This invaluable information is widely used in physics and chemistry for establishing energy balances in thermodynamics for obtaining entropy and enthalpy values, and for calculating changes in interaction enthalpies with temperature. Since the knowledge of the heat capacities is also required for evaluating the effect of temperature on phase and interaction equilibria, variations in heat capacities serve as a sensitive indicator of phase transitions and are an important tool for understanding changes in the structure of liquid solutions [7].

Although, in principle, more observables could be computed this set includes the most important thermodynamic properties of the liquids, including temperature derivatives of energy and volume. In this work, the thermodynamic properties of the pure ethanol, pure water, ethanol/ water mixture, and ethanol/water interaction were calculated in the thermal equilibrium state as well as the temperature dependence of these properties are studied. Also, we will present the details of simulations. The obtained results and their meaning are discussed in subsequent sections.

MOLECULAR DYNAMICS SIMULATION

In this research work, Molecular Dynamics Simulations were performed using the GROMACS (version 4.5.4) [8-10] at various temperatures ($T = 273.15, 283.15, 293.15, 298.15, 305.15, 311.15, 320.15, 333.15$ K) and the constant atmospheric pressure. We have prepared different boxes at various temperatures to do these calculations. One box contains pure water and the other box contains pure ethanol at various temperatures. Also, the binary system of (water + ethanol) prepared with the ethanol mole fractions

$X_{ethanol} = 0.5$ at various temperatures. number of total molecules is 1000 in the each simulation. In the first step, we assessed the quality of molecules topologies produced automatically through the server PRODRG [11, 12] under the grooms 43a1 force fields [13]. SPC water model were used to describe the interactions of water [14]. Temperature (v-rescale) and pressure (Parrinello-Rahman) were controlled by using weak coupling thermostats [15,16]. Electrostatic interactions were treated by means of Particle Mesh Ewald (PME) approach [17,18]. Initial atomic velocities were created on the basis of Maxwellian distribution at the absolute temperature [19,20]. Numerical integrations were calculated by the velocity verlet algorithm [21]. In the next step, the prepared mixtures, at various temperatures, were put into the $6.5nm \times 6.5nm \times 6.5nm$ cubic boxes. A steepest-descent algorithm was used to minimize the energy of each system with a cut-off distance for the short-range neighbor list (1 nm). In the last step, each system was simulated with a time step of $2fs$ for the total time $50ns$. To maintain number of molecules and also values of pressure and temperature (NPT ensemble) during simulation [22], the coupling time intervals was set at 0.1 ps and 2.0 ps for temperature and pressure, respectively. The compressibility was set at $4.5 \times 10^{-5} \text{ bar}^{-1}$ and it were used for a total time calculation. Also, the periodic boundary condition and integration of motion equations were carried out by the leap-frog algorithm [23] with a time step of 2 fs. LINCS algorithm [24] was used to fix the chemical bonds between the atoms. Coordinates were saved every 2 ps for subsequent analyses. Using a function called `g_energy` [25], we extract the enthalpy, H . The obtained results are finally shown in graphs and tables.

RESULT AND DISCUSSIONS

In this study, the values of change of enthalpy, ΔH , change of entropy, ΔS , change of heat capacity, ΔC_p , and change of Gibbs free energy, ΔG , for pure water, pure ethanol, water/ethanol mixture, and interaction of mixture (50% water + 50% ethanol) under thermal equilibrium condition at temperature range $T = 273.15 \text{ K}$ to $T = 333.15 \text{ K}$ and at atmospheric pressure were calculated using MD simulation. In these thermodynamic properties, the initial stage is $T = 273.15 \text{ K}$ (the reference temperature) and the final stages are higher temperatures. Thermodynamic properties of solution have many applications in research works and industries [26].

For a thermodynamic system, the enthalpy can be defined as the below:

$$H = U + PV \tag{1}$$

In equation 1, H is enthalpy, U is internal energy, P is the pressure, and V is volume of this system. At constant pressure, change of enthalpy can be obtained from below equation:

$$\Delta H = \Delta U + P\Delta V \quad (2)$$

In this theoretical study, all studied systems are closed. In a closed system, at constant pressure, the values of volume and ΔV as well as internal energy and ΔU increase as temperature increases. It shows that according to equation 2, in a closed system, the values of ΔH increase with temperature growth. It is well known that in closed systems, ΔV and ΔU have positive values.

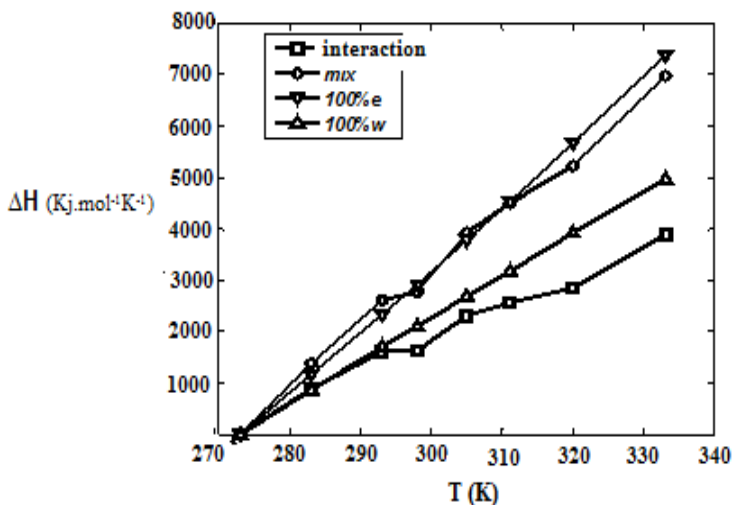


Figure 1. The change of enthalpy for interaction of mixture (50% water + 50% ethanol), water/ethanol mixture, pure ethanol, and the pure water as a function of temperature.

For our studied systems, the obtained values of ΔH (at various temperatures) have been plotted in Figure 1. This figure shows that ΔH for water/ethanol mixture, interaction of mixture (50% water + 50% ethanol), pure ethanol and pure water increases by temperature increasing. In addition, the lowest value of ΔH belongs to interaction of mixture (50% water + 50% ethanol) and also, the highest values of ΔH belong to mixture (ethanol + water) at $T = (270 - 295)$ K and pure ethanol at $T = (310 - 340)$ K.

The values of ΔH for systems of this study can be fitted by the following equation:

$$\Delta H = a_0 + a_1T + a_2T^2 + a_3T^3 \quad (3)$$

For studied systems of this work, the values of a_0 , a_1 , a_2 , and a_3 has been shown in Table 1.

Table 1. The values of a_0 , a_1 , a_2 , and a_3 (according to equation 3) for different systems of this study.

Systems	a_0	a_1	a_2	a_3
interaction	-6379	-85.7	0.6371	-0.0008657
water/ethanol mixture	-6379	-153.5	0.9623	-0.001147
pure ethanol	-6379	-95.31	0.5463	-0.0004092
pure water	-6379	-87.42	0.5918	-0.0006816

The change of specific heat capacity or specific heat (ΔC_p) is obtained by the following equation:

$$\Delta C_p = \left(\frac{d\Delta H}{dT}\right)_p \quad (4)$$

We can obtain equation 5 by considering equations 3 and 4:

$$\Delta C_p = a_1 + 2a_2T + 3a_3T^2 \quad (5)$$

Equation 5 can be used to calculate values of change of specific heat for studied systems of this work. Obtained data are listed in Table 2.

As it can be seen in Table 2 and Figure 2, the maximum and minimum values of ΔC_p belong to pure ethanol and interaction of mixture (50% water + 50% ethanol), respectively. As we know, the specific heat capacity or specific heat (C_p) is the amount of heat (usually in calories, kilocalories, or joules) needed to increase the temperature of a system by one degree (usually in Celsius or Kelvin). Among studied systems of this research work, pure ethanol has stronger intermolecular force. Therefore, there is need more amount of head to raise the temperature of this system by one degree.

Table 2. The values of change of specific heat (according to equation 5) for different systems of this study at various temperatures ($T = 273.15 \text{ K}$ to 333.15 K).

$\Delta C_p \text{ (Kj.mol}^{-1}.\text{K}^{-1})$							
273.15 K	283.15 K	293.15 K	298.15 K	305.15 K	311.15 K	320.15 K	333.15 K
interaction of mixture (50% water + 50% ethanol)							
68.5757	66.87004	64.64495	63.33762	61.28921	59.33085	56.04271	50.5504
water/ethanol mixture							
115.4683	115.572	114.9875	114.4372	113.3777	112.2012	109.9719	105.7676
pure ethanol							
111.5413	115.6382	119.4895	121.3231	123.787	125.8032	128.6618	132.4397
pure water							
83.31593	83.7767	83.82852	83.70107	83.35087	82.89121	81.92567	79.94619

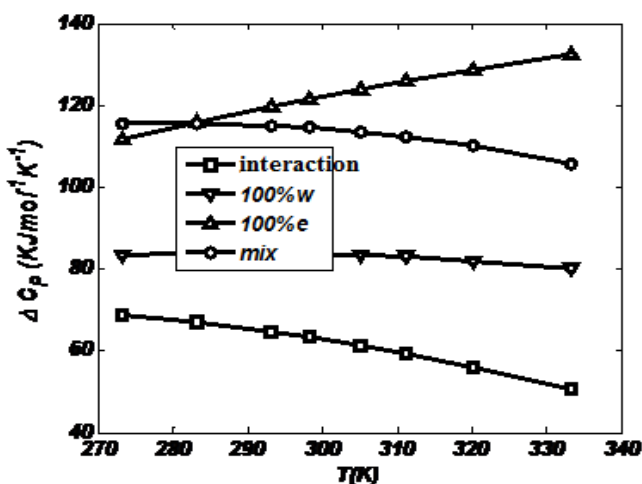


Figure 2. Changes of specific heat for interaction of mixture (50% water + 50% ethanol), water/ethanol mixture, pure ethanol and pure water as a function of temperature.

Figure 2 shows the changes of specific heat for studied systems of this work at different temperatures. In this figure it is obvious that the values of ΔC_p for interaction of mixture (50% water + 50% ethanol) and water/ethanol mixture decrease by temperature growth. Also, the value of ΔC_p for pure ethanol increases by temperature increasing.

Entropy change (ΔS) for our studied systems can be calculated as follows:

$$\Delta S = \int_{273.15}^{333.15} nC_p \frac{dT}{T} \quad (6)$$

For studied systems of this work, the obtained values of ΔS have been plotted in Figure 3 at different temperatures.

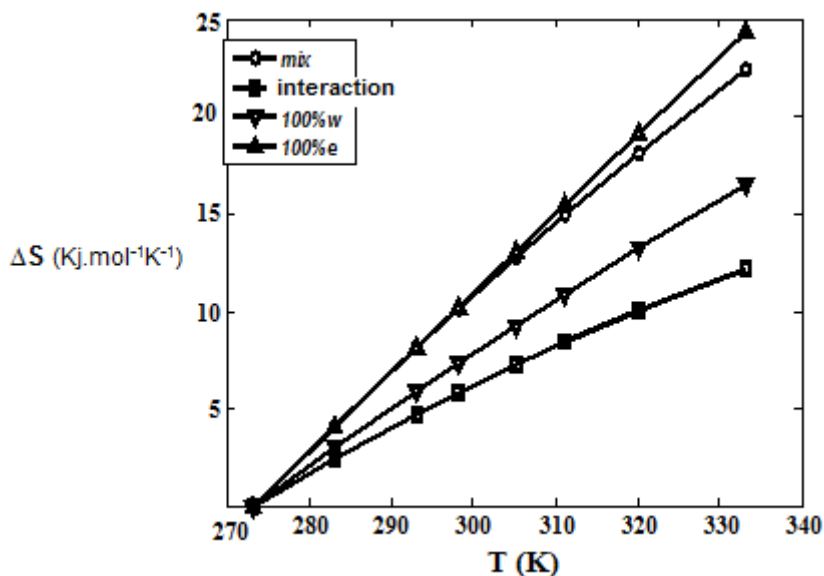


Figure 3. The entropy changes for interaction of mixture (50% water + 50% ethanol), water/ethanol mixture, pure ethanol, and pure water as a function of temperature.

As it can be seen in Figure 3, the values of ΔS for our studied systems obey from below order:

$$\Delta S_{(\text{pure ethanol})} > \Delta S_{(\text{water/ethanol mixture})} > \Delta S_{(\text{water})} > \Delta S_{(\text{interaction})} \quad (7)$$

The change of Gibbs free energy (ΔG) can be calculated by the following equation:

$$\Delta G = \Delta H - T\Delta S \quad (8)$$

Using Equation 8, for studied systems of this work, the values of ΔG were calculated and listed in Table 3. It is clear that interactions are possible which their values of ΔG are negative. As it can be seen in Table 3, for interaction of mixture (50% water + 50% ethanol) in this study, the value of ΔG are negative at 298.15 K, 311.15 K, 320.15 K, and 333.15 K. Therefore, this interaction will be possible only at 298.15 K, 311.15 K, 320.15 K, and 333.15 K.

Table 3. The values of change of Gibbs free energies for water/ethanol mixture, interaction of mixture (50% water + 50% ethanol), pure ethanol, and pure water at different temperatures (T = 273.15 K to 333.15 K).

ΔG (Kj.mol ⁻¹ .K ⁻¹)							
273.15 K	283.15 K	293.15 K	298.15 K	305.15 K	311.15 K	320.15 K	333.15 K
water/ethanol mixture							
0	186.313	221.247	-236.046	26.612	-156.849	-567.664	-489.658
interaction of mixture (50% water + 50% ethanol)							
0	175.970	227.397	-106.624	89.993	-53.814	-388.734	-176.397
pure ethanol							
0	-8.626	-72.928	-1140.167	-206.325	-292.195	-450.177	-742.278
pure water							
0	-3.979	-49.352	-84.635	-146.406	-210.192	-320.478	-503.548

Figure 4 displays self-diffusion coefficients (D) for pure ethanol, pure water and mixture as a function of temperature. Figure 5 shows the mutual diffusion coefficients (D_{ew}) for mixture (water + ethanol) at various temperatures. Figure 4 shows that by increasing temperature, the self-diffusion coefficient increases. In addition, self-diffusion coefficient for the pure water and water-ethanol mixture are maximum and minimum, respectively. The force of bond between atoms in water-ethanol mixture is stronger than that of in the pure ethanol and pure water. All these explanations show that the value of self-diffusion coefficients has inverse relationship with the force of bond between atoms in a mixture.

On the other hand, Figure 5 shows that for mixture (water + ethanol), the values of mutual diffusion coefficients (D_{ew}) increase by temperature growth.

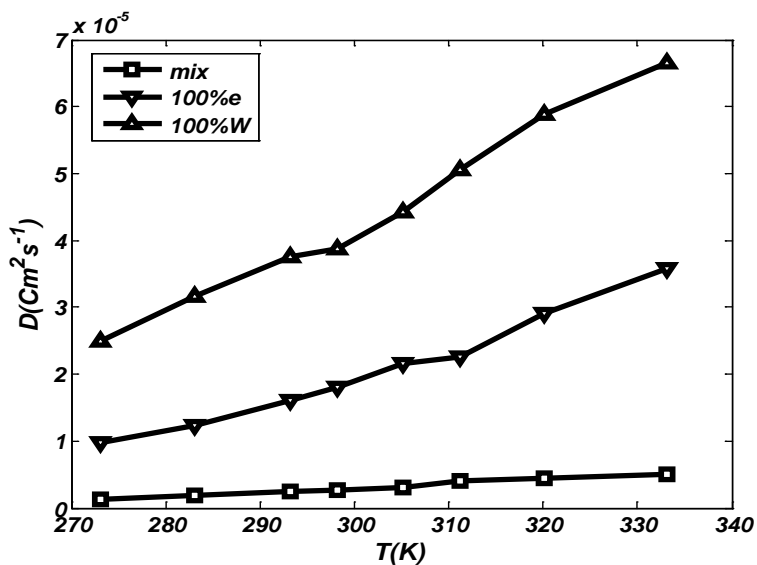


Figure 4. Self-diffusion coefficients of water/ethanol mixture, pure ethanol, and pure water as a function of temperature.

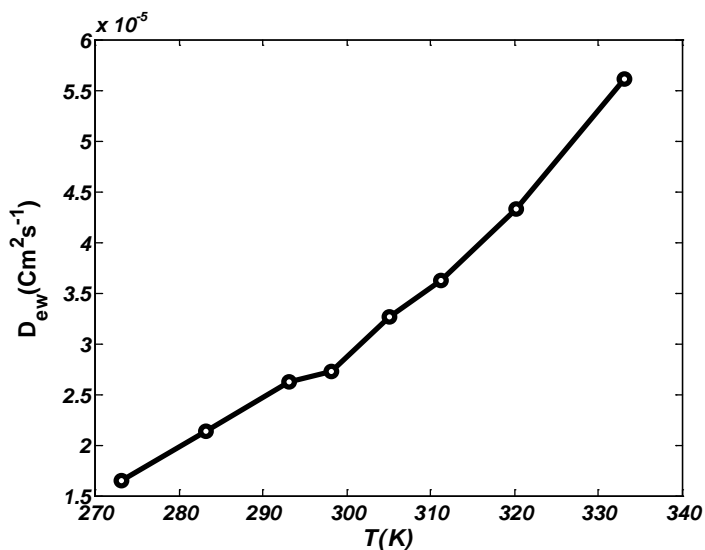


Figure 5. The mutual diffusion coefficients (D_{ew}) for water-ethanol mixture (D_{ew}) as a function of temperature.

In Figures 6, 7, and 8 the radial distribution functions (RDF) between various atoms in ethanol-water mixture, pure ethanol, and pure water have been plotted at $T = (273.15 \text{ and } 333.15) \text{ K}$. These data can be used to study the local structure in the mixture

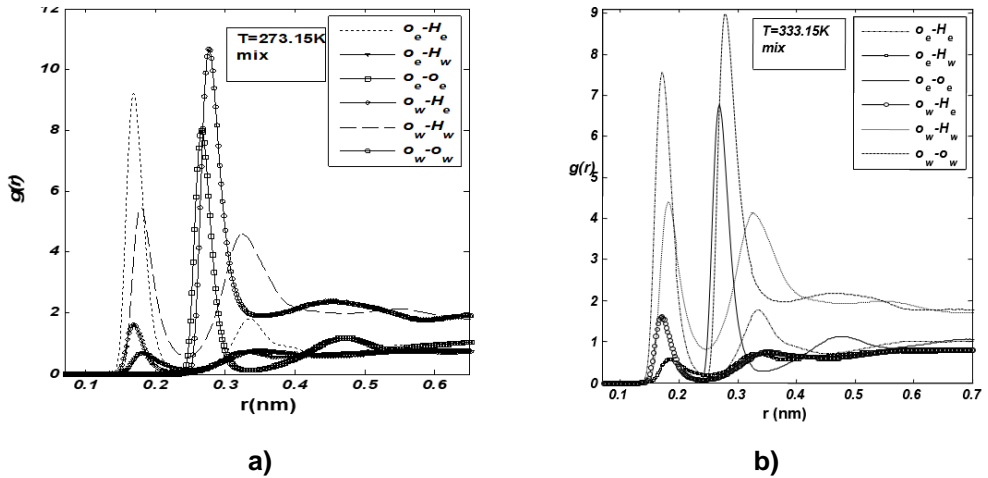


Figure 6. Various partial radial distribution functions for ethanol-water mixture at $T = 273.15 \text{ K}$ (a) and $T = 333.15 \text{ K}$ (b).

Figures 6, 7, and 8 show that the interaction between atoms decreases with temperature increasing. It is well known that by temperature increasing, atoms move faster and force of interactions between them decreases.

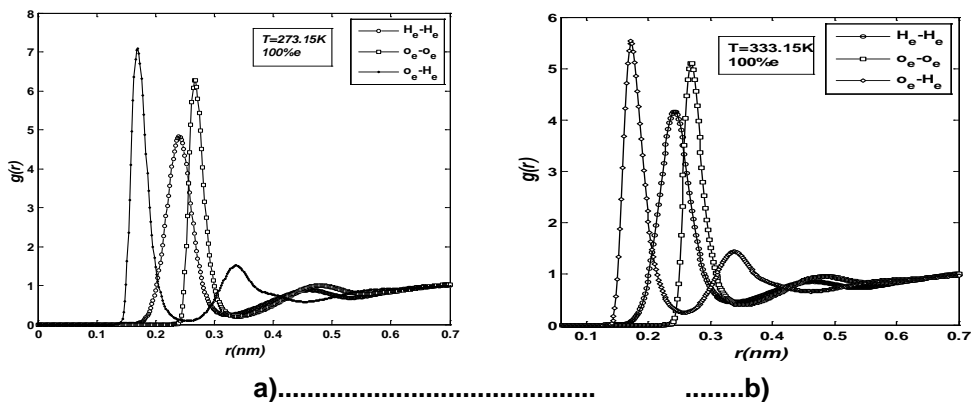


Figure 7. Various partial radial distribution functions for pure ethanol at $T = 273.15 \text{ K}$ (a) and $T = 333.15 \text{ K}$ (b).

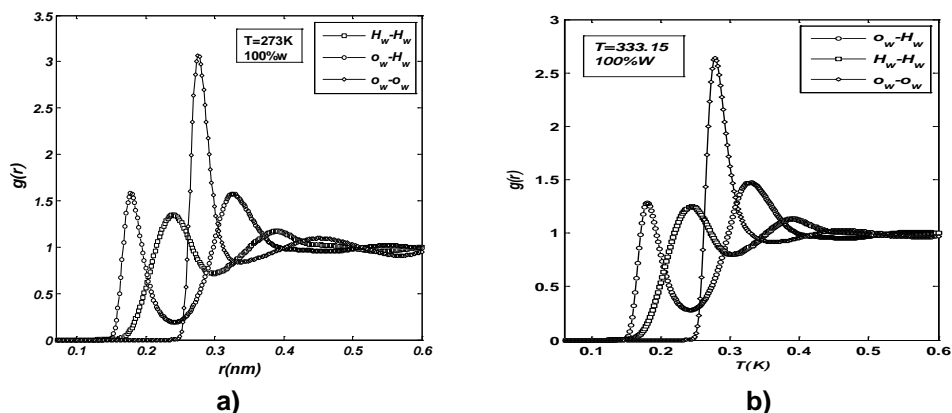


Figure 8. Various partial radial distribution functions for pure water at $T = 273.15$ K (a) and $T = 333.15$ K (b).

CONCLUSIONS

In this work, we calculated the thermodynamic properties (change of enthalpy, ΔH , change of entropy, ΔS , change of heat capacity, ΔC_p , and change of Gibbs free energy, ΔG) for pure water, pure ethanol, water/ethanol mixture, and interaction of mixture (50% water + 50% ethanol) under thermal equilibrium condition at $T = (273.15, 283.15, 293.15, 298.15, 305.15, 311.15, 320.15, 333.15)$ K and at atmospheric pressure. This theoretical calculation was done using Molecular Dynamic (MD) simulation. Results show that the enthalpy changes and entropy changes for ethanol/water mixture, interaction of mixture (50% water + 50% ethanol), the pure ethanol and pure water increases by temperature growth. Also, for mixture of ethanol/water and interaction of mixture (50% water + 50% ethanol), the changes of specific heat decrease by temperature increasing. In addition, the value of Gibbs free energy for interaction of mixture (50% water + 50% ethanol) at different temperatures show that this interaction can occur at $T = (298.15, 311.15, 320.15, 333.15)$ K.

REFERENCES

1. JC. Meyer, S. Kurasch, HJ. Park, V. Skakalova, D. Künzel, A. Groß, A. Chuvilin, G. Algara-Siller, S. Roth, T. Iwasaki, U. Starke, JH. Smet, U. Kaiser, *Nature Materials*, **2011**, 10, 209.
2. Y. Maréchal, *Journal of Molecular Structure*, **2011**, 1004, 146.
3. E. Yamamoto, T. Akimoto, M. Yasui, K. Yasuoka, *Scientific Reports*, **2014**, 4, 4720.

4. S. Le Caër, *Water*, **2011**, 3, 235.
5. S. Jamil, S. Rauf Khan, MRS. Ashraf Janjua, *Journal of the Chinese Chemical Society*, **2018**, 1-9.
6. H. Mevadaa, D. Patel, *Procedia Engineering*, **2016**, 144, 110.
7. JS. Alakali, SO. Eze, MO. Ngadi, 2nd International Conference on Environment, Energy and Biotechnology IPCBEE, IACSIT Press, Singapore, **2013**, 51, 149, doi:10.7763/IPCBEE.2013.V51.28.
8. T. Makarewicz, R. Kaźmierkiewicz, *Journal of Chemical Information and Modeling*, **2013**, 53, 1229.
9. H. Dong, F. Zonta, S. Wang, K. Song, X. He, M. He, Y. Nie, S. Li, *International Journal of Molecular Sciences*, **2018**, 19, 60.
10. Y. Zhang, Y. Ding, *BMC Bioinformatics*, **2016**, 17, 28.
11. JA. Lemkul, WJ. Allen, DR. Bevan, *Journal of Chemical Information and Modeling*, **2010**, 50, 2221.
12. A. Elengoe, MA. Naser, S. Hamdan, *International journal of molecular Science*, **2014**, 15, 6797.
13. M. Lundborg, E. Lindahl, *Journal of Physical Chemistry*, **2015**, 22, 810.
14. TT. Nguyen, MH. Viet, MS. Li, *The Scientific World Journal*, vol. 2014, Article ID 536084, 14 pages, **2014**, doi.org/10.1155/2014/536084.
15. SMJ. Rogge, L. Vanduyfhuys, A. Ghysels, M. Waroquier, T. Verstraelen, G. Maurin, V. Van Speybroeck, *Journal of Chemical Theory and Computation*, **2015**, 11, 5583.
16. M. Fernandez-Pendas, B. Escribano, T. Radivojević, E. Akhmatskaya, *Journal of Molecular Modeling*, **2014**, 20, 2487.
17. RC. Walker, MF. Crowley, DA Case. *Journal of Computational Chemistry*, **2008**, 29, 1019.
18. P. Johansson, A. Carlson, B. Hess, *Journal of Fluid Mechanics*, **2015**, 781, 695.
19. PS. Krstic, L. Han, S. Irle, H. Nakai, *Chemical Science*, **2018**, 9, 3803.
20. J. Yeow, KW. Tan, DA. Holdbrook, ZS. Chong, JK. Marzinek, PJ. Bond, SS. Chng, *Journal of Biological Chemistry*, **2018**, ASAP, doi: 10.1074/jbc.RA118.002441.
21. S. Toxvaerd, OJ. Heilmann, JC. Dyre, *The Journal of Chemical Physics*, **2012**, 136, 224106.
22. MP. Gajula, A. Kumar, J. Ijaq, Protocol for Molecular Dynamics Simulations of Proteins. Bio-protocol, **2016**, 6: e2051, doi: 10.21769/BioProtoc.2051.
23. D. Yu, X. Ma, Y. Tu, L. Lai, *Scientific Reports*, **2015**, 5, Article number: 8640.
24. F. Vitalini, F. Noé, BG. Keller, *Data in Brief*, **2016**, 7, 582.
25. D. van der Spoel, AR. van Buuren, MEF. Apol, PJ. Meulenhoff, DP. Tieleman, ALTM. Sijbers, B. Hess, KA. Feenstra, E. Lindahl, R. van Drunen, HJC. Berendsen, GROMACS User Manual version 3.3, Department of Biophysical Chemistry, University of Groningen, The Netherlands, **2001**.
26. F. Koohyar, AA. Rostami, MJ. Chaichi, F. Kiani, *Journal of Solution Chemistry*, **2011**, 40, 1361.

EFFECT OF MICROWAVE HEATING ON QUALITY AND FATTY ACIDS COMPOSITION OF VEGETABLE OILS

FLAVIA POP^{a, *}

ABSTRACT. The research was conducted in order to evaluate the microwave effect on fatty acids profile and quality parameters of safflower and rapeseed oils. To simulate conventional times used in microwave domestic cooking, different exposure times were tested: 1, 3, and 5, respectively. After 5 minutes of microwave exposure, the peroxide index showed a significant increase for both types of oil ($P \leq 0.05$). Rapeseed fatty acids profile was rich in oleic (C18:1), vaccenic (C18:1*n*-7), linoleic (C18:2), palmitic (C16:0) and linolenic (C18:3) fatty acids, followed by miristic (C17:0) and stearic (C18:0) acids. Microwave heating inflicted changes in fatty acids profile of both oils, the most affected fraction was the polyunsaturated fatty acids, directly related with their higher number of double bonds, with higher susceptibility to oxidation. Microwave heating exerted more aggressive effects on safflower oil, and rapeseed oil can be exposed for 5 minutes without negative effects.

Keywords: *fatty acids profile, microwave heating, peroxide index, iodine index*

INTRODUCTION

Vegetable oils and fats are found in nature in plant tissue, concentrated in seeds, pulp, fruit, tubers, or germs. They are rich in monounsaturated and polyunsaturated fatty acids and contain a low amount of saturated fat [1].

Fat products are an important source of energy and are indispensable to life. Fatty acids participate in the regulation of cholesterol metabolism and are the precursors of some hormones involved in wound healing, reducing of inflammation and blood clotting. Food containing low amounts of saturated fatty acids and high linoleic acid is recommended for the prevention of coronary and heart disease. Fats rich in linoleic acid are the best natural sources of E vitamin [2].

^a *Technical University of Cluj-Napoca, North University Center of Baia Mare, Chemistry and Biology Department, 76A Victoriei Str., 430122, Baia Mare, Romania.*

* *Corresponding author: flavia_maries@yahoo.com*

Safflower oil has a neutral flavor that combines well with many dishes and is a rich source of unsaturated fatty acids. Daily doses of safflower oil can help to improve blood sugar, blood cholesterol, and the level of inflammation in people with diabetes. Rapeseed oil is effective in treating mild burns, abscesses, furuncles, wounds and varicose ulcers [3].

Some of the major changes that occur during processing and final preparation of heated food are due to oxidation. Polyunsaturated fatty acids autooxidation is catalysed by heat, light, trace metals or enzymes and involves free radical generation. Oxidative rancidity consists in the formation of free radicals and hydroperoxides, the transformation of unstable hydroperoxides in stable peroxides, and finally, the split into aldehydes and acids with characteristic odor [4, 5]. It involves the oxidation of unsaturated fatty acids and generates compounds that affect food quality by altering of color, texture, nutritional value and food safety (Fig. 1).

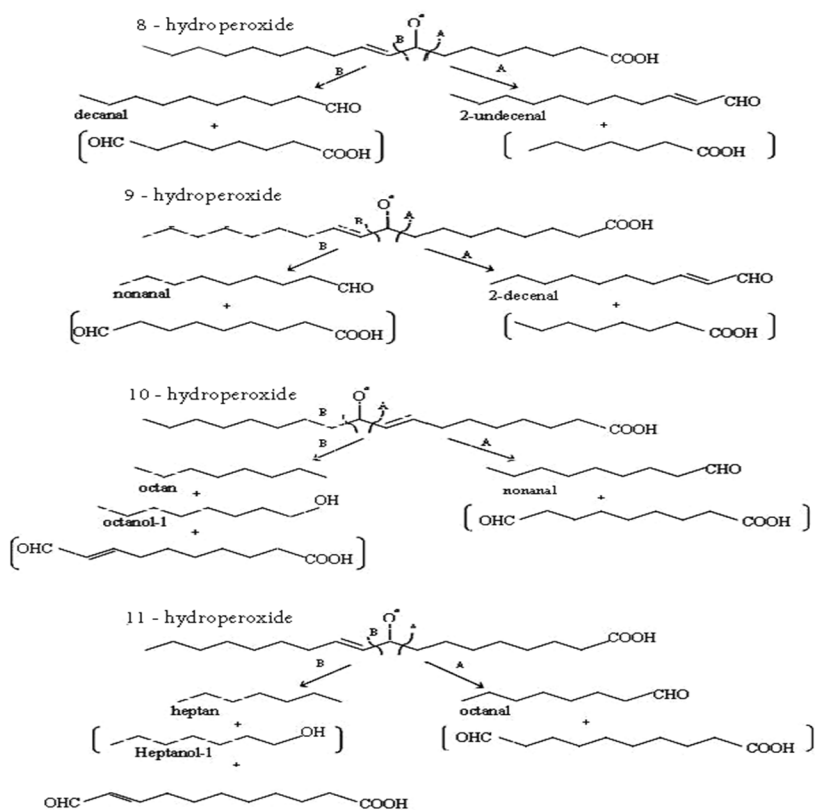


Figure 1. Breakdown of hydroperoxides from oleic acid [4]

Several studies report quality degradation of vegetable oils during microwave heating, fatty acids degradation, reduction in bioactive compounds and properties, pigments destruction, sensorial changes, and color modifications, as well as physical and rheological changes [6-10]. Comparatively to a conventional oven heating, microwave heating induces higher and faster oils deterioration [11, 12].

The objective of the study consisted in analysis the effect of microwave assisted heating on the quality and fatty acids profile of safflower and rapeseed oils subjected to heat treatment for 1, 3 and 5 minutes.

RESULTS AND DISCUSSION

Peroxide value, iodine value, refractive index value, acid value, moisture content and fatty acids profile were determined in order to asses the effect of microwave heating on safflower and rapeseed oils quality.

Free acidity represents an analytical parameter which is used to evaluate the hydrolysis extension in vegetable oils during thermal process. An increase in this parameter indicates a higher presence of free fatty acids in the vegetable oil, a direct consequence of hydrolysis, and it is an important indicator of oil chemical deterioration [13].

Safflower oil presented a lower content of free fatty acids compared to rapeseed oil. With the increase in microwave exposure, the two types of oil showed a different response. Safflower oil showed a significant increase in free acidity after 1 minute of heating compared to untreated oil ($P < 0.01$). Following 3 and 5 minutes of exposure to microwaves, the free fatty acids content increased steadily and continuously with heating time. The acidity of rapeseed oil was not significantly influenced by the increase in microwave exposure time ($P > 0.05$).

Borges et al., reported that soybean oil was not affected by the increasing exposition time, even at 15 minutes, while in baru oil, a significant increase of free fatty acids was recorded after 1 minute of heating, comparatively with unheated oils [14].

Peroxide value is a measure of primary lipid oxidation, indicating the amount of peroxides formed during oil oxidation. The products of lipid oxidation such as peroxides, free radicals, malonaldehyde and other cholesterol oxidation products are reported to promote coronary heart disease and atherosclerosis [5].

Untreated microwave oils showed lower values of the peroxide index. After 5 minutes of microwave exposure, the peroxide index showed a significant increase for both types of oil ($P \leq 0.05$). After 5 minutes of exposure to microwaves,

the amount of peroxides increased 2.1 times for safflower oil and 1.8 times for rapeseed oil. The results showed that safflower oil was more unstable to heating exposure, producing higher amounts of peroxides (Table 1). With higher heating periods, both oils become oxidized, with a higher degradation of polyunsaturated fatty acids and formation of oxidation compounds.

Table 1. Effect of microwave heating on quality parameters of vegetable oil

	t _{0min}	t _{1min}	t _{3min}	t _{5min}
Acid value (g oleic acid/100 g)				
Safflower oil	0.22 ± 0.02	0.41 ^b ± 0.04	0.44 ^{bc} ± 0.01	0.48 ^c ± 0.03
Rapeseed oil	0.38 ± 0.01	0.35 ^{ab} ± 0.02	0.37 ^b ± 0.05	0.40 ^{bc} ± 0.05
Peroxide value (mec O ₂ /kg)				
Safflower oil	3.8 ± 0.03	4.6 ^{bc} ± 0.06	5.9 ^c ± 0.02	8.1 ^d ± 0.01
Rapeseed oil	2.7 ± 0.01	3.5 ^b ± 0.04	3.1 ^b ± 0.05	4.9 ^c ± 0.02
Iodine value (g I ₂ /100 g)				
Safflower oil	83.1 ± 0.3	82.3 ^{ab} ± 0.4	80.2 ^b ± 0.5	76.5 ^c ± 0.1
Rapeseed oil	79.8 ± 0.2	78.9 ^{ab} ± 0.1	77.2 ^b ± 0.2	74.8 ^{bc} ± 0.3
Refractive index (refractometric degrees)				
Safflower oil	1.473 ± 0.01	1.470 ^{ab} ± 0.05	1.466 ^b ± 0.06	1.463 ^{bc} ± 0.04
Rapeseed oil	1.469 ± 0.04	1.467 ^a ± 0.07	1.464 ^{ab} ± 0.03	1.460 ^b ± 0.02
Moisture content (%)				
Safflower oil	0.723 ± 0.004	0.711 ^a ± 0.007	0.698 ^b ± 0.006	0.693 ^{bc} ± 0.003
Rapeseed oil	0.513 ± 0.008	0.504 ^a ± 0.005	0.498 ^{ab} ± 0.002	0.490 ^b ± 0.007

Values are means of triplicates ± standard deviation. Values with the same superscript in a column are not significantly different ($P > 0.05$).

Several authors have reported an increase in PV of oils during heating or frying [15-18]. Kreps et al., investigated the influence of microwave heating on sunflower and corn oil in two types of microwave oven. Oils were heated at progressively longer periods of 2, 4, 6, 8, and 10 minutes to reach approximately temperatures of 98, 121, 138, 149, and 158°C. The authors found that after a 6 minutes of microwave heating the content of hydroperoxides and conjugated dienes in oils grew significantly. The study showed that corn oil resisted much better to the deleterious effects of microwave heating, due to the 2.5 times higher content of tocopherols over sunflower oil. The researchers also observed that the effect of microwave radiation on oxidation stability and content of minor constituents in oils depended not on the magnetron output alone, but of more significance appeared to be the duration of magnetron pause, interrupting the microwave heating in order to allow for heat dissipation [19].

Refractive index value and iodine value are measures of the degree of unsaturation of fatty acids. Safflower oil presented a higher value of refractive index compared to rapeseed oil and the values decreased significant ($P \leq 0.05$) with the increase in microwave exposure time.

Iodine index values also decreased with the increase in microwave exposure time, as a result of the reduction in the degree of unsaturation, by the split of unsaturated fatty acids double bonds. Between the iodine index and the refractive index values, there was found a direct correlation.

Fatty acids represent the main constituents of the saponifiable fraction of vegetable oils, the fatty acids profile at $t_{0\min}$ and $t_{5\min}$ is reported for both oils.

Safflower oil fatty acids profile was dominant in oleic acid (C18:1), with levels exceeding 31%, followed by arachidonic acid (C20:4) with near 19%, eicosenoic acid (C20:1) with 11%, and palmitic acid (C16:0) containing approximately 9.2% (Fig. 2). The linoleic (C18:2) and linolenic acid (C18:3) amounts were also important (7.3 respectively 6.8%).

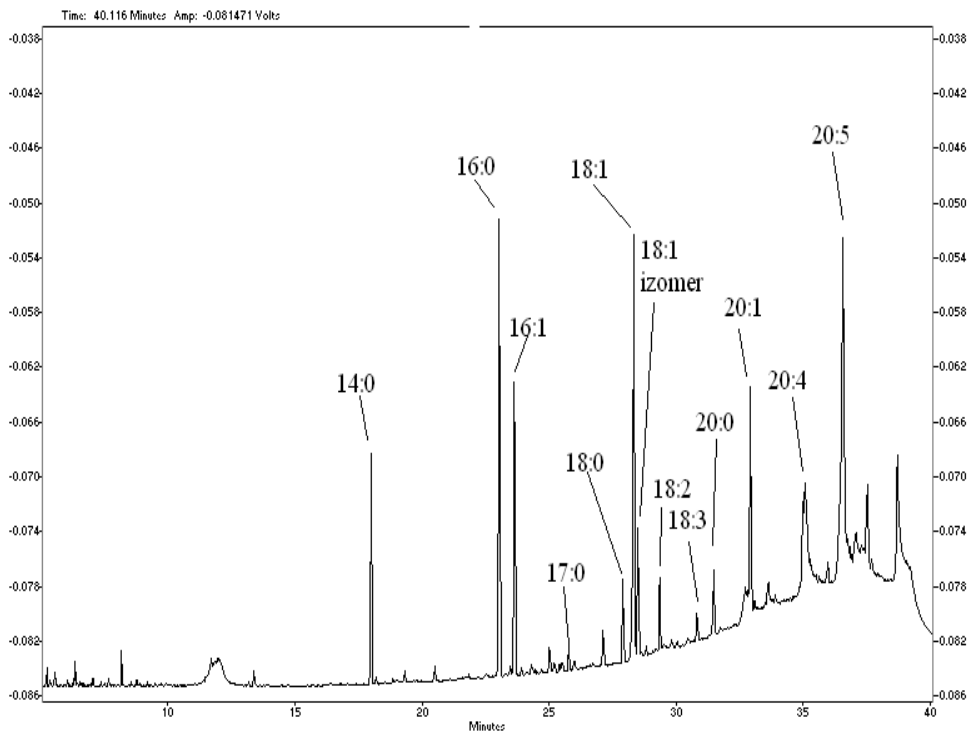


Figure 2. Gas chromatogram of unheated safflower oil

Rapeseed fatty acids profile was rich in olei (C18:1), vaccenic (C18:1_i), linoleic (C18:2), palmitic (C16:0) and linolenic (C18:3) fatty acids, followed by miristic (C17:0) and stearic (C18:0) acids (Fig. 4). Safflower oil was predominantly polyunsaturated, while rapeseed oil was mainly monounsaturated.

Microwave heating inflicted changes in fatty acids profile of both oils. Analyzing the fatty acids by their common nature, the most affected fraction was the polyunsaturated fatty acids (PUFA), directly related with their higher number of double bonds, with higher susceptibility to oxidation (Fig. 3, Fig. 5). With $t_{5\text{min}}$ of heating, PUFA content decreased around 10% in both oils.

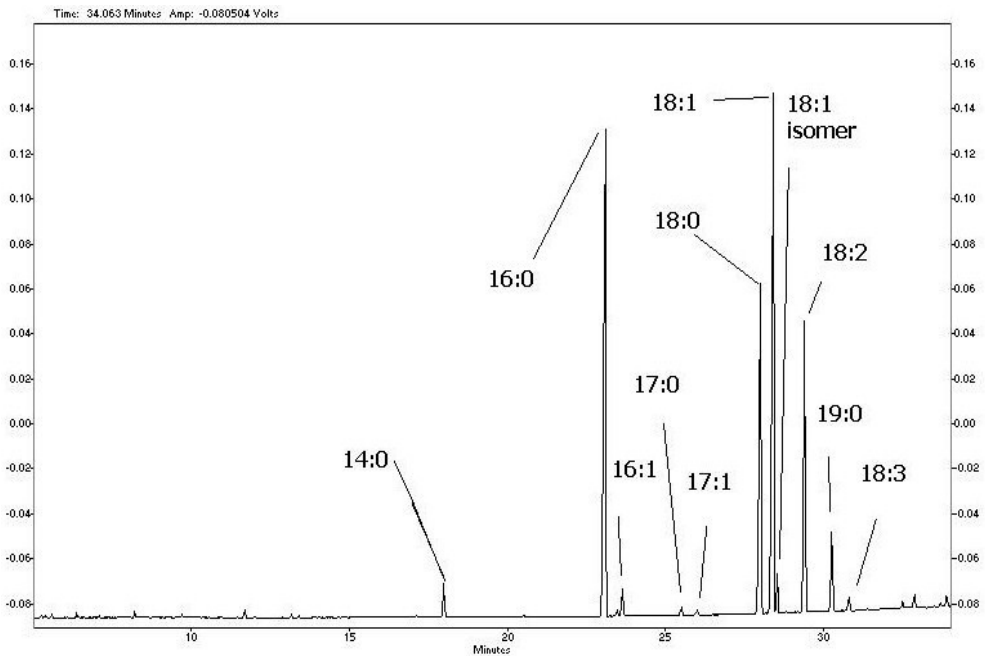


Figure 3. Gas chromatogram of safflower oil after 5 minutes of microwave heating

Kreps et al., studied the influence of microwave heating on fatty acids composition in different types of microwave oven. The researchers observed that after 10 minutes of microwave heating vegetable oils contained less than 50% original content of linolenic acid, and further heating led to complete degradation of linolenic acid in oils. Linoleic acid in microwave-heated corn oil was less degraded than in sunflower oil [19].

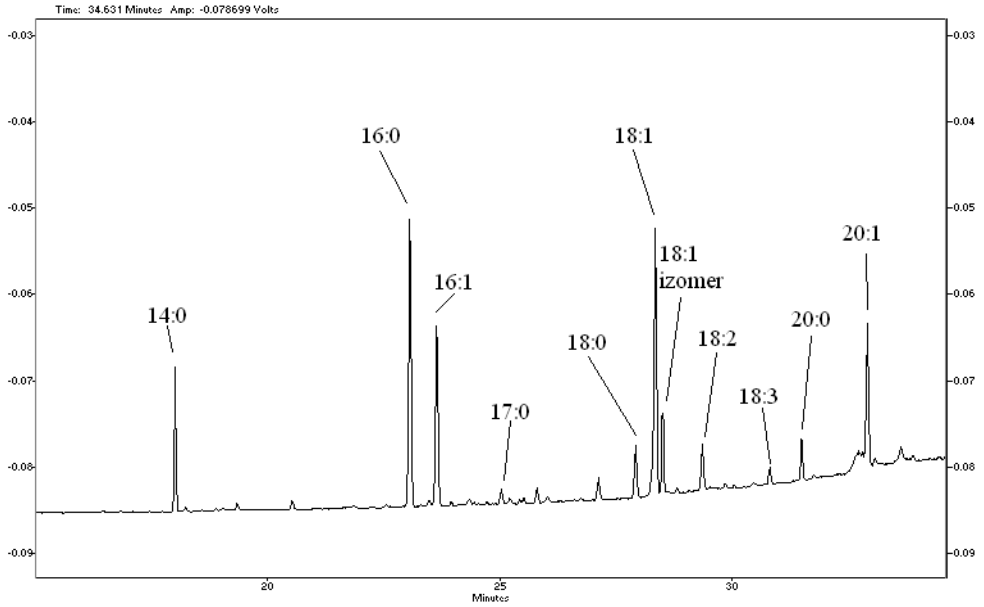


Figure 4. Gas chromatogram of unheated rapeseed oil

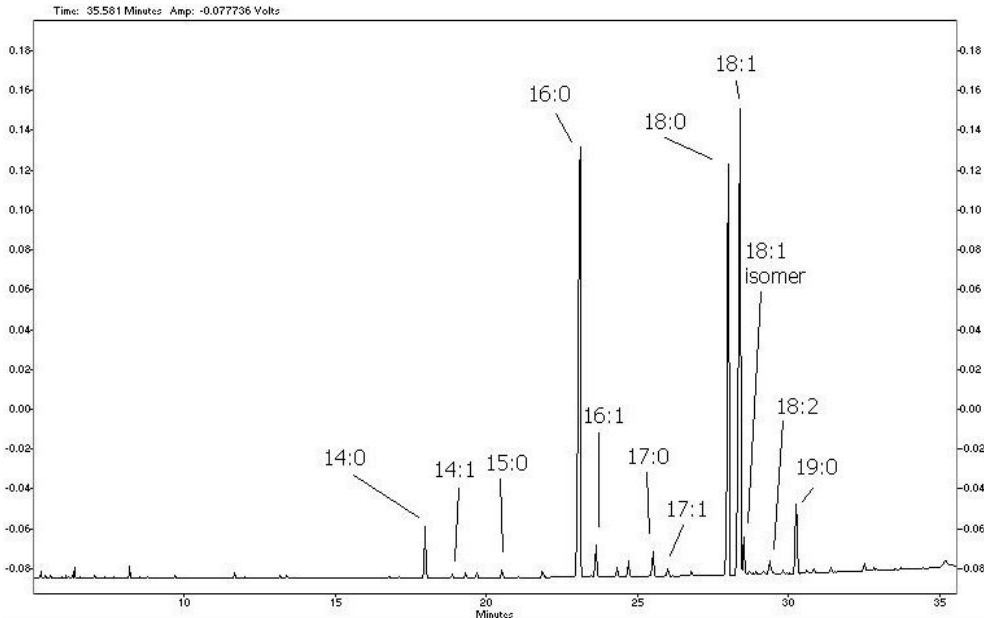


Figure 5. Gas chromatogram of rapeseed oil after 5 minutes of microwave heating

CONCLUSIONS

Safflower oil showed a significant increase in free acidity after 1 minute of microwave exposure. For safflower oil, there was observed a strong correlation between acidity and exposure to heat treatment, and for rapeseed oil no correlation was observed. During heat treatment no significant changes in peroxide index values were observed for exposure up to 3 minutes for both types of oil. Safflower oil was more unstable at heat treatment, producing higher amounts of hydroperoxides.

Microwave heating inflicted changes in fatty acids profile of both oils, the most affected fraction was the polyunsaturated fatty acids, directly related with their higher number of double bonds, with higher susceptibility to oxidation.

Microwave heating exerted more aggressive effects on safflower oil, and rapeseed oil can be exposed for 5 minutes without negative effects. Based on the results obtained in this work, we can state that safflower oil is very unstable when subjected to microwave heating and we recommend the use of this oil with minimal thermal processing in order to maintain its stability.

EXPERIMENTAL SECTION

Samples

To assess the behavior of safflower and rapeseed oils under microwave heating conditions, commercial samples were obtained from local markets. To simulate conventional times used in microwave domestic cooking, different exposure times were tested: 1, 3, and 5, respectively. Within each studied oil, one sample was used as control sample (unheated - t_{0min}). Approximately 50 g of oil were individually heated in Petri dishes in a domestic microwave oven at maximum power (900 W). The cold samples were transferred to glass tubes and kept under refrigeration until analysis. Three replications were carried out to examine each sample.

Physicochemical examination

Peroxide value was determined using UV-VIS spectrophotometer. Thiocyanate ions (SCN^-) react with Fe^{3+} ions to give a red-violet chromogen that can be determined spectrophotometrically, the absorbance of each solution was read at 500 nm. To quantify PV, a calibration curve (absorbance at 500 nm vs. Fe^{3+} expressed in μg) was constructed and peroxide value was expressed as meq O_2/kg sample. Iodine value was determined using Hanus method, was calculated as $g I_2/100 g$ sample [20].

To determine the refractive index we used the PAL-RI (Tokyo, Japan) with the following technical characteristics: field: 1,3306-1,5284; resolution: 0.0001; accuracy: ± 0.0003 ; measuring temperature: 5-45°C (resolution 1°C); measuring time: 3s; in accordance with the requirements of EMC Directive 93/68/EEC. Acid value determination consists in neutralizing acidity with sodium hydroxide 0.1 N, using phenolphthaleine, as an indicator. Acidity was expressed as oleic acid grams to 100 grams sample [20].

Fatty acids composition was determined using a Shimadzu GC-17 A gas chromatograph (Tokyo, Japan) coupled with a flame ionization detector. The gas chromatography column is Alltech AT-Wax, (60 m x 0.32 mm x 0.5 μm), stationary phase (polyethylene); helium was used as a carrier gas at a pressure of 147 kPa, temperature of the injector and detector was set to 260°C, and the oven program was the following: 70°C for 2 minutes, then the temperature was raised to 150°C with a gradient of 10°C/minute, a level of 3 minutes, and the temperature was raised to 235°C with a gradient of 4°C/minute. Identification and quantification of FA were performed by comparison with standards. Results were expressed as g/100 g fat [21].

Statistical analysis

All analytical determinations were performed at least in triplicate. Values of different parameters were expressed as the mean \pm standard deviation ($X \pm SD$). Significant differences between mean were determined by using "Student" ("t") distribution.

REFERENCES

1. B. Sultana, F. Anwar, R. Przybylski, *Food Chemistry*, **2007**, *104*, 997.
2. C.A. Costa, A.S. Carlos, G.P. Gonzalez, R.P. Reis, *European Journal of Nutrition*, **2012**, *51*, 191.
3. S. Wang, K.A. Meckling, M.F. Marcone, Y. Kakuda, R. Tsao, *Journal of Agricultural and Food Chemistry*, **2011**, *59*, 960.
4. E. Choe, D.B. Min, *Comprehensive Reviews in Food Science and Food Safety*, **2006**, *5*, 169.
5. O. Roman, B. Heyd, B. Broyart, R. Castillo, M. N. Maillard, *LWT - Food Science and Technology*, **2013**, *52*, 49.
6. B. Roszkowska, M. Tanska, S. Czapliski, I. Konopka, *European Journal of Lipid Science and Technology*, **2015**, *117*, 673.
7. S. Azadmard-Damirchi, F. Habibi-Nodeh, J. Hesari, M. Nemati, B.F. Achachloei, *Food Chemistry*, **2010**, *121*, 1211.

8. M. Wroniak, K. Krygier, M. Kaczmarczyk, *Polish Journal of Food and Nutrition Sciences*, **2008**, 58, 85.
9. A. Biswas, A. Adhvaryu, D.G. Stevenson, B.K. Sharma, *Industrial Crops and Products*, **2007**, 25, 1.
10. A. Bendini, E. Valli, L. Cerretani, E. Chiavaro, G. Lercker, *Journal of Agricultural and Food Chemistry*, **2009**, 57, 1055.
11. F. Caponio, A. Pasqualone, T. Gomes, *European Food Research and Technology*, **2002**, 215, 114.
12. R.M. El-Abassy, P. Donfack, A. Materny, *Food Research International*, **2010**, 43, 694.
13. N. Rodrigues, R. Malheiro, S. Casal, M.C. Manzanera, *Food and Chemical Toxicology*, **2012**, 50, 2894.
14. T.H. Borges, R. Malheiro, A. Marques de Souza, S. Casal, J.A. Pereira, *European Journal of Lipid Science and Technology*, **2015**, 117, 503.
15. K. Warner, *Journal of Agricultural and Food Chemistry*, **2005**, 23, 9906.
16. H. Yoshida, S. Takagi, *Journal of the Science of Food and Agriculture*, **1999**, 62, 41.
17. F.A. Aladedunye, *European Journal of Lipid Science and Technology*, **2014**, 116, 688.
18. F. Caponio, A. Pasqualone, T. Gomes, *International Journal of Food Science and Technology*, **2003**, 38, 481.
19. F. Kreps, L. Vrbíková, S. Schmidt, S. Sekretár, O. Híreš, *European Journal of Lipid Science and Technology*, **2014**, 116, 1685.
20. F. Pop, L. Mihalescu, *International Journal of Food Properties*, **2017**, 20, 1085.
21. F. Pop, L. Giurgiulescu, A. Dumuța, Z. Voșgan, *Studia Universitatis Babeș-Bolyai Chemia*, **2013**, 58, 31.

THE INFLUENCE OF TEMPERATURE AND DOLOMITE ADDITION ON THE DRYING KINETICS OF SUGAR BEET PULP (BETA VULGARIS L.)

ADINA GHIRIŞAN^a, SIMION DRĂGAN^{a*}, CONSTANTIN COŢA^b,
NICOLAE CIOICA^b, ELENA-MIHAELA NAGY^b, VASILE MICLEAŞ^a

Abstract. The aim of this study is to investigate the hot air drying kinetics of sugar beet pulp, without and with dolomite addition, in order to establish the drying mechanism. The influence of temperature and dolomite addition on the drying rates is observed. The drying constant rates and the activation energies for different working conditions are determined. The obtained results show that the drying took place in falling rate period. The obtained activation energy values correspond to the mechanism mass transfer at low amount of dolomite addition and combined mechanism, mass transformation (evaporation process) – mass transfer, at higher amount.

Keywords: *sugar beet pulp, hot air drying, dolomite, constant rate, activation energy*

INTRODUCTION

Sugar beet processing operations comprise several steps, including extraction of sucrose by diffusion, juice purification, evaporation, crystallization, dried-pulp manufacture, and sugar recovery from molasses [1, 2]. The extraction of sucrose by hot water diffusion from the plant "beta vulgaris L." is an important production operation in the sugar industry. The extraction products are: a) the liquid phase containing all water-soluble components called raw juice and b) the solid phase, the wet pulp, containing the insoluble components of the sugar beet.

^a Universitatea Babeş-Bolyai, Facultatea de Chimie și Inginerie Chimică, Str. Kogălniceanu, Nr. 1, RO-400084, Romania

^b Institutul Național de Cercetare - Dezvoltare Pentru Mașini și Instalații Destinate Agriculturii și Industriei Alimentare, Filiala Cluj-Napoca, Str. Al. Vaida-Voievod, Nr. 59, RO-400458, Romania

* Corresponding author: sdragan@chem.ubbcluj.ro

The raw juice proceeds to the juice purification operations in order to obtain sugar. Byproducts of sugar beet processing include the pulp and the molasses. These products may be used separately or combined. They may be dried or otherwise processed in a variety of ways to produce a range of high-quality animal feeds whose nutritional value is close to that of the hay [2, 3].

The sugar-enriched water from the diffusion contains 10 -15 % sugar. The insoluble compounds of the beet, which remain after complete aqueous extraction of the soluble constituents under industrial processing conditions, called "marc", is sent to the dried-pulp manufacture operations. The sugar beet pulp is made of: hemicelluloses (26%), pectin (24%), cellulose (23%), coagulated protein substances (9%), sucrose (6%), lignin (4.5%), soluble mineral matter (4.0%), insoluble mineral matter (3.0%) and fat (0.5%) [4].

Considering the nature of the compounds entering this byproduct, as well as the large amount resulting from diffusion extraction, 350-400 kg/tonne of sugar product, sugar beet pulp is also an important source of raw material for the production of animal food, adhesives based on of pectin glue with properties similar to the Arabic gum or dextrin solutions [2].

The use of sugar beet pulp as animal feed shows two disadvantages: the high volume and high moisture content 80-90% [4]. These lacks lead to high transport costs and limited storage period due to deterioration by fermentation and molding. For conserving sugar beet pulp are used silage and drying [5]. The reduction of moisture content by drying will decrease or inhibit the microbial growth in the storage period.

In addition, the nutritional value of sugar beet pulp can be enhanced by the addition of micro- and macro-minerals and other nutrients, supplements which maintain a good health and increase milk production. Animal feeding practice uses numerous mineral supplements to provide calcium. Limestone (calcium carbonate) is the most widely used [6]. The effects of calcium magnesium carbonate (dolomite) supplementation on performance of cows dairy production and on the diet and metabolism, was already studied [7, 8]. With the addition of dolomite (CaCO_3 , MgCO_3), calcium and magnesium pectinates are formed, and thus Ca^{2+} and Mg^{2+} ions are easily assimilated [2].

The drying kinetics of the sugar beet pulp, without and with dolomite (CaCO_3 – MgCO_3) addition, is carried out in the present study. Different authors investigated hot air drying of sugar beet pulp, but not in the presence of dolomite. The most of them tried to find the proper model to describe or simulate the drying process of sugar beet pulp [9, 10]. In the present research, the influence of temperature and the addition of dolomite on the drying rate was observed and analyzed. Constant rates and activation energies for different working conditions were calculated in order to establish the drying mechanism.

RESULTS AND DISSCUSION

The drying rates (kg/kg.h) obtained as a function of moisture content, are calculated by the relation (1) [11]:

$$D_R = \frac{M_i - M_{i-1}}{\Delta t} \quad (1)$$

where M_i is the moisture content dry basis (kg water/kg dried matter) at the moment t_i .

Figure 1 shows the influence of temperature on the drying rate for two cases: a. without dolomite and b. with 5.0 grams dolomite.

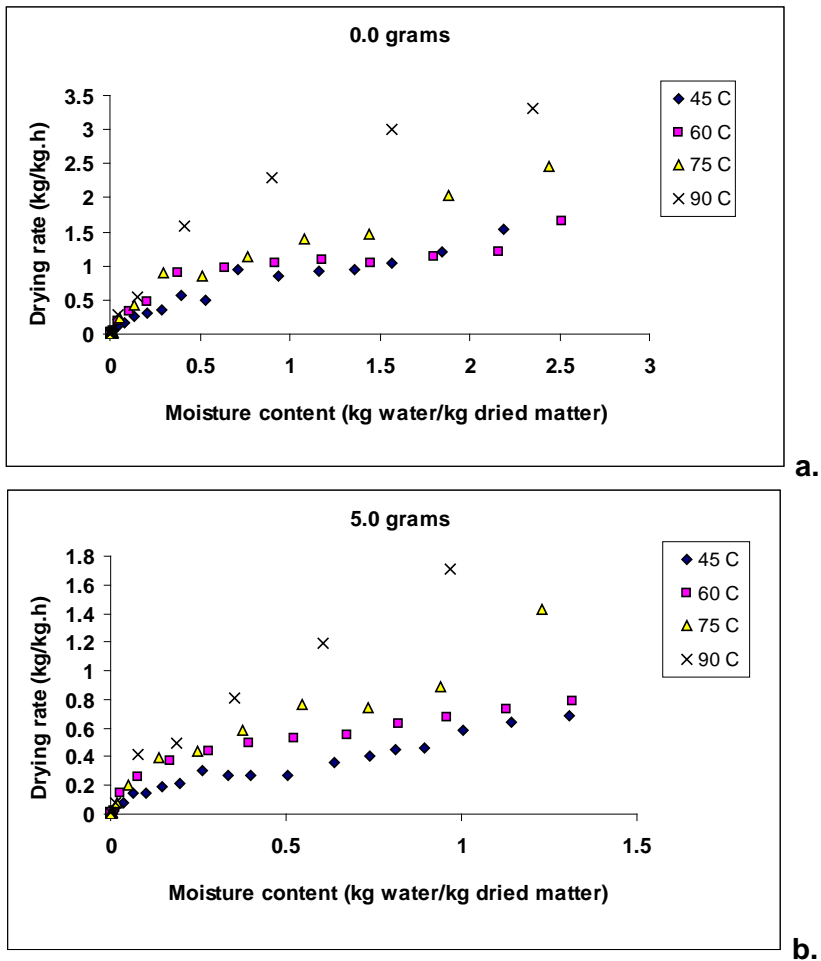


Figure 1. Influence of temperature on drying rates

It can be observed that in both cases dolomite-free sample (Figure 1.a) and dolomite sample (Figure 1.b), the drying rates decrease over the whole range of material moisture content. The continuously decreasing of the drying rate with the moisture content indicates the specific curve of falling rate period [12]. This behavior could indicate that the moisture of the material is bound by different binding energy and/or the moisture transfer within the solid porous material is made by different mechanism [13].

Falling rate period can be observed also when the influence of dolomite addition for the same temperature (e.g., at 75 °C) is followed (Figure 2).

The analysis of the drying curves shows that the temperature has a positive strongly influence on drying rates (Figure 1.a, 1.b) comparative to the dolomite addition which has a negligible influence on drying rates (Figure 2).

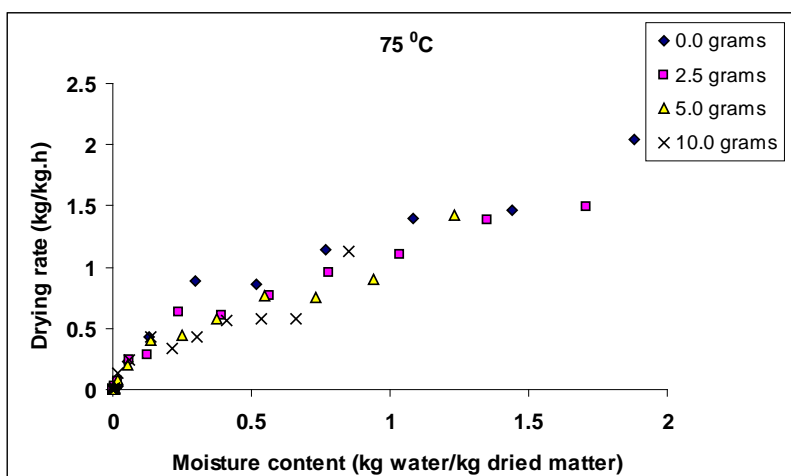


Figure 2. Influence of dolomite addition on drying rates

This behavior is confirmed for all analyzed cases at temperatures lower than 75 °C, by the variation of drying degree, η (Figure 3). Determinations have been made for all working temperatures and for all dolomite additions specified in the experimental section.

It can be observed that at a drying time of 50 minutes, the drying degree value is two times higher at 90 °C than at 45 °C. At 100 minutes drying degree reaches unit value, $\eta=1$, in both cases, with and without dolomite addition.

Experimental data on the drying degree versus time were further used to determine the constant drying rates, k , calculated by next equations [14]:

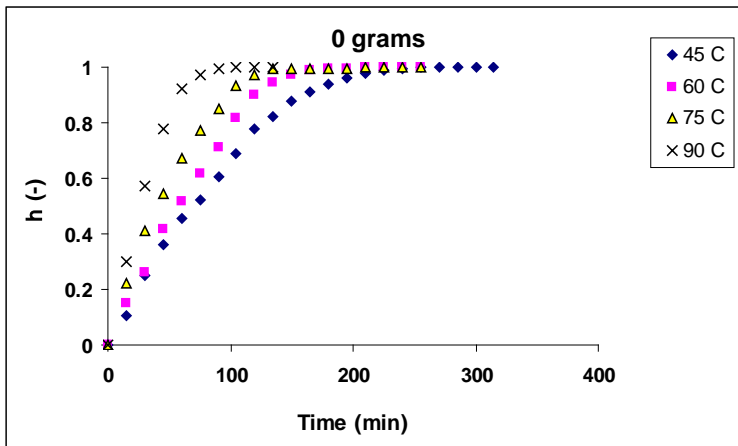
$$-\frac{dM}{dt} = k \cdot M \quad (2)$$

$$M = M_0(1 - \eta) \quad (3)$$

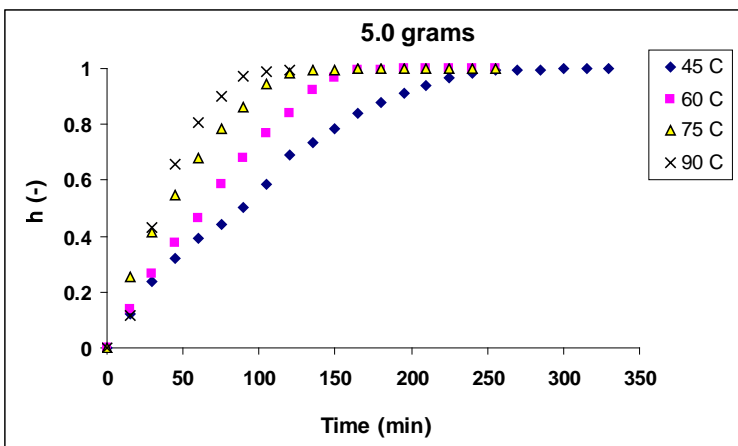
$$-\frac{dM}{M} = k dt \quad (4)$$

The integration of equation (4) at the limitation conditions, leads to the equation:

$$-\ln(1 - \eta) = k \cdot t \quad (5)$$



a.



b.

Figure 3. Influence of temperature and the dolomite addition on drying degree

For two of the analyzed cases, the results are presented in the diagrams in Figure 4.

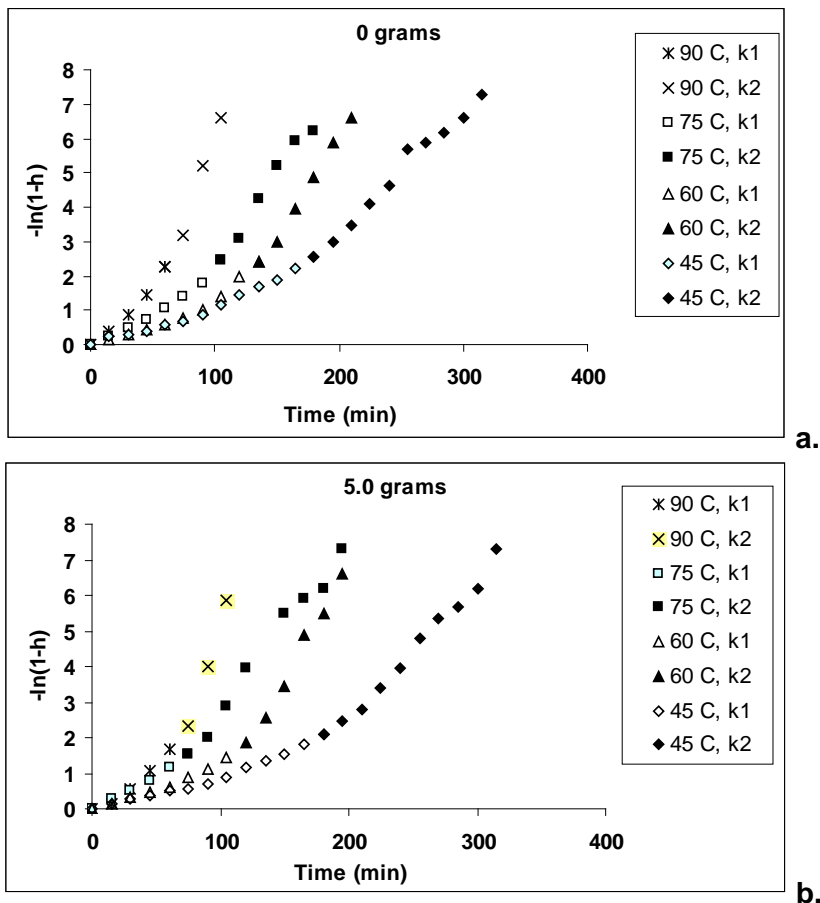


Figure 4. Diagrams $-\ln(1-\eta)$ vs. Time

Diagram analysis (Figure 4) for all working conditions shows that the points are not collinear. Changing the slope suggests the change of drying mechanism. The values of the constant rates determined from the slope of each linear representation $-\ln(1-\eta)$ vs. time, are shown in Table 1.

It can be noted that the values of constant rates decrease with the increase of added dolomite. It is also observed that the values of constant rates for the beginning of drying are smaller than those obtained for the second drying period at each temperature.

The numerical values of the constant drying rates were mathematically processed and plotted in the coordinates of the $\ln k$ vs. $1/T$ (Figure 5).

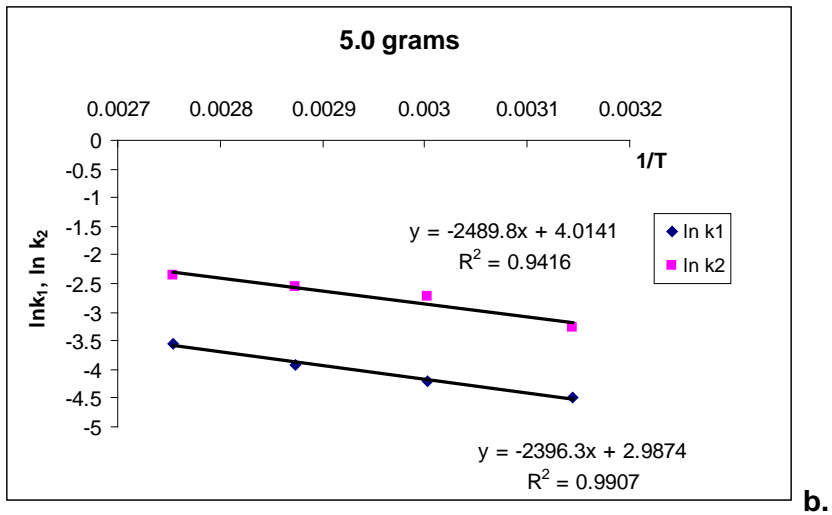
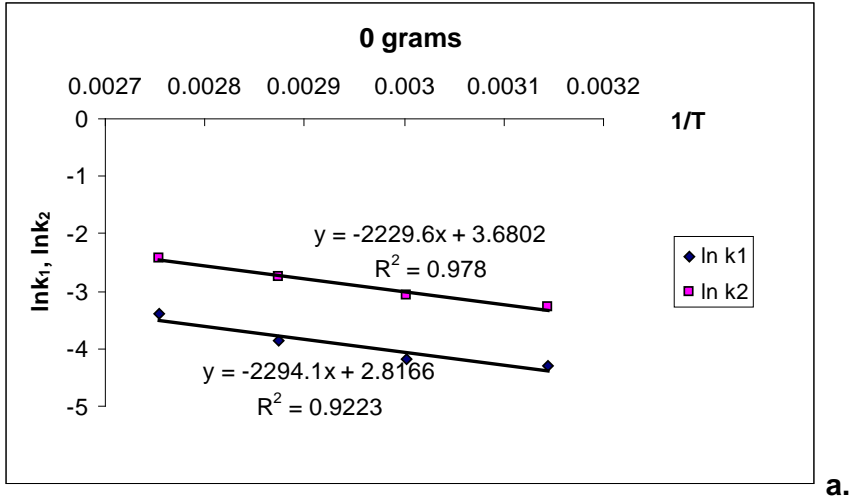


Figure 5. $\ln k$ vs. $1/T$ (a. 0 grams, b. 5.0 grams)

From the slopes of the obtained lines, the activation energies of the drying process were calculated. Values are shown in Table 1.

Table 1. Constant rates and activation energies

Addeed dolomite (grams)		Constant rates (min ⁻¹)		Activation energy (kJ/mol)	
0.0					
T	1/T	k ₁	k ₂	Ea ₁	Ea ₂
318	0.003145	0.0135	0.0376	19.00	18.48
333	0.003003	0.0154	0.0459		
348	0.002874	0.0209	0.0637		
363	0.002755	0.0333	0.0890		
2.5					
318	0.003145	0.0138	0.0354	19.78	18.60
333	0.003003	0.0171	0.0581		
348	0.002874	0.0224	0.0536		
363	0.002755	0.0367	0.0908		
5.0					
318	0.003145	0.0112	0.0379	20.25	19.42
333	0.003003	0.0124	0.065		
348	0.002874	0.020	0.078		
363	0.002755	0.0286	0.1178		
7.5					
318	0.003145	0.0085	0.0209	22.81	22.17
333	0.003003	0.0110	0.0343		
348	0.002874	0.0153	0.059		
363	0.002755	0.0253	0.0979		
12.5					
318	0.003145	0.0086	0.0213	26.18	23.81
333	0.003003	0.0098	0.0469		
348	0.002874	0.0153	0.069		
363	0.002755	0.0253	0.0711		

All obtained activation energy values are lower than 42.0 kJ/mol, which show that the drying process takes place following the mass transfer mechanism [14]. Analyzing the results, it can be observed the increase of activation energy values with the amount of dolomite addition.

This increase confirms the trend of drying mechanism modification from mass transfer to the combined mechanism, mass transformation (evaporation) – mass transfer.

CONCLUSIONS

The drying kinetics of the sugar beet pulp, without and with dolomite addition, was studied in this research work.

The experimental results have shown that the drying rates decrease with the moisture content decrease, being characterized by the specific falling rate period. The analysis of the drying curves shows that the temperature strongly influences the drying rates comparative to the dolomite addition which only slightly influences the drying rates.

The obtained values of activation energy (19.00 -26.18 kJ/mol) indicate that internal mass transfer mechanism for low amount of dolomite addition and the combined mass transformation (evaporation) - mass transfer mechanism control of the drying process.

EXPERIMENTAL SECTION

Sugar beet pulp was obtained from "TEREOS" sugar factory, Luduș, Romania. In order to determine the drying rates, several sets of experiments were carried out. During the experiments, the moisture removed from sugar beet pulp at four temperatures: 45⁰, 60⁰, 75⁰ and 90⁰ Celsius, and for various dolomite additions: 0.0, 2.5, 5.0, 7.5 and 12.5 grams were measured. Drying was carried out in a dryer under constant conditions [11]. Each sample was obtained by intimately mixing of the dolomite with marc in the proportions shown above. The material so prepared was placed in a thin-layer of 8 mm, in 100 mm diameter Petri dishes and then in dryer. Gravimetric measurements were made at each 15 minute, as described in literature [15].

The used dolomite has a content of 21.5% MgO, 32.6% CaO, 1.85% R₂O₃ (R = Fe, Al, Si) and particles size of less than 0.125 mm.

ACKNOWLEDGMENTS

This work was supported by Ministry of Research and Innovation, Project NUCLEU code PN 18 30 01 03.

REFERENCES

1. R.A. McGinnis, "Beet-Sugar Technology", Third Edition, Beet Sugar Development Foundation, Fort Collins, CO, **1982**.
2. Domnica Culae, V. Platon, "Tehnologia zaharului", Ed. Tehnica, Bucuresti, **1983**.
3. J.I. Harland, "The Sugar Beet Crop", Springer Link, **1993**, chapter 16.
4. N. Broughton, C. Dalton, G. Jones, E. Williams, *International Sugar Journal*, **1995**, 97, 57.
5. M.A. Salgado, A. Lebert, H.S. Garcia, J.J. Bimbenet, *Drying Technology*, **1994**, 12(4), 955.
6. F. Alibegovic-Zecic, A. Gagic, S. Piplica, C. Crnkic, D. Tahirovic, A. Kavasovic, *Veterinaria*, **2011**, 60(3-4), 121-125.
7. R.E. Rauch, P.H. Robinson, L.J. Erasmus, *Animal Feed Science and Technology*, **2012**, 177(3-4), 180.
8. G.I. Crwford, C.D. Keeler, J.D. Wagner, C.R. Krehbiel, G.E. Erickson, M.B. Crombie, G.A. Nunnery, *Journal of Animal Science*, **2008**, 86, 2998.
9. M.A. Salgado, H.S. Garcia, A.M. Lebert, J.J. Bimbenet, *Drying Technology*, **1994**, 12(4), 955.
10. A. Merino, R. Alves, L.F. Acebes and C. Prada, *Drying Technology*, **2017**, 35(4), 1765.
11. A. Ghirișan, S. Drăgan, *Studia Universitatis Babeș-Bolyai, Chemia*, **2013**, 58(2), 35.
12. A. Jokic, Z. Zavargo, N. Lukic, B. Ikonc, J. Markovic, J. Dadic, J. Grahavoc, *Journal on Processing and Energy in Agriculture*, **2013**, 17(1), 24.
13. A.A. Shevtrov, A.V. Drannikov, A.A. Derkanasova, A.S. Muravev, A.V. Kvasov, *Journal of Engineering and Applied Sciences*, **2017**, 12(1), 5754.
14. S. Drăgan, I. Siminiceanu, "Studii de caz în procese chimice gaz-lichid și gaz-solid necatalitice", Ed. Risoprint, Cluj-Napoca, **2006**.
15. A. Ghirișan, S. Drăgan, V. Miclăuș, *Studia Uiversitatis Babeș-Bolyai, Chemia*, **2017**, 62(1), 7.

XRD AND IR INVESTIGATIONS OF SOME COMMERCIAL POLYSTYRENE SAMPLES THERMALLY DEGRADED

CARMEN NICULĂESCU^a, LOREDANA OLAR^b, RĂZVAN STEFAN^b,
MIHAI TODICA^a AND CORNEL-VIOREL POP^{a,*}

ABSTRACT. Thermal degradation of commercial polystyrene was investigated by XRD and FT-IR methods. The samples were heated 30 minutes at temperatures 140°C, 200°C, 250°C, 300°C and 350°C and then brought back to room temperature. XRD investigation denotes structural modification for samples heated above 200°C. This modification is confirmed by FT-IR measurements. Some vibration bands are affected by thermal degradation at temperatures higher than 200°C. Both FT-IR and XRD methods reveal modification of microscopic structure of the polystyrene submitted to thermal degradation.

Keywords: *thermal degradation, commercial polystyrene, FT-IR, XRD*

INTRODUCTION

One of the most important challenges of our days is the destruction and recycling, without pollutant effects, of enormous quantity of polymeric materials produced daily by the humanity. Thermal degradation is the simplest method of destroying, but its use could produce undesired products. The aim of this work is the study of structural changes caused by thermal degradation of one of the most used polymer, the polystyrene. The absorption of energy by heating might cause reversible or irreversible modification of physical and chemical properties of samples by oxidation. Similar studies performed by ESR method on UV-irradiated polystyrene showed possible ionization and breaking of chemical bonds of the polymeric chains, [1]. Gamma irradiation of such materials induces a crystallization effect, as confirmed by NMR, [2].

^a Babeş-Bolyai University, Faculty of Physics, 1 M. Kogalniceanu str., RO-400089, Cluj-Napoca, Romania

^b University of Agricultural Science and Veterinary Medicine, Faculty of Veterinary Medicine, 3-5 Calea Mănăştur Street, 400372, Cluj-Napoca, Romania

* Corresponding author: cornel.pop@phys.ubbcluj.ro

RESULTS AND DISCUSSION

Polystyrene is a thermoplastic material consisting in unbranched linear macromolecules, obtained by the polymerization of the styrene, with or without a catalyst (Fig. 1).

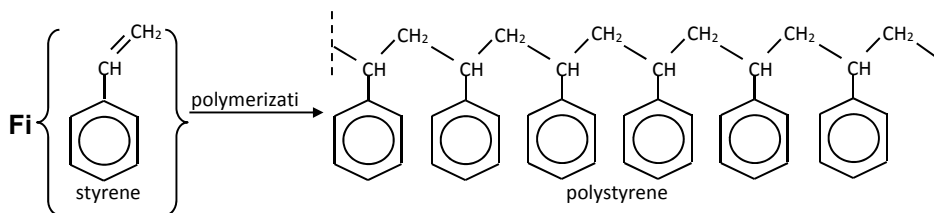


Figure 1. Molecular structure of polystyrene

Generally, these materials are amorphous, but under certain circumstances they can acquire slightly local arrangement. During the synthesis process, it is possible that small quantities of water or solvent to be included in the polymer structure. By heating these residues might be removed by evaporation, which would conduct to a variation of the mass of samples. At high temperatures it is possible that parts of the sample to be oxidized, resulting in the production of chemical compounds different from the initial polymer, which would be later removed by degassing. This process would also have the effect of reducing of the mass of the sample. Our observations have firstly focused on this aspect. The mass variation has been studied in the regard of the temperature. Between 22°C and 140°C variations of the mass and the color were not observed. Modifications appear above 200°C. This behavior was associated with the evaporation of water and residual solvents trapped into the polymeric matrices. Above the temperature of 300°C the samples become black, and the weight decreases again, (Fig. 2). At this temperature the samples fail to burn and become to degage black smoke, which is responsible for coloring the sample in black. These observations lead us to the supposition that below 140°C the samples are stable, but above this temperature evaporation of the residual water and solvents and oxidation process can occur.

The polymeric materials are known as amorphous materials with very low degree of ordering, [3].

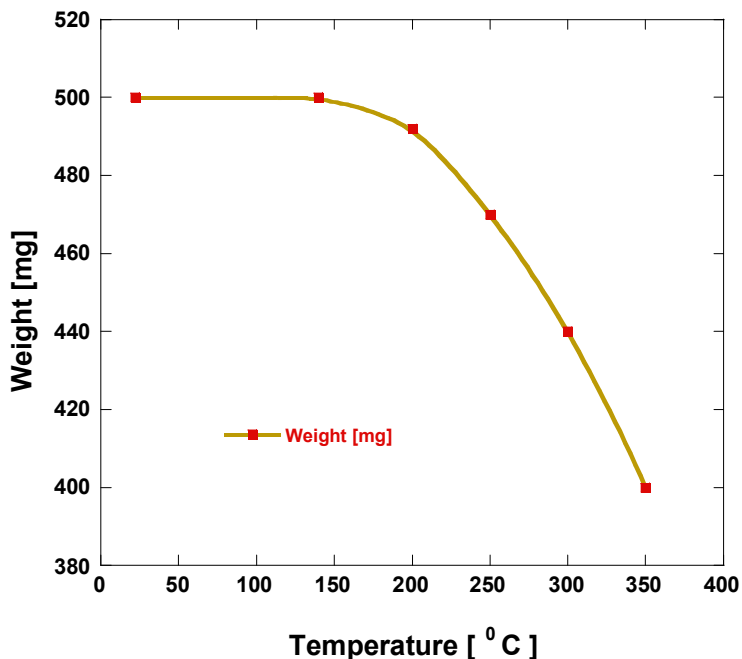


Figure 2. Temperature dependence of the weight of the heated samples.

However it is possible that parts of the same polymeric chain, or parts of different neighboring chains, adopt parallel local arrangement. Such structures behave like the crystalline planes when they are irradiated by X rays, producing the diffraction phenomena. In the XRD spectrum each ordered domain, with the same inter-planar distance, gives a narrow diffraction peak. But in the polymeric materials these domains are characterized by very different inter-planar distance, giving diffraction peaks at different angles. The resulting spectrum is a superposition of the individual peaks giving a broad spectrum, [4]. For polymers the degree of ordering depends on synthesis process, but external factors as UV, X, gamma irradiation or heating process can affect the so called crystalline structure. In our case we were interested to observe possible modifications of the local ordering after heating. The samples were investigated before and after thermal treatment. The unheated polystyrene shows a broad and weak peak centred at $2\theta=17.8^\circ$, (Fig.3).

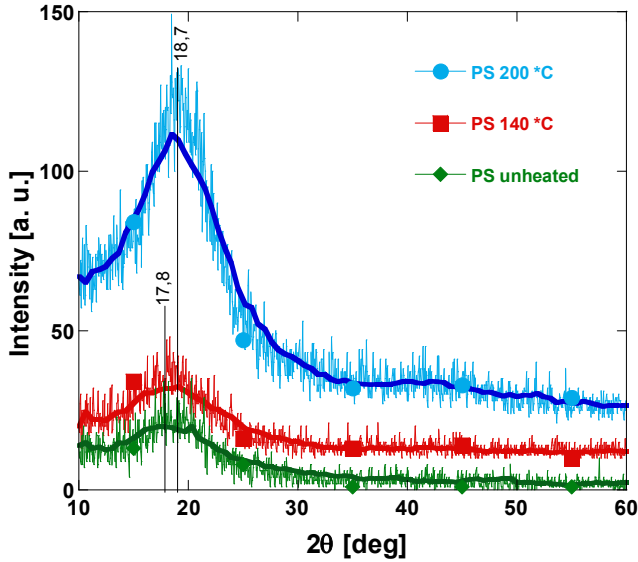


Figure 3. XRD patterns undegraded and, thermally degraded polystyrene at 140 °C and 200 °C.

From the diffraction theory we can calculate the inter-planar distance with the Bragg equation:

$$d = \frac{k \cdot \lambda}{2 \sin \theta} \quad (1)$$

where k is the diffraction order and 2θ is the diffraction angle, [4]. We found the value $d=5.0 \text{ \AA}$. The area S under the diffraction peak is proportional with the concentration of the ordered domains in the sample and the width of the signal is correlated with the size of the ordered domains, [5]. Using Scherrer's formula we found the value $D=14.1 \text{ \AA}$ of the size of ordered domains.

$$D = \frac{K \cdot \lambda}{\beta \cdot \cos \theta} \quad (2)$$

D is the size of the ordered domains, $K = 0.9$ is a proportionality factor and β is the half line width. The sample heated at 140°C doesn't show major modifications; the shape and the amplitude of the diffraction peak are almost similar with those of the unheated sample. That shows that the thermal treatment below this temperature doesn't modify the local order of the polymer. Important changes appear at 200°C . The amplitude of the peak and the area under the graphic increase compared with the unheated sample. The rappings of the areas is $R=3.80$ at 140°C and $R=4.20$ at 200°C .

The thermal treatment facilitates the local ordered arrangement of polymeric chains and the increase of ratio of the crystalline phase, [6-8]. It can be observed a weak shift towards higher diffraction angles of the main peak at 18.7° , (Fig. 3). The new inter-planar distance is $d = 4.7 \text{ \AA}$, showing a more compact structure of the polymer. If the heating process is continued, above 200°C , there is a decrease of the intensity and area of the diffraction peaks, (Fig. 4). This reduction is associated with the destruction of the ordered phase determined by the oxidation.

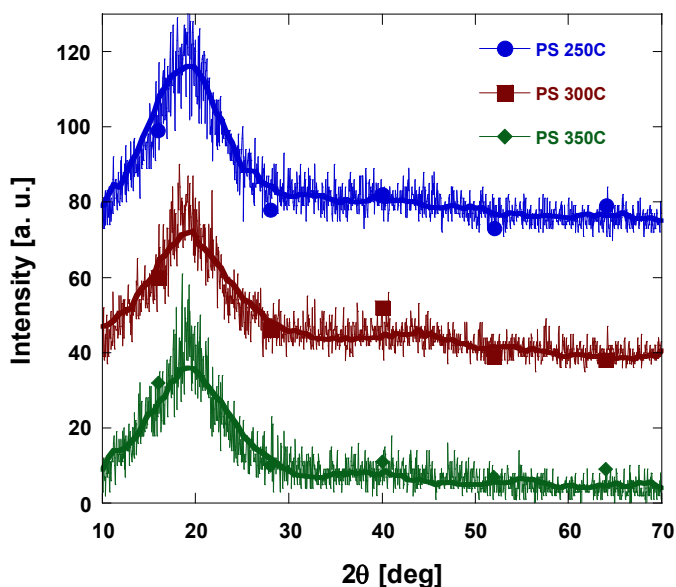


Figure 4. XRD patterns of unheated and thermally degraded polystyrene at 250°C , 300°C and 350°C .

The modifications induced by thermal treatment were analyzed also by IR measurements. Usually the heating at moderate temperatures has small effects on the vibrations of the molecular bonds and on the IR spectrum. The IR spectra of polystyrene heated at different temperatures are shown in figure 5. The most intense vibration bands can be observed at 1041 cm^{-1} , 1232 cm^{-1} , 1485 cm^{-1} , 1600 cm^{-1} , 2854 cm^{-1} and 2926 cm^{-1} . These bands are assigned as follows: the peak at 2926 cm^{-1} represents H – C – H asymmetric stretching vibration of chain backbone. The peak at 1600 cm^{-1} is associated to the phenyl ring stretching vibration of C = C – C conjugative system.

The peak at 1485 cm^{-1} represents either out of plane or in plane C – H bending vibration of the chain backbone. The peak at 1232 cm^{-1} is assigned to C – C – O – C – C stretching. The peak at 1041 cm^{-1} corresponds to phenyl in plane C – H bending vibration, [5, 9, 10, 13]. Low amplitude of the bands in the 1250 cm^{-1} range are in accord with other works reported in literature, [14]. The heating below 200°C doesn't have major effect on the shape, intensity and position of the vibration bands. At 200°C a new band appears at 896 cm^{-1} , showing the apparition of a vibration determined by the crystallization of the sample.

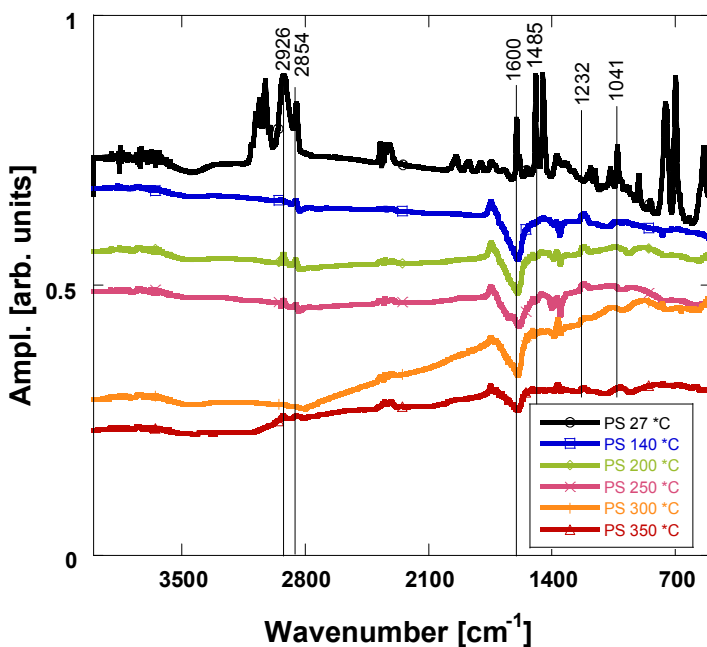


Figure 5. IR spectra of polystyrene at different temperatures between 27°C and 350°C

This observation is in accord with the XRD measurements, which indicate structural modification at high temperature. At 300°C the intensity of the majority of the vibration bands diminishes, (1486 cm^{-1} , 2854 cm^{-1} and 2926 cm^{-1}). At 350°C the intensity of the vibration bands diminishes again and some bands almost vanish (2854 cm^{-1} and 2926 cm^{-1}).

CONCLUSIONS

Commercial polystyrene heated at different temperatures was investigated by XRD and IR methods. XRD investigation reveals some structural changes of heated samples. Heating up to 200°C facilitates the local arrangement of the polymeric chains in ordered structures. This is demonstrated by the increase of the intensity and the area of the diffraction peaks. The slight shift of the diffraction peak from 17.8° to 18.7° indicated the evolution of the polymeric chain towards a more compact structure. Heating above 200°C is followed by oxidation of the polymer and the reduction of the ordered structure.

The conclusions deduced from XRD investigation have been confirmed by IR measurements. At room temperature a very neat spectra is obtained. At 200°C a vibration band appears at 896 cm⁻¹, determined by the crystallization of the sample. Above this temperature the intensity of the majority of the vibration bands diminishes, and some bands almost vanish. This behavior is associated to the oxidative process of the sample.

EXPERIMENTAL SECTION

Samples of commercial polystyrene, used as thermal insulation for building, were heated 30 minutes at different temperatures, 140°C, 200°C, 250°C, 300°C and 350°C and then investigated by XRD and IR methods. XRD measurements were performed with Brucker X-ray diffractometer with Cu K α ($\lambda=1.54$ nm) at 45 KV and 40 mA. The 2θ range of 10–60° was recorded [11, 12]. The IR absorption spectra were recorded in 400–4000 cm⁻¹ spectral range with JASCO FTIR 4100 spectrometer.

The polystyrene was divided into 6 samples, each sample having 500 mg weigh. One sample has been studied separately in the initial state and the other 5 samples were heated at 140°C, 200°C, 250°C, 300°C, 350°C for 30 minutes. For some samples a variation of the mass and color with the temperature was observed, (Table 1).

Table 1. Variation of the properties of polystyrene samples upon heating.

Samples	Initial weigh [mg]	Final weigh [mg]	Temperature [° C]	Color
PS1	500	500	22	White
PS2	500	500	140	White
PS3	500	492	200	White-gray
PS4	500	470	250	Gray
PS5	500	440	300	Black-gray
PS6	500	400	350	Black

REFERENCES

1. A. Martínez-Romo, R. González-Mota, J.J. Soto-Bernal, I. Rosales-Candel, *Hindawi Publishing Corporation. Journal of Spectroscopy*, **2015**. Article ID: 586514.
2. M. Pop, S.Traian, L. Daraban, R. Fechete, *Studia UBB Chemia*, **2011**, *56*, 129.
3. J.P. Cohen, "Addad Physical properties of polymeric gels", Chichester (UK): John Wiley & Sons, **1996**.
4. Barbara Stuart, "Polymer Analysis". Chichester (UK), John Wiley & Sons, **2002**.
5. M. Todica, V. Simon, T. Stefan, D.L.Trandafir, I. Balasz, *Indian Journal of Pure and Applied Physics*, **2015** *53*, 359.
6. M. Todica, T. Stefan, S. Simion, I. Balasz, L. Daraban, *Turkish Journal of Physics*, **2014**, *1*.
7. M. Todica, M. Nagy, C. Niculaescu, O. Stan, C. Nicolae, C.V. Pop, *Journal of Spectroscopy*, **2016**, Article ID: 9605312.
8. M. Todica, N. Cioica, L.E. Olar, I. Papuc, C. Cota, E. Marin, D. Manea, E.M. Nagy, *Romanian Biotechnological Letters*, **2016**, Vol. *21*, No. *5*, 11825.
9. M. Todica, L. Udrescu, "Metode experimentale în fizica polimerilor", Presa Universitară Clujeană, **2013**, 56.
10. H. Zhen-Li, L. Lie-Xiong, L. Hong, Z. Yuan-Di, *Journal of Molecular Structure*. **2005**, *738*, 155.
11. R. Hirian, S. Mican, O. Isnard, L. Barbu-Tudoran, V. Pop, *Journal of Alloys and Compounds*, **2017**, *697*, 19.
12. H. Mocuta, Marieta Mureșan-Pop, Irina Kacsó, G. Borodi, S. Simon, I. Bratu, *Studia UBB Chemia*, **2012**, *57*, *4*, 135.
13. M.M. Radhi, A.J. Haider, Z.N. Jameel, T.W. Tee, M. Z.B. Rahman, A.B. Kassim, *Research Journal of Chemical Sciences*, **2012**, *2*(11), 1.
14. C.P. Ennis, R.I. Kaiser, *Physical Chemistry Chemical Physics*, **2010**, *12*, 45, 14884.

IN VITRO BEHAVIOUR OF NEW EXPERIMENTAL ADHESIVE SYSTEMS

**DIANA SUCALĂ^a, CODRUȚA SAROSI^{b*}, CĂȚĂLIN POPA^a,
ILEANA COJOCARU^c, MARIOARA MOLDOVAN^b AND
AUREL GEORGE MOHAN^d**

ABSTRACT. Bonding of current adhesives to dentin is usually through the formation of the interfacial hybrid layer between adhesives and dentin. Inter-tubular and intra-tubular resin infiltration leads to an increase of the quality regarding the dentinal adhesion. The aim of this study is in vitro testing of new experimental adhesives in comparison with commercial adhesive, regarding sorption and solubility as well as to investigate molecular chemical features of the adhesive/dentin interfaces. We used 4 experimental adhesives systems A1, A2, A3, A4 and IBond® (Heraeus) as reference material. Organic phase adhesive system consists of a mixture of monomers. As filler for these systems, besides hydroxyapatite, we used TiO₂ nanoparticles. FTIR spectroscopy was used to investigate molecular chemical features of the adhesive/dentin interfaces. The obtained data show the main advantages and disadvantages of the tested adhesive systems. The best values of water sorption and solubility both in water and artificial saliva present A2 and A3 adhesives.

Keywords: FTIR spectroscopy, TiO₂, dental adhesives, sorption, solubility

INTRODUCTION

The increase in the use of composite resins as a restorative material in dentistry is mainly due to their aesthetic features, favorable physical and mechanical properties, including high resistance to compression and wear,

^a Technical University of Cluj-Napoca, Materials Science and Engineering Department, Cluj-Napoca, Romania

^b Babes Bolyai University - Raluca Ripan Chemistry Research Institute, Department of Polymer Composites, Cluj-Napoca, Romania

^c University of Craiova, 13 Al. I. Cuza, 200585, Craiova, Romania

^d University of Oradea, 1 Universitatii Street, 410087, Oradea, Romania

* Corresponding author: codruta.sarosi@ubbcluj.ro

relatively low costs and simple application. Many studies have found failures of composite resins restoration due to the loss of integrity of the adhesive interface. A number of possible mechanical and chemical mechanisms have been proposed as reasons of dentin adhesion [1, 2]. The resin impregnation creates a transitional hybrid layer, that is neither resin nor tooth, but a hybrid of the two. The thin layer of resin reinforced dentin locks the two dissimilar substances together on a molecular level, sealing the surface against leakage. This layer that connects the adhesive to the subjacent dentin is believed to be both chemically and structurally heterogeneous, since its formation relies on many processes such as acid etching to remove mineral phase, adhesive penetrating into the demineralized collagen network in the presence of water and photo-polymerization of the adhesive [3, 4].

The characterization of the heterogeneity of the adhesive/dentin interfacial layer has thus been a topic of great interest. Fourier transform infrared (FTIR) spectroscopy has proven to be a good technique to investigate the physicochemical interactions at the dentin/adhesive interface [4]. Using FTIR spectroscopy, the degree of cure, relative chemical composition and homogeneity across the length and breadth of the adhesive/dentin interface can be determined [4].

Sorption and water solubility leads to a lot of chemical and physical effects, resulting negative influences upon the structure and functions of dental polymers including their capacity of dental adhesion retention. Ideally, the polymeric structure must be insoluble, with a high chemical and physical stability. However, most of the monomers used in the dental materials can absorb water and environment chemical substances, and can release components too.

The water contamination of adhesive materials during their preparation or application, significantly reduce their mechanical properties by 50%. A low solubility of the adhesive materials components is a fundamental condition to insure clinical success. Manufacturers have added hydrophilic monomers to hydrophobic dimethacrylates in an attempt to promote effective bonding between hydrated dentin and resin composites.

Many studies have found failures of composite resin restorations, due to the less of integrity of the interface [3]. This failure can lead to micro leakage and consequently post operator sensitivity, marginal discoloration and secondary caries. Moreover, it has been shown that the movement of water from hydrated dentin may cause the formation of waterfilled channels within the polymer matrices of contemporary hydrophilic dentin adhesives [5,6]. Some findings suggest that the fluid sorption may lead to a plasticizing of the organic matrix and to its hygroscopic expansion witch can reduce the shrinkage stress [7].

The purpose of this study was to determine sorption, solubility and the physico-chemical interactions at the hard dental /adhesives interface.

RESULTS AND DISCUSSION

Water sorption and solubility mean values ($\mu\text{g}/\text{mm}^3$) are presented in figures 1, 2, 3 and 4. In the graphs are presented the weekly values of solubility, respectively of sorption. One way ANOVA showed that water sorption and solubility was different for tested materials ($p < 0.05$). The experimental adhesive A2 showed the lowest value, both in water and artificial saliva, followed by adhesive A3, with a small difference between them. That is due to the higher content of their filler (15% compared with 5% of A1 and A4). Adhesives A1 and A4 showed a higher water sorption and solubility, with a considerable difference between them and the first group adhesives. Regarding all tested adhesives, the values of sorption and solubility was stabilized after 21 days. In the same time, the solubility in water was higher than in artificial saliva in all tested adhesives. The negatives solubility values were recorded in this study. This can be explained by the presence of hydroxyl and carboxyl groups in monomers and their resultant polymers make them more hydrophilic and, supposedly, more prone to water sorption and increase the mas of the specimen.

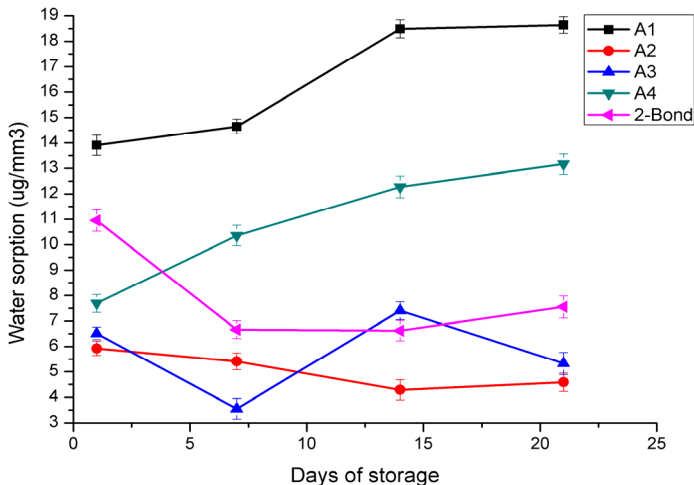


Figure1. Mean values and standard deviation for **water sorption** ($\mu\text{g}/\text{mm}^3$) of the adhesive materials tested after 1, 7, 14 and 21 days of **water storage**.

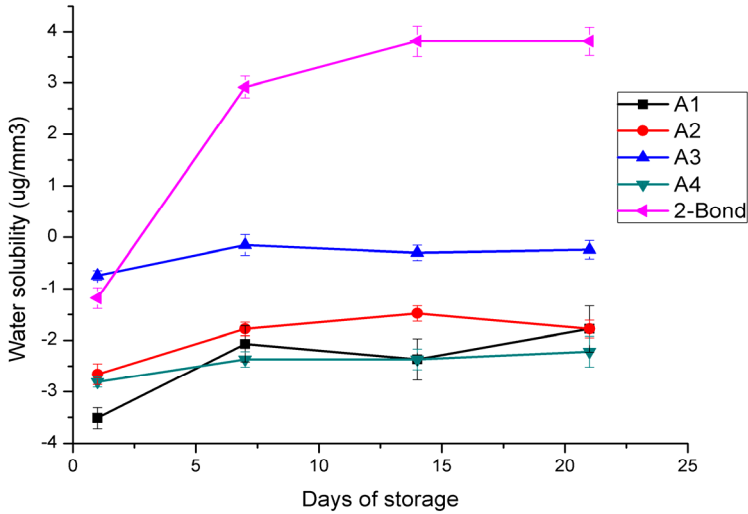


Figure 2. Mean values and standard deviation for **water solubility** ($\mu\text{g}/\text{mm}^3$) of the adhesive materials tested after 1, 7, 14 and 21 days of **water storage**.

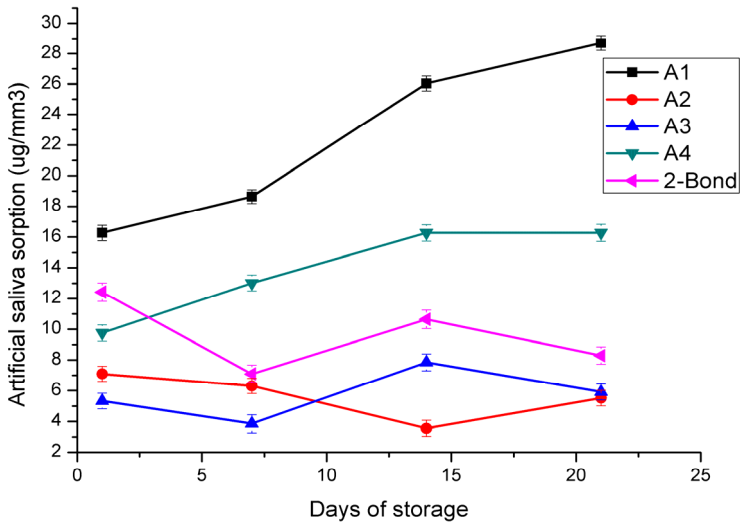


Figure 3. Mean values and standard deviation for (a) **artificial saliva sorption** ($\mu\text{g}/\text{mm}^3$) of the adhesive materials tested after 1, 7, 14 and 21 days of **artificial saliva storage**.

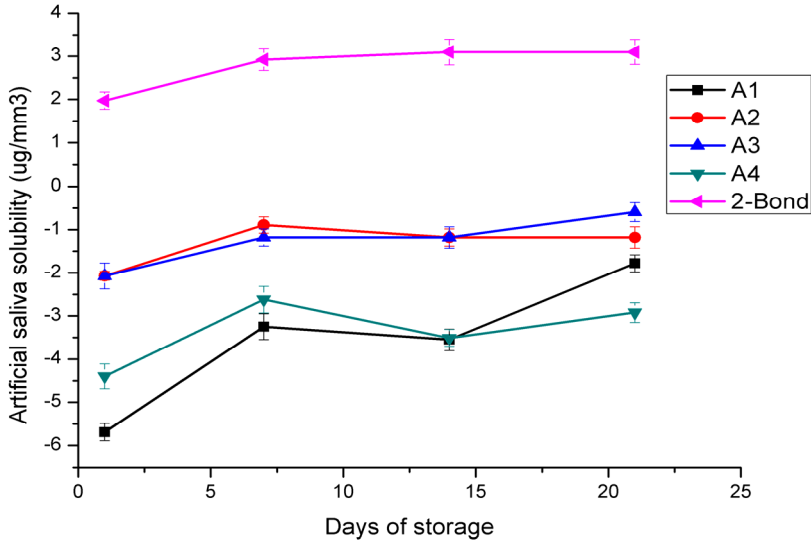


Figure 4. Mean values and standard deviation for **artificial saliva solubility** ($\mu\text{g}/\text{mm}^3$) of the adhesive materials tested after 1, 7, 14 and 21 days of **artificial saliva storage**.

The one-way ANOVA revealed highly significant differences between the materials for all the sorption and solubility values with some exceptions ($p < 0.05$). After storage in water, there was no significant difference between A2 and A3 at 1 day, between A2 and 2-Bond at 7 days as well as between A2 and 2-Bond at 14 days for the sorption (S). Additionally, there were no significant differences between all materials for the solubility (SL) and SL%, ($p = 0.196$ and $p = 0.245$, respectively). But there were significant differences between storage mediums. As shown in Fig. 1, and 3 the highest sorption (S) was obtained for A1 adhesive when it was immersed in artificial saliva followed by A4 and 2-Bond. A higher amount of TiO_2 in experimental adhesive composition, decrease the sorption and solubility. Moreover, no significant differences were noted between A2 and 2-Bond after 14 and 21 days sorption period. Water sorption and solubility of the experimental and commercial dental adhesives were all significantly dependent on material composition.

Thin sections of the adhesive/dentin interface specimens were analyzed using FTIR spectroscopy. In table 1 are presented the infrared spectroscopic ν (cm^{-1}) wavenumbers of absorption maxima of dentin/ adhesive/ enamel interface of experimental dental TiO_2 adhesives and 2-Bond commercial adhesive.

Table 1. Infrared spectroscopic ν (cm^{-1}) wavenumbers of absorption maxima of dentin/adhesive/enamel interface of experimental dental TiO_2 adhesives and commercial adhesive

Band name of dental inter-face	Amide I	Amide II	Amide I II	C=O	C=C	O-H	C-O	Collagen	PO_4^{3-}	Bis-GMA aromatic ring	TiO_2
Enamel							1405		1080 964 632		
Dentin	1660	1550	1240	1719	1637	1607	1039	1676 1458 1253	1076 965 588		
Adhesive					1639 1721		1182		1080 632	1610 1635	399
Dentin-adhesive			1240		1639 1721		1182	1458	1080 638	1635	400

It can be observed that the phosphate band ($900\text{--}1200\text{ cm}^{-1}$) of the dentin overlaps with the band of SiO_2 filler in the adhesive. In addition, the amide I region more or less overlaps the $1620\text{--}1680\text{ cm}^{-1}$ region of the adhesive.

The wavenumbers of absorption maxima from the dentin/adhesive interface spectra are specific from adhesive and dentine, in accordance with other studies [8-10].

Haller et al [11] reported an increase in the amount of interface with gaps over time of storage in water. He explained this occurrence as the effect of degradation of the polymeric structure, with hydrolytic degeneration of resin composite as the water diffuses along adhesive interface. In order to observe the gaps, some authors [6, 5-12] did not use a scanning electron microscope because it would require vacuum, causing loss of water from dentin and composite resin, which could alter the adhesive interface integrity. Instead of it, they used an optical microscope. The adhesive resin should create the hybrid layer (consisting of a collagen network exposed by etching and embedded in adhesive resin). This layer is an interface between dentin and adhesive and the quality of the dental restoration depends greatly on its properties. The quality and structure of the hybrid layer depends on a few factors. One of those is the adhesive type (Total etch/Self etch).

Eliguzeloglu et al [13] reported that hybrid layer thickness showed a significant difference between total etch and self-etch systems in non-carious sclerotic lesions without removal of the superficial layer. Hybrid layer thickness was increased when superficial dentin was removed.

Our study showed that all the tested adhesives are stabilized after 14 days when sorption and water solubility registered the best values. Adhesive A2 and A3 showed low solubility comparing with adhesive A1 and A4. This can be explained by the different composition of filler which is three times higher in adhesives A2 and A3. In the same time, the hydrophilicity of functional monomers can affect the chemical interaction and can influence water absorption and solubility in different adhesives.

Some studies have found that the water sorption causes expansion of the adhesive material until an equilibrium value [14-17]. Another study shows that most of the hygroscopic expansion occurs in the first two weeks, with the balance achieved in about eight weeks [18]. The process of water sorption depends on the composition of the adhesive (volume of filler, type of monomer of the resin matrix, volume of restoration and the cavity configuration [19, 20]. Contemporary adhesives contain increased concentration of hydrophilic resin monomers (HEMA, BPDM, MDP, Bis-GMA), to enhance their bonding to the wet dentine substrate [21-23]. The hydrophilic nature of copolymers facilitates water sorption from the oral environment when exposed to saliva and hydrated dentine. The absorbed moisture can alter the properties of adhesive resin [24]. The temperature at which the process is carried out is very important. In his study, Diamant et al [25] showed that the exposure to water at elevated temperature can produce irreversible effects in polymers that contain high concentration of very hydrophilic monomers. There is a correlation between the nature of monomers regarding their hydrophilicity, the high of moisture and temperature. Intra oral temperature changes can occur following eating and drinking. Under such conditions, formation of cracks as a result of swelling stress and chemical degradation through hydrolytic reactions may compromise the adhesion [26]. Additions of TiO_2 nanoparticles increase the stability of adhesive, and the resistance to water sorption and solubility. Other studies revealed that TiO_2 present unique photocatalytic, antibacterial and UV-absorbing properties that recommend as beneficial additives in adhesives and resin composites [8, 27].

The strengths of bonding to dentin, especially bonding to the clinical relevant substrates, continue to drop as a function of time [28, 29]. Durability of this bond relies on the quality of the interface between adhesive and dentin. Understanding of the interfacial structure and chemistry is critical to reveal reasons for the low durable bond. The mechanical test techniques measure fracture resistance of adhesive/dentin specimens, and are not sensitive enough to identify interfacial defects that lead to crack initiation or

aqueous degradation [30, 31]. The differences in the distribution patterns of two adhesive regions within the specimens may be caused by different substrates during wet bonding processes. When bonding to dentin, the tubules perpendicular to the surface are filled with water after acid etching and water rinsing. The system of dental adhesive is considered to be the first choice in the treatment of dental restoratives. The results show that the introduction in the polymeric matrix of TiO_2 , improves the physico-chemical properties of the adhesive and gives an antibacterial effect.

CONCLUSIONS

The reinforcement of TiO_2 in polymer matrices has shown interesting results in improving the water sorption and solubility properties. Based on the obtained results, we could consider that the TiO_2 (two-step self-etch systems – A2) could be a very promising filler for the dental adhesives.

Durability of the tooth restoration relies on the quality of the interface between adhesive and dentin. Understanding of the interfacial structure and chemistry is critical to reveal reasons for the low durable bond.

EXPERIMENTAL SECTION

Four new adhesives based on TiO_2 and a commercially available dental adhesive were tested: two “etch and rinse systems” adhesives (A2, A3), and two “two-step self-etch systems” adhesives (A1, A4) and the 2Bond® (Heraeus), etch and rinse adhesive system. The composition of the experimental adhesives is presented in table 2.

We used 20 extracted erupted human teeth, stored in artificial saliva. In each tooth were produced class I occlusal cavities following steps to prepare cavities by Black. All the cavities were etched with phosphoric acid (37%) for 15 seconds, followed by washing in running water for 20 seconds and drying. The adhesive solution was brushed onto the entire dentin surface, gently air-dried; the adhesive coated dentine surface was light-cured for 20 seconds using a conventional halogen light unit with an output intensity of $600\text{mW}/\text{cm}^2$. A resin composite (Herculite XRV®, Kerr) was placed in three 1 mm thick increments over the adhesive and light-cured for 120 seconds. The prepared teeth were fixed on a methacrylate support and stored for 8 weeks in artificial saliva at 37°C before being sectioned in 3 microns thick sections using a tungsten carbide knife fixed on a microtome (IsoMet 1000, Buehler). These sections were placed directly on the motorized stage for FTIR with a spectrometer (JASCO).

For the water sorption and solubility measurements, a teflon mold was used with 15 mm diameter x 1 mm thickness, according to ISO 4049. A glass cover slip was placed on top of the adhesive, which was light-cured for 40 s using a visible light (Woodpeker LED). After removing the specimen from the mould, photoactivation was repeated on its opposite surface for another 40 s. The obtained surfaces must be smooth and flat. Immediately after polymerization, the specimens were placed in a desiccator at 23°C, repeatedly weighed (Analytical balance – Partner AS160/C/2, Partner Corporation, RO) after 24 h intervals until a constant mass (m_1) was obtained. The specimens were immersed in distilled water and maintained 7 days. The weight was daily determined by extracting from water and wiped with absorbing paper. After 10 minutes the specimens must be weighed thus registering the weight (m_2). The specimens were replaced in desiccator again, 4 hours long, until a constant weight had been achieved (m_3). This process will be repeated at 14 and 28 days. The test was done both in distilled water and artificial saliva ARTISIAL® (Jouveinal Laboratoires, France).

Table 2. The composition of experimental and commercial adhesive system

Adhesive system	Composition	Ratio
A1	(1) <i>Adhesive</i> - Bis-GMA, HEMA, TEGDMA, Polyacrylic acid, Ethanol and initiators, HAp-TiO ₂ (5%)	95/5
A2	(1) <i>Primer</i> - Bis-GMA, HEMA, Polyacrylic acid, Ethanol, Water and initiators; (2) <i>Adhesive</i> - Bis-GMA, HEMA, TEGDMA and initiators, TiO ₂ (15%)	85/15
A3	(1) <i>Primer</i> - Bis-GMA, HEMA, Polyacrylic acid, Ethanol, Water and initiators; (2) <i>Adhesive</i> - Bis-GMA, HEMA, TEGDMA and initiators, HAp-Ag (5%), HAp-ZnO (5%), TiO ₂ (5%)	85/15
A4	(1) <i>Adhesive</i> - Bis-GMA, HEMA, TEGDMA, Polyacrylic acid, Ethanol and initiators, TiO ₂ (5%)	95/5
2Bond, Heraeus Kulzer GmbH	(1) <i>Adhesive</i> - 4-META, Urethane dimethacrylate, Glutaraldehyde, acetone, water and initiators	100
Bis-GMA- 2,2-bis(3-(2'-hydroxy-3'methacryloyl-oxypropoxy)phenyl)propane [synthesised in ICCRR laboratory]; HEMA- 2-Hydroxyethyl methacrylate [Aldrich]; TEGDMA - triethyleneglycol- dimethacrylate [Aldrich]; 4-META- 4-methacryloyloxyethyl trimellitate anhydride, Polyacrylic acid M2000 [Aldrich]		

Sorption and solubility were calculated for each specimen according to formulas:

$$W_{sp} = (m_2 - m_1)/V \text{ and } SL = (m_1 - m_3)/V \text{ } (\mu\text{g}/\text{mm}^3)$$

where: m_1 - sample weight before water immersion (μg);
 m_2 - sample weight after water immersion 24 hours (μg);
 m_3 - sample weight which was maintained in the desiccators until a constant weight had been achieved (μg);
 V - sample volume (mm^3).

ACKNOWLEDGMENTS

This work was funded by the Romanian Ministry of Education and Research, National projects 101PED/2017 and 142PED/2017.

REFERENCES

1. N. Nakabayashi, M. Nakamura, N.J. Yasuda, *Aesthetic and Restorative Dentistry*, **1991**, 3, 133.
2. H. Sano, M. Yoshiyama, S. Ebisu, M.F. Burrow, T. Takatsu, B. Ciucchi, R. Carvalho, D.H. Pashley, *Operative Dentistry Journal*, **1995**, 20(4), 160.
3. Y. Wag, X. Yao, R. Parthasarathy, *Journal of Biomedical Materials Research Part A*, **2009**, 91(1), 251.
4. P. Spencer, Y. Wang, M.P. Walker, D.M. Wieliczka, J.R. Swafford, *Journal of Dental Research*, **2000**, 79, 1458.
5. T.A. Xavier, I.S. Medeiros, E.F. Rosa, R.Y. Ballester, *Journal of Research in Dentistry, Tubarao*, **2013**, 1(2), 119.
6. J. Malacarne, R.M. Carvalho, M.F. de Goes, N. Svizero, D.H. Pashley, F.R. Tay, C.K. Yiu, M.R. de Oliveira Carrilho, *Dental Materials*, **2006**, 22, 973.
7. Y. Xu, J. Zhang, *Journal of Materials Science: Materials in Medicine*, **2008**, 19(6), 2477.
8. J. Sun, E.J. Petersen, S.S. Watson, C.M. Sims, A. Kassman, S. Frukhtbeyn, D. Skrtic, M.T. Ok, D.S. Jacobs, V. Reipa, Q. Ye, B.C. Nelson, *Acta Biomaterialia*, **2017**, 53, 585.
9. M. Hashimoto, H. Ohno, M. Kaga, K. Endo, H. Sano, H. Oguchi, In vivo degradation of resin-dentin bonds in humans over 1 to 3 years, *Journal of Dental Research*, **2000**, 79(6), 385.

10. V.C. Dumont, R. Menezes Silva, L.E. Almeida-Júnior, J.P. Bretas Roa, A.M. Botelho, M.H. Santos, *Journal of Materials Science and Chemical Engineering*, **2013**, 1(7),13.
11. B. Haller, N. Hofmann, B. Klaiber, A. Pfannkuch, *Deutsche Zahnärztliche Zeitschrift Journal*, **1993**, 48, 100.
12. D. Sucala, C. Sarosi, S. Cuc, M. Moldovan, C. Popa, *Key Engineering Materials*, **2017**, 752, 18.
13. E. Eliguzeloglu, H. Omurlu, G. Eskitascioglu, S. Belli, *Oper. Dent.*, **2008**, 33(3), 338.
14. U. Ortengren, H. Wellendorf, S Karlsson, I.E. Ruyter, *Journal of Oral Rehabilitation*, **2001**, 28(12), 1106.
15. A. Albaladejo, R. Osorio, M. Toledano, M. Ferrari, *Medicina Oral, Patología Oral y Cirugía Bucal*, **2010**, 15(1), 112.
16. L. Tjaderhane, F.D. Nascimento, L. Breschi, A. Mazzoni, I.L.S. Tersariol, S. Geraldeli, A.T. Mutluay, M. Arrilho, R.M. Carvalho, F.R. Tay, D.H. Pashley, *Dental Materials*, **2013**, 29(10), 999.
17. M. Păstrav, A.M. Chisnoiu, O. Pastrav, L. Silaghi-Dumitrescu, C. Sarosi, V. Tarmure, *Studia UBB Chemia*, **2017**, LXII(4), 201.
18. J.L. Ferracane, *Dental Materials*, **2006**, 22(3), 211.
19. C.K. Yiu, N.M. King, D.H. Pashley, B.I. Suh, R.M. Carvalho, M.R. Carrilho, F.R. Tay, *Biomaterials*, **2004**, 25, 5789.
20. L.R. Archegas, D.B. Caldas, R.N. Rached, S. Vieira, E.M. Souza, *The Journal of Contemporary Dental Practice*, **2008**, 9(2), 73-80.
21. A. Reis, A.D. Loguercio, R.M. Carvalho, R.H. Grande, *Dental Materials*, **2004**, 20, 669.
22. U. Lohbauer, S.A. Nikolaenko, A. Petschelt, R.J. Frankenberg, *The Journal of Adhesive Dentistry*, **2008**, 10, 97.
23. D. Cornea, L. Silaghi-Dumitrescu, R. Balazsi, R. Oprean, D. Dude, M. Moldovan, *Studia UBB Chemia*, LXI(2), **2016**, 239.
24. X. Wang, G. Huyang, S.V. Palagummi, X. Liu, D. Skrtic, C. Beauchamp, R. Bowen, J. Sun, *Dental Materials*, 2018, 34(2), 228.
25. Y. Diamant, G. Marom, J. Broutman, *J. Appl. Polym. Sci.*, **1981**, 26, 3015.
26. J. Kim, S. Mai, F.R. Tay, *Dent. Research*, **2010**, 89(5), 482.
27. J. Kovács, S. Beszédes, S. Kertésza, G. Veréb, C. Hodúr, I.Z. Papp, A. Kukovecz, Z. László, *Studia UBB Chemia*, **2017**, LXII(1), 249.
28. S. Kenshima, C. Francci, A. Reis, A.D. Loguercio, L.E.R. Filho, *Journal of Dentistry*, **2006**, 34(10), 775.
29. R.H. Sunfeld, C.H. Oliviera, A. Silva, A.L. Briso, M.L. Sundefeld, *The Bulletin of Tokyo Dental College*, **2005**, 46(3), 43.
30. K.I. Yiu, N.M. King, M.R.O. Carrilho, S. Sauro, F.A. Rueggeberg, C. Prati, R.M. Carvalho, D.H. Pashley, F.R. Tay, *Biomaterials*, **2006**, 27,1695.
31. S.R. Armstrong, J.C. Keller, D.B. Boyer, *Dental Materials*, **2001**, 17(3), 268.

CHARACTERIZATION OF SOILS IN THE ALMASU MARE AREA THROUGH THE DETERMINATION OF LEAD CONCENTRATIONS

ADRIANA MIHAELA CHIRILĂ BĂBĂU^{a*}, VALER MICLE^a,
IOANA MONICA SUR^a

ABSTRACT. The present study consisted in the determination of lead concentrations in soil samples and sterile material dumped collected from the Almaşu Mare mining area. The lead concentration in the samples collected were determined by atomic adsorption spectrometry (AAS). In spite of the fact that all mines from area are nowadays inactive, the results of the chemical analysis showed that the soils in the area are still highly polluted with lead, except at the base of the “Radeş” dump, where the lead concentrations were below the intervention thresholds.

Keywords: *mining area, “Radeş” dump, lead concentration.*

INTRODUCTION

In the very beginning the curiosity and interest of researchers was probably devoted to herbs which were able to grow on heavy metals contaminated soils, restricting metals uptake or accumulating them in their tissues [1-7]. Sterile dumps are detrimental to natural plant growth due to their physicochemical characteristics, such as low pH, high heavy metal concentrations, deficiencies in soil organic matter and low fertility. Thus, the remediation of sterile dumps has become a key issue in environmental science.

High concentrations of lead in soils are associated with long-term pollution [4, 5]. Lead has been known to be toxic since the 2nd century BC in ancient Greece. Lead is one of the most common contaminants found in soils. It is toxic both to humans and animals, especially to young children [6].

^a *Technical University of Cluj-Napoca, Faculty of Materials and Environmental Engineering, Department of Environmental Engineering and Sustainable Development Entrepreneurship, 103-105 Muncii Ave, Cluj Napoca, Romania,*

* *Corresponding author: adriana.babau@yahoo.com*

Where the soil is acid Pb is mobile and is available for uptake by plants, but the effect of pH on Pb availability is not large [8, 9].

Current remediation of Pb contaminated soils by stabilization/solidification (immobilization) technique is in the development stage [6].

The phytoremediation contaminated soil with lead, using plants, also is a technology in development. Phytoremediation is a concept that has been in use since the early 1990 and is composed of a set of natural technologies that use plants to clean up contaminated areas. This technology has become in the last period a great money saver and its applications can contribute with great success at cleaning up and healing the contaminated soils [2]. The researchers suggest that this technology will be economically feasible only if systems can be developed to employ high biomass plants that can accumulate greater than 1% Pb in their shoots [10]. Phytoremediation, an in situ cost-effective and friendly technology, is emerging as the most promising remediation method for mine tailings by introducing tolerant plant species [3].

The possibility of applying phytoremediation technology to lead-polluted soils

The technologies of phytoremediation are based on different mechanisms which include: phytoextraction, phytostabilization, phytovaporation, rhizofiltration and rhizodegradation. The primary attention is given to the phytoextraction and phytostabilization as the most widespread and alternative methods of soil remediation.

Phytoextraction (also known as phytoaccumulation or phytoabsorption) is the uptake of contaminants from soil by plant roots and their translocation and accumulation in above ground biomass and shoot [11] and the phytostabilization is the immobilization of contaminants through absorption by roots, precipitation, complexation or metal valence reduction in rhizosphere. In this case, the plants are used to limit the mobility and bioavailability of pollutions in the environment and to prevent the contaminant migration caused by wind and water erosion [2].

In order to know which plant is best for phytoremediation it is very important to determine the concentrations of heavy metal from soil and from the parts of the plant. These data are employed in the determination of the bioaccumulation and the translocation factor which indicate the plant's capacity to remediate a contaminated soil by phytoextraction and phytostabilization. The bioaccumulation factor (BAF) is defined as the total element concentration in shoot tissue/total element concentration in mine tailings [1]. Pb bioaccumulation from shoot and soil can be calculated by the equation (1)[13]:

$$BAF=C_{\text{shoot}}/C_{\text{soil}} \quad (1)$$

where: C_{shoot} and C_{soil} are metal concentration in the plant shoot (mg/kg^{-1}) and soil (mg/kg^{-1}), respectively. BAF was categorized further as hyperaccumulators, accumulator and excluder to those samples which accumulated metals >1 mg/kg^{-1} , and < 1 , respectively [13, 14, 15].

The translocation factor (TF) or shoot/root (S/R) ratio is defined as the total element concentration in shoot tissue/total element concentration in root tissue [12]. Pb translocation from shoot to root can be measured by the equation (2), [13]:

$$TF = C_{\text{shoot}}/C_{\text{root}} \quad (2)$$

where: C_{shoot} and C_{root} are metals concentration in the shoot (mg/kg^{-1}) and root of plant (mg/kg^{-1}), respectively. $TF > 1$ represent that translocation of metals effectively was made to the shoot from root [13, 14, 16, 17, 18].

Plants with both factors >1 are suitable for phytoextraction while, plants with both factors <1 are suitable for phytostabilization [1].

The immobilization of lead was tested in experiments using different additives (lime, activated carbon, clay, zeolite, sand and cement) and artificially lead contaminated soil samples, according to the Toxicity Characterization Leaching Procedure (TCLP) developed by U.S. EPA [6]. Results showed that, activated carbon, clay, zeolite and sand are not very efficient for Pb immobilization. Lime and cement are significantly effective in Pb immobilization with 88% efficiency at 1:21 lime: soil ratio and 99% efficiency at 1:15 cement: soil ratio.

Otherwise, besides the importance of choosing the most suitable plant in phytoremediation, it has been found that another important aspect in the bioaccumulation of heavy metals from the soil in the plant is the addition of inorganic and organic substances. Microorganisms release CO_2 during their metabolism, which solubilize in soil water as HCO_3^- which produces CaCO_3 at high pH in presence of Ca^{2+} [19]. Precipitation of CaCO_3 can be enhanced by the addition of organic compounds rich in nitrogen because the microorganisms hydrolyze urea leading to the production of CO_3^{2-} at neutral/basic pH [20].

Thus, in order to improve the bioaccumulation and translocation of heavy metals from soil in plants, it is important to contribute to soil quality and fertility, lowering the mobility of metals and accelerating plant growth [21]. Numerous studies have shown that the plants of the *Acacia* family can be used successfully in phytostabilization of degraded lands, being a good ground fixer [22].

The aim of this paper was to determine the lead concentration from soil and sterile material samples collected from Almaşu Mare mining area in order to apply the most suitable technique of phytoremediation.

RESULTS AND DISCUSSION

Lead concentrations determined from soil samples were compared with the intervention thresholds established by the Romanian legislation [24]. The variation of lead concentration from the soil and sterile material samples taken from mining perimeter studied are highlighted in the figure 1, 2 and 3. The results obtained at the determination of the lead concentration of the sterile material samples taken from the three particular points are shown in Figure 1.

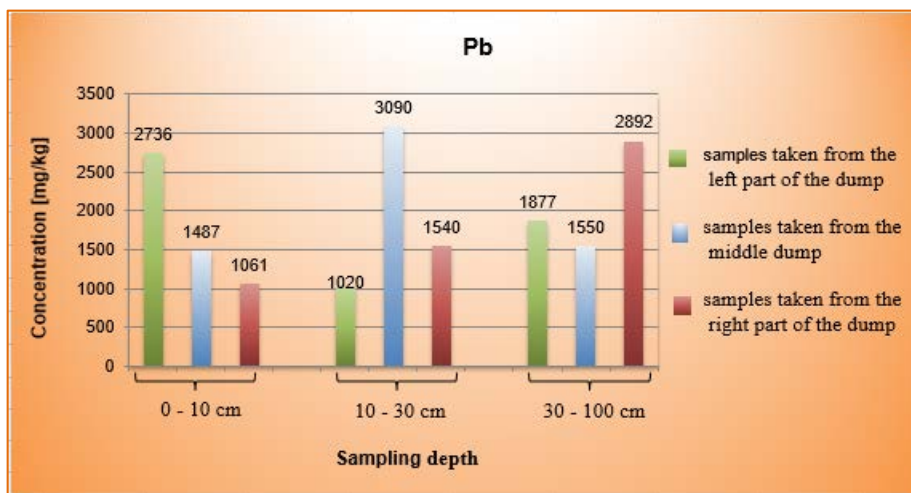


Figure 1. Lead concentrations present in samples taken from the surface of the “Radeș” dump

The analyzes performed on samples of sterile material collected from the left side of the “Radeș” dump showed that the Pb concentration on the first sampling layer (0 - 10 cm) was 2736 mg/kg, decreasing to a depth of 10-30 cm to 1020 mg/kg, and the third sampling layer (30-100 cm) increased to 1877 mg/kg. In the middle part of the dump, the Pb concentration was 1487 mg/kg on the first sampling layer, increased to 3090 mg / kg at 10-30 cm depth and the third sampling layer (30-100 cm) decreased again to 1550 mg/kg.

On the right side of the dump the lead concentration increased with the depth. The value at the depth of 0-10 cm was 1061 mg/kg 1540 mg/kg in the depth of 10-30 cm, and 2892 mg/kg at the depth of 30-100 cm.

The lead concentrations at the base of the dump are shown in Figure 2.

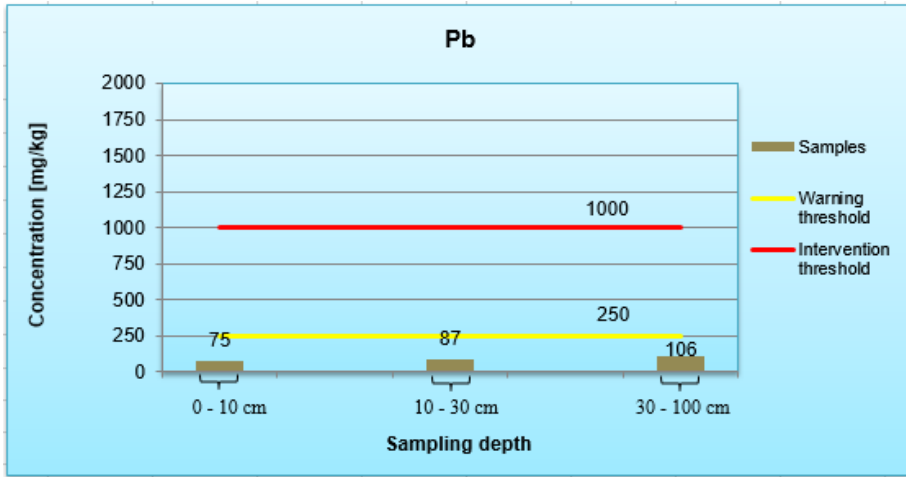


Figure 2. Lead concentrations present in samples taken at the base of the “Radeş” dump

At the base of the dump, the concentrations of Pb measured from the samples taken does not exceed the alert and intervention threshold.

Figure 3 highlights Pb concentrations upstream and downstream of the dump.

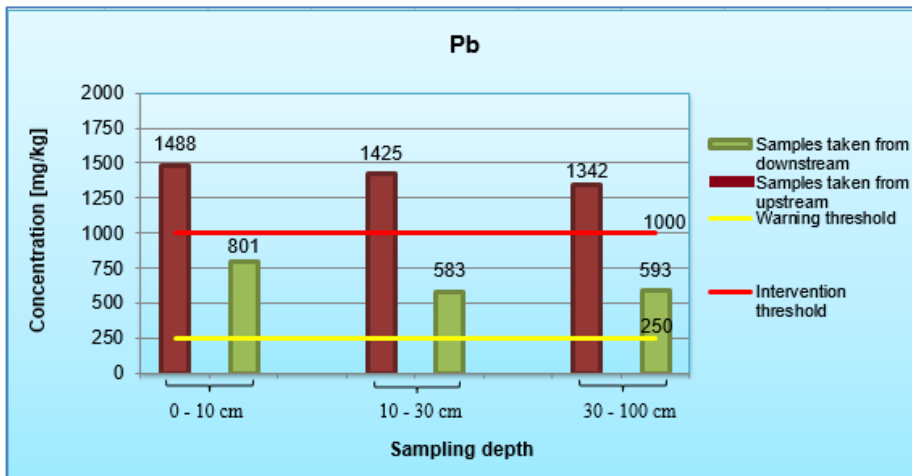


Figure 3. Lead concentrations present in samples taken from upstream and downstream of the “Radeş” dump

Upstream from the sources of pollution in the Almaşu Mare area, lead concentrations decrease with the depth and exceed the alert threshold of more than 4 times and the threshold for intervention at all sampling depths.

Downstream, Pb concentrations have fallen above the alert threshold, but are slightly lower compared to concentrations upstream from sterile dump.

CONCLUSIONS

The sterile dumps are considered to widespread contamination of the environment. On the surface of the "Rades" dump the lead concentrations resulted from the analysis performed showed values ranging from 1020 - 3090 mg/kg. At the base of the dump, the Pb concentrations measured did not exceed the intervention threshold. Upstream and downstream of the "Radeş" dump, Pb concentrations exceeded the intervention thresholds at all sampling depths. In this area it is necessary to apply remediation methods.

The most suitable phytoremediation technique that can be applied to the sterile dumps in the studied area is phytostabilisation. *Robinia Pseudoacacia* is suitable for use in phytostabilization of polluted soils because it has the capacity to absorb and agglomerate Pb concentrations in roots and around it.

EXPERIMENTAL SECTION

Study area

The investigation site is located in the Almaşu Mare village, in the southern outskirts of the Apuseni Mountains from Romania, in the subunit of Metaliferi Mountains, bordering the town Zlatna and Alba County [23]. The total area of this village is 9330 ha. Since 1900, in this area were performed mining activities which are making their presence felt even today through the enormous quantities of mining waste deposited inappropriately and through the waste water which flows into the rivers due to rainfall over them. The "Radeş" sterile dump is located in Almasu Mare village (Figure 4) and stretches over a distance of 100 m, with a height of 30 m. In the front of dump, at 50 m away is "Radeş" mine and at 5 m distance is the Ardeu stream that flows into the Ampoi River.

This dump is not subject to conservation or reforestation process, it being still below the target mining strategy for the period 2008-2020 which aims to restore the environment affected by mining. The people and their households are very close to this dump at no 2 m from it. This fact this represents a source of risk and negative impact on human health [25].

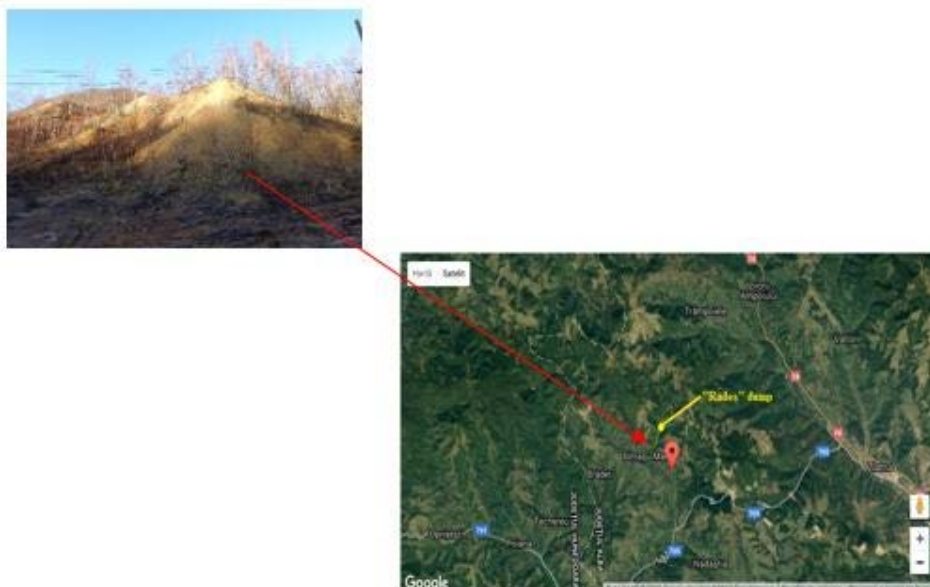


Figure 4. The image of the study area

Sampling and analyzing

In order to evaluate the quality of soil in the Almaşu Mare mining area were collected nine samples of soil and waste material from three different points (the dump “Radeş”, upstream dump and downstream of it) at the following depths: 0-10 cm, 10-30 cm and 30-100 cm.

Soil sampling was performed in November, 2016 and analysis of heavy metals concentrations from samples was performed in the Laboratory of soil quality analysis and depollution processes at the Technical University of Cluj Napoca by Atomic Absorption Spectrometry (AAS) using a SHIMADZU AA-6800 spectrometer.

The preparation of samples for analysis consisted of the following: the moist soil and sterile material was crumbled, dried at 40 °C, sieved and milled. Prior analyzing heavy metal content, 3 g of prepared samples were placed in a 100 beaker with 21 ml of HCl concentrated and 7 ml of HNO₃ concentrated. Then, the glasses were covered with glass plate and left for mineralization. After these, samples were filtered and analyzed for heavy metal content. Reference solutions for calibration, were also prepared using analytical grade chemicals and deionized water.

ACKNOWLEDGMENTS

The authors gratefully acknowledge the financial support provided by the Romanian National Authority for Scientific Research, CNCS – UEFISCDI, under grant no. PN-II-PT-PCCA-2013-4-1717.

REFERENCES

1. A. Buscaroli, *Ecological Indicators*, **2017**, *82*, 367.
2. M. Boroş, V. Micle, *Scientific Papers. Series E. Land Reclamation, Earth Observation & Surveying, Environmental Engineering*, **2014**, *Vol. III*, 2285.
3. L. Wang, B. Ji, Y. Hu, R. Liu, W. Sun, *Chemosphere*, **2017**, *Vol. 184*, 594.
4. I.M. Sur, V. Micle, T. Gabor, *Studia UBB Chemia*, **2016**, *LXI*, 3 (2), 364.
5. V. Farkas, A. Hegedúsova, S. Jakabova, C. Majdik, T. Pernyeszi, *Studia UBB Chemia*, **2011**, *56(2)*, 65.
6. B. Alpaslan, M. Ali Yukselen, *Water, Air and Soil Pollution*, **2002**, *133(1–4)*, 253.
7. G.A. Seilkhanova, A. N. Imangaliyeva, D.N. Akbayeva, Z.Z. Kenzhalina, *Studia UBB Chemia*, **2017**, *62(1)*, 35.
8. E.B. Culbard, I. Thornton, J. Watt, M. Wheatley, S. Moorcroft, M. Thompson, *Journal of Environmental Quality*, **1988**, *17*, 226.
9. J. Watt, I. Thornton, J. Cotter-Howells, *Applied Geochemistry, Supplementary*, **1993**, *2*, 269.
10. A.A. Juwarkar, A. Nair, K.V. Dubey, S.K. Singh, S. Devotta, *Chemosphere*, **2017**, *68(10)*, 1996.
11. A. Mahar, P. Wang, A. Ali, M. K. Awasthi, A.H. Lahori, Q. Wang, R. Li, Z. Zhang, *Ecotoxicology and Environmental Safety*, **2016**, *126*, 111.
12. R.R. Brooks, *Microbiology, Archaeology, Mineral Exploration and Phytomining. CAB International*, Wallingford, Oxford, UK, **1998**, 384.
13. M. Rezvani, F. Zaefarian, *Australian Journal of Agricultural Engineering*, **2011**, *2(4)*, 114.
14. L.Q. Ma, K.M. Komar, C. Tu, W. Zhang, T. Cai, E.D. Kenelly, *Nature*, **2001**, *409*, 579.
15. C. Cluis, *Biotech J.*, **2004**, *2*, 60.
16. A.J.M. Baker, R.R. Brooks, *Biorecovery*, **1989**, *1*, 81.
17. W.H. Zhang, Y. Cai, C. Tu, Q.L. Ma, *Science of the Total Environment*, **2002**, *300*, 167.
18. A.Q. Fayiga, L.Q. Ma, *Science of the Total Environment*, **2006**, *359*, 17.
19. J.M. Arocena, V.J.M. Mourik, A. Faz-Cano. *Canadian Journal of Soil Science*, **2012**, *Vol. 92*, 243.
20. K. Rowshanbakht, M. Khamehchiyan, R.H. Sajedi, M.E. Nikudel, *Ecological Engineering*, **2016**, *Vol. 89*, 49.

21. R. Zornoza, M. Gómez-Garrido, S. Martínez-Martínez, M. Dolores, G. López, Á. Faz, *Science of the Total Environment*, **2017**, Vol. 593 - 594, 357.
22. R. Budău, I. A. Timofte, N. Kopacz, *Annals of the University of Oradea, Faculty of Environmental Protection*, **2014**, Vol. XXIII, 337.
23. S. Varvara, M. Popa, R. Bostan, G. Damian, *Journal of Environmental Protection and Ecology*, **2013**, 14 (4), 1506.
24. ORDER 756/1997 published in *Monitorul Oficial* 303 from 06.11.1997, modified by Order 592/2002 published in *Monitorul Oficial* from 21.10.2002.
25. *Mining Industry Strategy in Romania 2008-2020*.

IN VITRO TESTING OF A POLYLACTIC POLYMER SYNTHESIZED FROM WHEY

ALEXANDRA DREANĂ^a, RADU A POPESCU^{a, b}, AMALIA NEAGU^a,
GEORGE ENACRACHI^a, IULIA CIMPOEȘ^a, NICODIM FIȚ^a,
MARIOARA MOLDOVAN^{c*}, LAURA SILAGHI DUMITRESCU^b,
ANCA JURJ^d, IOANA BERINDAN-NEAGOE^d, IOAN MARCUS^a

ABSTRACT. The main purpose of this research is *in vitro* biocompatibility testing of a polylactic acid polymer (PLA) synthesized by the condensation of lactic acid separated from whey (Zonar). The experimental PLA obtained was characterized by: Scanning Electron Microscopy which pointed a homogeneous microstructure of the polymer without a separation phase and differential scanning calorimetry (DSC) analysis which indicated a melting point of 174°C of the biomaterial. The cytotoxicity test for experimentally obtained polymer was performed according to ISO 10 993 -12³. Six solutions of different concentrations were prepared (30 mg/ml, 20 mg/ml, 10 mg/ml, 5 mg/ml, 2.5 mg/ml and 1.25 mg/ml) and were tested on a fibroblast culture at 48 hours using MTT cell viability and proliferation assay. At 48h the obtained polylactic polymer showed good compatibility with an IC 50 of 64.82 mg/ml. The results showed that the cytotoxicity level can be influenced by the period of time in which the extract acts on the cell culture.

Keywords: *whey, polylactic acid, cytotoxicity, biocompatibility, eco-friendly*

INTRODUCTION

Whey is a waste product of dairy industry, with numerous valuable ingredients such as proteins, minerals, vitamins and lactose. Global dairy production is estimated at 160 million tones liters / year, of which about 50%

^a *University of Agricultural Sciences and Veterinary Medicine, Faculty of Veterinary Medicine, No.3-5 Calea Manastur str.,400372 Cluj-Napoca, Romania*

^b *Babeș-Bolyai University, Interdisciplinary Research Institute on Bio-Nano-Sciences, Nanostructured Materials and Bio-Nano-Interfaces Center, 400271, Cluj-Napoca, Romania*

^c *Babeș-Bolyai University, Raluca Ripan Chemistry Research Institute, Cluj-Napoca, Romania*

^d *Iuliu Hațieganu University of Medicine and Pharmacy, Faculty of Medicine, Institute of Molecular Biology, Cluj-Napoca, Romania*

* *Corresponding author: mmoldovan2004@yahoo.com*

is produced in EU Member States [1]. In Romania, the annual whey production was estimated to 300 million liters in 2013 [2]. Zonar [3] is a sweet whey beverage with an ecological and medicinal purpose. Beyond its direct applications in the food and pharmacological fields, lactose is a valuable raw material for processing by fermentation or chemical transformation [3]. Due to its high content in lactose (4.82g/100ml), whey (Zonar) processing takes a biotechnological innovative direction of lactic acid production [4]. Through chemical synthesis, the production of lactic acid is developed using waste products from food industry and agricultural production [5]. Among these potential sources are: starch materials (potatoes, wheat, corn, etc.), waste products (whey, molasses) and cellulose products (rice, corn straw, wheat, etc.). Lactic acid is used in the production of polylactic polymers [5, 6].

Polylactic acid (PLA) and its copolymers have a wide range of applications in fields such as: biomedicine, pharmacy, food industry, packaging [7]. Polylactic acid is an aliphatic polyester derived from exclusively renewable sources [8]. It is an ideal material, suited for many applications, such as: packaging, paper coating, fibers, films, molded articles, etc. Polylactic polymers, due to their exceptional properties are the most used medical devices in various fields: orthopedics, delivery systems, tissue regeneration. PLA may be implemented in tissue engineering applications such as: scaffolds, autografted skin, wound covers, stents, anastomose systems [9]. Polymers based on lactic and glycolic acids could be a great choice to substitute traditional metallic or ceramic materials [10].

The synthesis of PLA may be achieved by three polymerization routes: condensation (generating low molecular weight PLA), ring opening polymerization and chemical catalysis respectively (which are producing high molecular weight PLA) [11,12], completed by numerous studies reporting progresses in the methods development as well as mechanical, physical and chemical properties of the polymer. It is known that the mechanical and crystallization behavior of PLA is dependent on the molecular weight and the stereo chemical makeup of the backbone [13].

Polylactic acid production offers advantages such as renewable resources, biocompatibility, processability and energy saving [7, 9]. Biocompatibility is the most attractive property of PLA with respect to the biomedical field [14]. PLA *in vivo* is not toxic, nor has any carcinogenic effects in tissues [10]. Polylactic polymer degradation occurs by hydrolysis in living organisms and by thermal activation in nature [7]. The degradation products are water and dioxide carbon, which are non-toxic products further metabolized by cells. Biocompatibility and biodegradability offer a broad spectrum of applications in many different areas including regenerative medicine.

The aim of this research was the *in vitro* biocompatibility testing of a polylactic polymer synthesized from whey (Zonar) in comparison with a commercial PLA. The study also described physical properties of the experimental sample by scanning electron microscopy and calorimetric analysis. Additionally, the sterilization capacity of UV light on solid commercial and experimental polymer was determined.

RESULTS AND DISCUSSION

Some of the physico-chemical properties of polymeric biomaterials, which may have an effect on their biocompatibility include: chemical properties, hydrophilicity/hydrophobicity, molecular weight, solubility, water absorption, shape and structure, degradation and erosion mechanism.

Scanning electron microscopy

SEM images have revealed that the synthesis polymer displayed good morphology. A homogeneous microstructure of the polymer was noticed, without a separation phase (Fig. 1), unlike a previous study where it was stated that neat PLA undergoes a brittle fracture and only a combination between PLA and another polymer was capable to ensure a smooth and homogenous microstructure [15]. Another study demonstrated that pure PLA scaffolds had a honeycomb surface with a microporous structure. It also showed that the polymers surface structure influences the biologic activity (adhesion, migration and proliferation) of cultured cells [16]. Additionally, other studies stated that micro particles or nanoparticles made of low molecular PLA had smooth and non-porous surface [17]. Microspheres of PLA or other PLA blends presented no signs of collapse [17]. It was found that the polymer type and molecular weight did not affect the morphology of the micro or nanoparticles [18], suggesting that our material is a good candidate for future composite biomaterial synthesis.

Thermal analysis investigation

Auras et al, 2004 stated that the crystallization formation of PLA depends on thermal history and stereochemistry [19]. Studies showed that polymers melting temperature increases directly proportional with its PLLA content. Our synthesis polymer has PLLA stereochemistry. The DSC analysis revealed a melting point of 168°C and commercial PLLA of 174°C (Fig. 2).

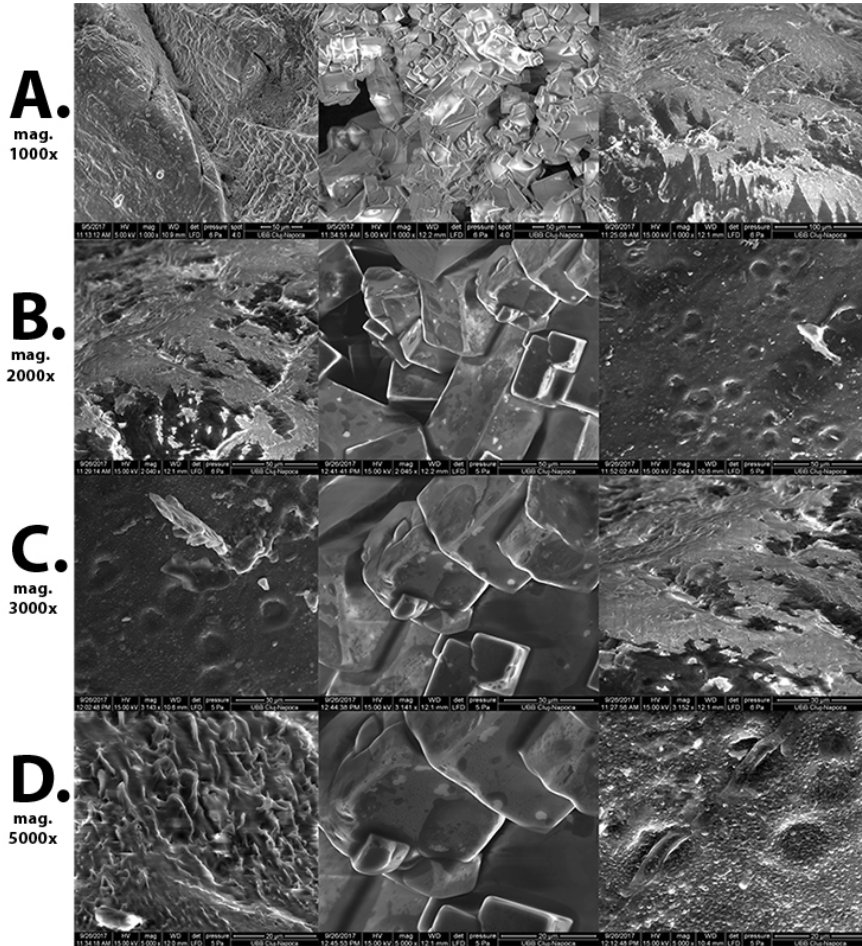


Figure 1. SEM micrograph of the poly(lactic acid) polymer after chemical engineering process.

The thermal behavior, specifically the melting point of the newly synthesized PLA was similar with results from previous studies, where the melting temperatures of PLA obtained through polycondensation were between 173-178°C [9]. Additionally, authors stated that PLLA thermal and mechanical properties were higher than other stereoisomeric ratios [20]. Another thermal investigation showed a melting point of 127°C for low molecular PLA [21]. Palacio et al, 2011 stated that the thermal behavior of low molecular PLA and high molecular PLA are similar, but low molecular PLA starts to decompose at lower temperature than the high molecular one [21].

Cell viability

The mitochondrial dehydrogenase performance measurement is a rapid assessment of cell proliferation and cytotoxicity [17]. The MTT assay is currently the most used method to test cytocompatibility of medical devices. Our study revealed that both, experimental and commercial polymer showed a good cytocompatibility (Fig. 3, Fig. 4). Only control cells treated with DMSO showed a decrease in viability (51.89%) in comparison with the control and all the other concentrations. The cells viability treated with extract from the commercial polymer showed a slight decrease at the concentration of 20 mg/ml (82%) ($p < 0.01$) in comparison to the control. However, this decrease was not under 80%, showing thus a good cytocompatibility (Fig. 3). The percentage of cellular viability was above 89% for all the tested extract concentrations from the experimental polymer. Moreover, cells treated with concentrations of 20 mg/ml, 10 mg/ml, 5 mg/ml and respectively 1.25 mg/ml showed an increase in cell viability, exceeding 100%, indicating that these concentrations promoted cell proliferation (Fig. 4). Additionally, the low cytotoxicity of the experimental PLA was demonstrated by calculating the IC 50 of the extract (Fig. 5). It showed that a concentration of 64.82 mg/ml or a higher concentration could reduce the number of viable cells at half. The results of the research were comparable to a previous study, in which it was reported that PLA scaffolds were biocompatible at 24, 48 and 96 hours [16], demonstrated by MTT test and also by direct contact test, showing cell adhesion and migration on the scaffold. Similar results to our study were reported by Vergnol et al, 2015 as well [24]. Good biocompatibility of PLA composites was demonstrated using Presto Blue assay at 6 and 10 days after incubation, although the authors stated that cell viability decreased with the increase of the concentration of the extract [24]. Even PLA nanoparticle formulations were found to be non-toxic in the concentrations studied. Cell viability was between 80% and 120% after treatment with different concentrations of PLA nanoparticles extract [18]. The MTT test was declared a useful method for measuring the subtle toxicity of biomaterials, regarding cell metabolism and functions, even if cells do not die in 24-72 hours, the usual time for a cytotoxicity test. Biomaterials display different rates of toxicity, being cytostatic, affecting a cell function or damaging a whole cell compartment [25]. The results of the current study have proved that the cytotoxicity level of PLA can be determined by the period of time in which the polymers extract acts on the cell culture. In addition, the cellular viability can be affected by the method used to obtain PLA and by the compounds used in the lactic acid extraction process [24]. When aqueous extracts of the biomaterials are used, they seem

to provide suitable samples of potentially hazardous substances that may leach out from a device [26]. According to the previous statement, the synthesis method used to create the polylactic polymer from ZONAR is safe and reliable. Also, according to our data both polymers, commercial and experimental, showed no toxicity, the cellular viability being unaffected.

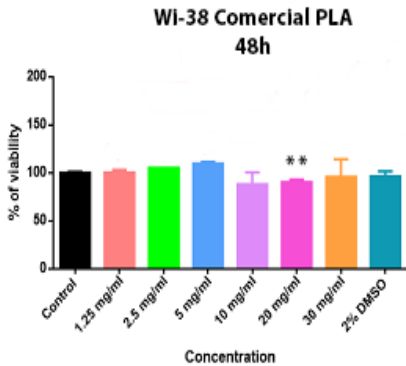


Figure 3. Cytotoxicity assessment of commercial PLA extract using MTT assay on fibroblasts cells at 48 hours, ** $p \leq 0.01$.

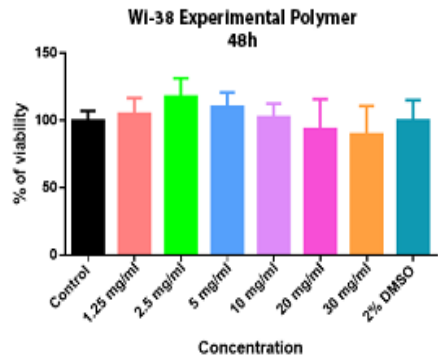


Figure 4. Cytotoxicity assessment of experimental PLA extract using MTT assay on fibroblasts cells at 48 hours.

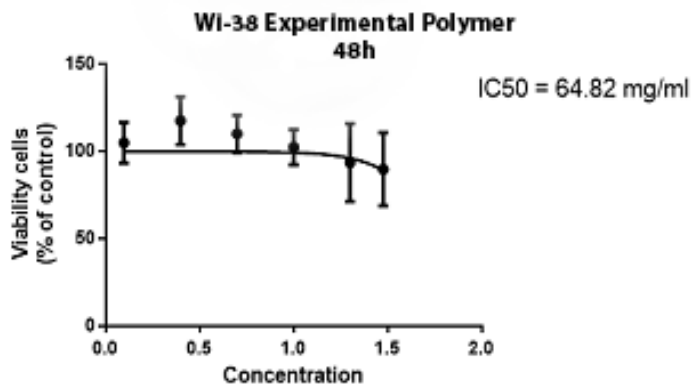


Figure 5. Assessment of the IC 50 on viability of fibroblasts cells after treatment with PLA extract at 48 hours.

CONCLUSIONS

Extracting lactic acid from whey (ZONAR) and converting it into PLA represents an innovative & promising technology, providing biomaterials for many economical fields. The poly-L lactic polymer synthesis from the whey Zonar is a reliable & eco-friendly process, able to provide a low molecular polymer fulfilling 3 essential features, such as nontoxicity, renewability and high biocompatibility.

EXPERIMENTAL SECTION

Samples synthesis

For Synthesis of lactic acid by fermentation, we used whey (Zonar SC Embrion, Satu Mare, Romania), molasses (Tereos Romania, Ludus), and Ecoflorina (*Lactobacillus bulgaricus*) to pH= 5,0-6,0, temperature 44-45°C and the lactic acid polymerization, was done by polycondensation.

Commercial PLA A commercial PLLA was purchased from Sigma Aldrich, with the following characteristics: Lot: BCBP2966V, 81273-10G, molecular weight: 260 000, viscosity: 2.0 dl/g.

Material characterization

Scanning electron microscopy

The experimental PLA obtained was characterized by: Scanning Electron Microscopy (SEM-Inspect S, FEI Company), with an acceleration voltage of 15 kV in order to observe the biomaterials surface.

DSC analysis

A differential scanning calorimetry (DSC) analysis using a Mettler Toledo DSC 823e/700 °C was performed, in order to obtain the melting point of the biomaterial.

Sterility test

Samples of the experimental and standard polymer were placed in glass recipients and sterilized through UV light, for 24 hours. A microbiological test was performed in order to assess the sterilization capacity of UV light. The method used was the indirect method for the evaluation of the total germ number (ufc) on solid medium for mesophilic germs. It was considered that each colony on the surface of the testing medium was the result of the multiplication of one bacteria [27]. Both products have been included in 0.1 ml

sterile nutrient broth. The solution was subsequently passed in the Petri dishes with the Muller Hinton agar by flooding method. The samples were incubated at 37^o C and then evaluated at 24, 48 and 72 hours.

Cell viability – The in vitro test for cytotoxicity was performed according to International Organization for Standardization (ISO) - ISO 10993-5 " Test for in Vitro Cytotoxicity [28].

Polymer extract. The extracts for the experimental and commercial polymer regarding the cytotoxicity test was performed according to ISO 10 993-12 "Sample Preparation and Reference materials" [29].

Cell culture For the experiment were used human fibroblast cell line, Wi-38. Wi-38 cell line was cultured in Gibco® MEM Medium, supplemented with 10% Fetal bovine serum (FBS - Gibco®), 2 mM L-glutamine (Gibco®), MEM-NEAA (MEM Non-Essential Amino Acids Solution (100X) - Gibco®) and 1% Penicillin-Streptomycin. Cells were incubated in a 5% CO₂ incubator at 37°C.

MTT assay Cell survival was assessed using MTT assay. Adherent cells were cultivated at sub confluence before being washed twice with phosphate-buffered saline (PBS 1X). After trypsinization, cells were resuspended in culture medium with FBS 10%, counted and seeded for the experiments. A number of 10⁴ cells were seeded in 96-well plate and incubated for 24 hours. After incubation, cells were treated with the experimental polymer obtained through synthesis and with the extract from the commercial PLA, using six solutions of different concentrations, respectively 30 mg/ml, 20 mg/ml, 10 mg/ml, 5 mg/ml, 2.5 mg/ml and 1.25 mg/ml. The cell viability was related to the negative control wells. DMSO was used for positive cytotoxic control. For each concentration of the extract, the test was performed in triplicate. The proliferation activity of the cells was evaluated after 48 hours using MTT (Thiazolyl Blue Tetrazolium Bromide, Sigma-Aldrich, Germany) test. Cells were incubated for 3 hours with 150 µl MTT and the metabolized formazan salt was resolubilized in 100 µl DMSO, incubated for 10 minutes on a shaker. Afterwards, we read the absorbance at 570 nm with a multi-plate spectrophotometer BioTek Synergy.

Statistical analysis

All data is reported as mean ± SD from the experiment performed on triplicate samples. The differences between experimental conditions and controls were analyzed using T test. Statistical significance was at p<0.05 (95% confidence interval). Statistical values and figures were obtained using GraphPad Prism version 6.0 for Windows, GraphPad Software, San Diego California USA. Cell viability was determined as a percentage of the negative control (untreated cells).

ACKNOWLEDGMENTS

This work was supported by a grant of the Romanian National Authority for Scientific Research and Innovation, "CNCS/CCCDI – UEFISCDI, project number PN-III-P2-2.1-BG-2016-0335, within PNCDI III". The authors wish to thank associate professor doctor Lucian Baia and CSIII Klara Magyari from the Institute on Bio-Nano-Sciences for providing commercial polylactic acid and advice in terms of physical characterisation.

REFERENCES

1. P.M.R. Guimarães, J.A. Teixeira, L. Domingues, *Biotechnology Advances*, **2010**, 28, 375.
2. www.wheyeurope.com
3. C. Spalatel, *Innovative Romanian Food Biotechnology*, **2012**, 10, 1-8.
4. P.S. Panesar, J.F. Kennedy, D.N. Gandhi, K. Bunko, *Food Chemistry*, **2007**, 105, 1.
5. S. Maslanka, M. Siolek, L. Hamryszak, D. Lopot, *Chemik*, **2014**, 68(8), 703.
6. S. Maslanka, A. Kos, M. Bankzyk, I. Kzopek, L. Adam, *Chemik*, **2015**, 69(4), 241.
7. L. Xiao, B. Wang, G. Yang, M. Guthier, *Biomedical Science, Engineering and Technology*, **2012**, 11, 248.
8. R.E. Drumright, P.R. Gruber, D.E. Henton, *Advanced materials*, **2000**, 12(23), 1841.
9. S.M. Davachi, B. Kaffashi, *Polymer-Plastics Technology and Engineering*, **2015**, 54(9), 944.
10. M.S. Lopez, A.L. Jardini, R. Maciel Filho, *Procedia Engineering*, **2012**, 42, 1402.
11. A.J.R. Lasprilla, G.A.R. Martinez, B.H. Lunelli, J.E.J. Figueroa, A.L. Jardini, R. M. Filho, *Chemical Engineering*, **2011**.
12. L.T. Lima, R. Auras, M. Rubino, *Progres in Polymer Science*, **2008**, 33, 820.
13. D. Garlotta, *Journal of Polymers and the Environment*, **2001**, 9(2), 63.
14. S. Farah, D.G. Anderson, R. Langer, *Advanced Drug Delivery Reviews*, **2016**, 2.
15. V.S. Giita Silverajah, A.I. Nor, Z. Norhazlin, Y. Wan Md Zin Wan, A.H. Hazimah, *Molecules*, **2012**, 17, 11729.
16. S. Shi, X.H. Wang, M. Fan, M.J. Huang, Z.Y. Qian, *International Journal of Nanomedicine*, **2010**, 5, 1049.
17. S. Zhou, X. Deng, X. Li, W. Jia, L. Liu, *Journal of Applied Polymer Science*, **2004**, 91, 1848.
18. A. Basarkar, D. Devineni, R. Palaniappan, J. Singh, *International Journal of Pharmaceutics*, **2007**, 343, 247.
19. R. Auras, B. Harte, S. Selke, *Macromolecular Bioscience*, **2004**, 4, 835.

20. T.M. Quynh, H. Mitomo, M. Yoneyama, N.Q. Hien, *Polymer Engineering and Science*, **2009**, 49(5), 970.
21. J. Palacio, V.H. Orozoco, B.L. Lopez, *Journal of Brazilian Chemical Society*, **2011**, 22(12), 2304.
22. www.tainstruments.com
23. M. Silindir, A.Y.Ozer, *Fabad Journal of Pharmaceutical Sciences*, **2009**, 34, 43.
24. G. Vergnol, N. Ginsac, P. Rivory, S. Meille, J.M. Chenal, S. Balvay, J. Chevalier, D.J. Hartmann, *Journal of Biomedical Materials Research Part B*, **2015**, 00B:000-000.
25. G. Ciapetti, E. Cenni, L. Pratelli, A. Pizzoferrato, *Biomaterials*, **1993**, 14(5), 359.
26. L.S. Desai, L. Lister, *Toxikon Advancing your innovation*, 1-19 www.toxikon.com
27. USP 40, 61, 1-7
28. International Organization for Standardization, ISO 10993-5, 2009, 1-34.
29. International Organization for Standardization, ISO 10993-12, 2004, 1-20.

PALLADIUM AND RUTHENIUM DERIVATIVES STABILISED BY BIS-SULFONE LIGAND

NOÉMI DEAK^{a,b}, RALUCA SEPTELEAN^a, IONUT-TUDOR MORARU^a,
SONIA MALLET-LADEIRA^c, DAVID MADEC^{b*}, GABRIELA NEMES^{a*}

ABSTRACT. The synthesis and characterization of new palladium and ruthenium derivatives using the bis-sulfone 1,3-bis{(4-methylphenyl)sulfonyl}-5-tert-butylbenzene ligand is presented. The new compounds were characterized in solution by multinuclear NMR spectroscopy and for the palladium derivative the molecular structure in solid state was also determined by single crystal X-ray diffraction. The work was completed with a DFT study in order to better understand the electronic effect in the stabilization of the new complexes containing *bis*-sulfone ligand.

Keywords: *bis-sulfone, palladium and ruthenium derivatives, NBO analysis*

INTRODUCTION

Inorganic and organometallic chemistry developed significantly in the last period, mainly due to the possibility to control the properties of designed compounds by using versatile ligands with modulated structures connected to the central atom.

Structural modifications of the ligand backbone and its functional groups allowed access to a large number of compounds whose properties change depending on the connection mode to the metal atom.[1–4] Additionally, the metallic center plays also an important role in the properties of the new compounds; this fact must to be considered at the design of new species. It is well known that organometallic derivatives containing a transition metal

^a *Universitatea Babeş-Bolyai, Facultatea de Chimie și Inginerie Chimică, str. Arany Janos, nr. 11, RO-400028, Cluj-Napoca, Romania.*

^b *Université de Toulouse, UPS, LHFA, 118 Route de Narbonne, F-31062 Toulouse, France, CNRS, LHFA, UMR 5069, F-31062 Toulouse Cedex 9, France.*

^c *Institut de Chimie de Toulouse, FR2599, Université Paul Sabatier, UPS, 118 Route de Narbonne, F-31062 Toulouse Cedex 9, France.*

* *Corresponding authors: sgabi@chem.ubbcluj.ro, madec@chimie.ups-tlse.fr*

are used mainly in various catalytic processes[5,6] as compounds with biological activity[7–10] or used as building blocks for obtaining of inorganic polymers or supramolecular structures,[6,11–14] these important applications being the reason for significant developments of this field of chemistry in the last period. There are numerous examples of palladium and ruthenium complexes obtained with different ligands whose coordination modes determine not only the stability of the species but also the chemical properties they display. Among the large variety of ligands used for these complexes are for example different phosphines,[15] sulfoxides,[16] Schiff bases[17] or pincer ligands.[13,14,18–20]

Furthermore, the preparation of ligands with properties modulated by the presence of several functional groups like: metallylenes,[21–23] oxathia- derivatives,[24] germil-aminophosphoric esters,[25] phophaalkenyl derivatives[26–28] or organometallic halogenated derivatives[29–31] as well as their study for the stabilization of transition metals derivatives of palladium, ruthenium, gold, tungsten, etc., is a continuous concern in our team.

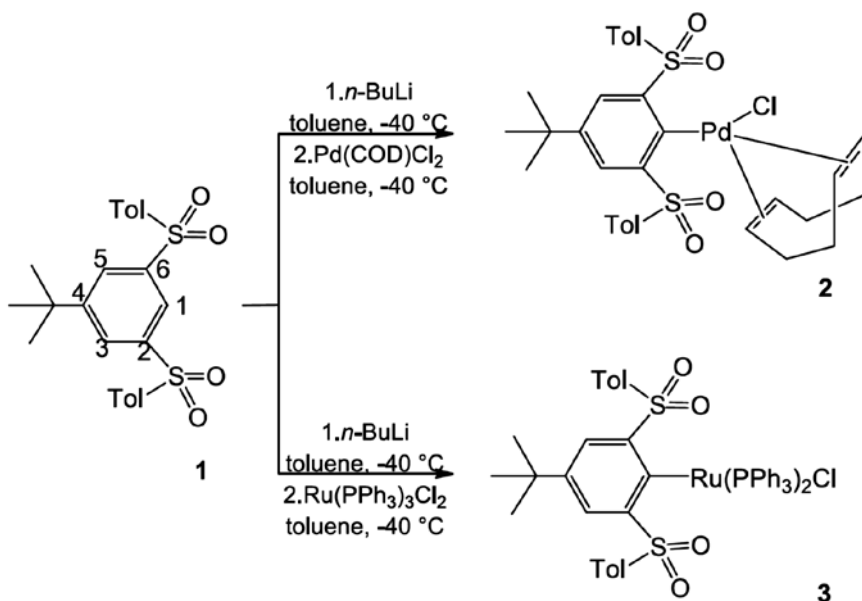
Recently, we highlighted the utility of the bis-sulfone ligand 1,3-bis{(4-methylphenyl)sulfonyl}-5-tert-butylbenzene, containing two sulfonyl groups, as a pincer ligand for the stabilization of metallylenes and their transition metal compounds and cycloadducts.[32,33] In order to evaluate the properties and stability of organometallic derivatives containing a heavy *p-block* element or transition metal, additionally the effect induced by a ligand containing sulfonyl groups was studied. It's worth mentioning that in the literature there are several examples for transition metal containing derivatives stabilized by sulphur based, sulfonyl or sulfinyl containing ligands, where the transition metal is bonded either through the coordination of the sulphur or the oxygen atom,[16,34–37] however, there are only a few examples for such compounds containing a bis-sulfonyl ligand.[37]

Herein, we present the results obtained with the before mentioned bis-sulfone ligand in the synthesis of new palladium and ruthenium derivatives.

RESULTS AND DISCUSSIONS

The 1,3-bis{(4-methylphenyl)sulfonyl}-5-tert-butylbenzene ligand, hereafter named bis-sulfone **1**, was synthesized according to the previously described procedure.[32] For this study, compound **1** was tested to obtain transition metal complexes with the aim to further investigate the connection ability of **1** towards transition metals. The synthetic pathway to obtain the palladium and ruthenium derivative is shown in Scheme 1.

In the case of both palladium **2** and ruthenium **3** derivatives, the ^1H NMR spectra indicate the formation of the new compounds by the disappearance of the signal for the H1 proton from bis-sulfone **1** (Scheme 1) at 8.90 ppm. The signals for the *ortho* protons of the tolyl groups are downfield shifted to 8.55 ppm for palladium complex **2** and to 8.61 ppm for ruthenium complex **3** from 7.82 ppm in bis-sulfone **1**, while an upfield shift can be observed for the signals corresponding the *meta* protons H3 and H5 of the central aromatic ring to 8.06 ppm for palladium complex **2** and 7.32 ppm for ruthenium complex **3** from 8.25 ppm in bis-sulfone **1**. For the palladium complex **2** in the ^1H NMR spectrum signals at 2.48, 2.81 ppm and 5.44, 6.38 ppm can be seen, suggesting that the cyclooctadiene is still linked to the metal center. In the case of the ruthenium complex **3**, the signals at 6.87-7.03, 7.84, 7.55 ppm corresponding to 30 protons indicate the presence of two triphenylphosphine groups bonded to the ruthenium atom.



Scheme 1. Synthesis of palladium complex **2** and ruthenium complex **3**

The $^{31}\text{P}\{\text{H}\}$ NMR of the ruthenium derivative **3** presents two doublet signals at 52.3 ppm ($^2J_{\text{P-P}}=23.39$ Hz) and 25.4 ppm (d, $^2J_{\text{P-P}}=23.45$ Hz), also confirming that two triphenylphosphine groups are linked to the metal. The ^{13}C NMR data for both derivatives **2** and **3** support these observations. All the NMR data are presented in the experimental part.

Crystals of palladium complex **2** were obtained by diffusion of pentane in dichloromethane solution and were analyzed by single crystal X-ray diffraction; the solid state molecular structure of compound **2** is shown in Figure 1.

The solid state molecular structure confirms the formation of the complex, where the palladium atom is linked to the C1 carbon atom of the bis-sulfone ligand. It also confirms the structure deduced from the ^1H and ^{13}C NMR spectra, that not only a chlorine atom is linked to the palladium atom, but also the cyclooctadiene group remains coordinated.

The palladium atom is four coordinated, with the usual square planar geometry. The geometrical features are in agreement with values from the literature for other palladium complexes with similar ligands.[13,14,19,20] The tolyl groups are situated on the same side of the central aromatic ring, not on opposite sides, as seen in the case of the previously reported metallylenes, as a consequence of the steric hindrance of the cyclooctadiene group. This effect was also observed in the previously reported transition metal complexes of the metallylenes.[32]

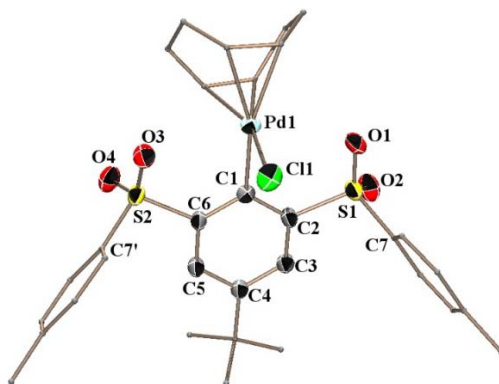


Figure 1. Molecular structure of compound **2** the solid state (50 % probability level for the thermal ellipsoids). For clarity, hydrogen atoms are omitted, tolyl and *t*-butyl and cyclooctadiene groups are simplified. Selected bond distances [Å] and bond angles [deg]: S1-O1 1.433(4), S1-O2 1.450(4), S2-O3 1.440(3), S2-O4 1.422(4), Pd1-C1 2.004(5), Pd1-Cl1 2.343(2), C1-Pd1-Cl1 86.04(14), C2-S1-C7 105.7(2), C6-S2-C7' 106.1(2), Pd1-C1-C2 122.7(3), Pd1-C1-C6 122.1(3)

The distance O1-Pd1 is 2.803(4) Å, while O3-Pd1 is 2.806(3) Å, values almost equal and significantly larger than the sum of the covalent radii of the Pd and O atoms (2.05).[38–40] The C1-Pd1, S1-O1, S2-O3 bonds are situated roughly in the same plane with the central aromatic ring (S1-O1 0.074 Å, S2-O3 0.277 Å out of the plane), arrangement favorable for interaction between the oxygen and palladium atoms. However, interaction

cannot be possible because of the presence of the cyclooctadiene group, thus in this case the bis-sulfone ligand **1** does not function as a pincer ligand as in the case of the previously reported metallylenes and their transition metal derivatives.

Furthermore, the oxygen atoms being a hard donor while the palladium atom a soft one, also effects the formation a coordinative bond. However, in the literature, a few examples can be found where an oxygen atom coordinates to a palladium atom.[20] The molecular structure of palladium compound **2** was additionally analyzed through DFT calculations. The calculated lengths of selected Pd-C (2.023 Å), Pd-Cl (2.353 Å) chemical bonds are in agreement with the solid-state data, as well as the Pd-O distances (2.855 Å and 2.867 Å). For the two $\eta^2(\text{C}=\text{C})\rightarrow\text{Pd}$ coordinative bonds, the distances between the palladium atom and the centroids of the C=C bonds, have calculated values of 2.179 Å for the one oriented in *trans* with respect to the Pd-Cl bond, and of 2.290 Å for the other one. These lengths indicate strong interactions between the palladium atom and cyclooctadiene group.

NBO calculations, carried-out on the optimized structure of species **2**, revealed also strong $\eta^2(\text{C}=\text{C})\rightarrow\text{Pd}$ interactions. According to these calculations, the energy corresponding to the short (C=C) \rightarrow Pd coordinative bond (with calculated length of 2.179 Å) was computed to be around 78 kcal/mol, with about 64.1 kcal/mol corresponding to the $\pi(\text{C}=\text{C})\rightarrow\text{Pd}$ interactions and 13.9 kcal/mol to the $\sigma(\text{C}-\text{C})\rightarrow\text{Pd}$ ones; the NB orbitals involved within these donor-acceptor interactions are illustrated in Figure 2. For the other (C=C) \rightarrow Pd chemical bonding, NBO data revealed an interaction energy of about 49.5 kcal/mol, with 11.9 kcal/mol arising from $\sigma(\text{C}-\text{C})\rightarrow\text{Pd}$, and the rest up to the total amount from the $\pi(\text{C}=\text{C})\rightarrow\text{Pd}$ electron departures.

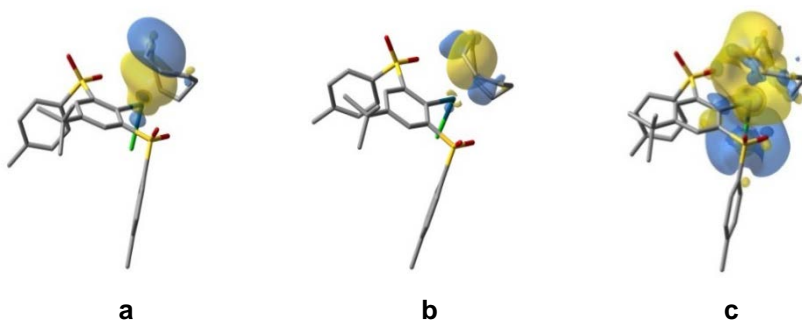


Figure 2. NB orbitals involved in the charge transfer interactions of the type $\eta^2(\text{C}=\text{C})\rightarrow\text{Pd}$ for one of the two coordinative bonds; a) $\pi(\text{C}=\text{C})$ donor component on cyclooctadienyl species; b) $\sigma(\text{C}-\text{C})$ donor component on cyclooctadienyl species; c) acceptor orbital situated on the palladium atom; H atoms were omitted for clarity. NBOs with similar shapes were obtained for the other $\eta^2(\text{C}=\text{C})\rightarrow\text{Pd}$ chemical bonding.

A potential chemical reaction involving palladium derivative **2** (see Figure 3) could be of interest due to the formation of a chelated O,C,O-coordinating pincer-type Pd complex, **2_a**. DFT calculations, performed on species **2_a**, indicate Pd-O bond lengths of 2.173 Å and 2.176 Å. According to NBO analyses, the calculated energies corresponding to these O→Pd chemical bondings is around 78 kcal/mol for each contact (77.4 kcal/mol and 78.1 kcal/mol, respectively).

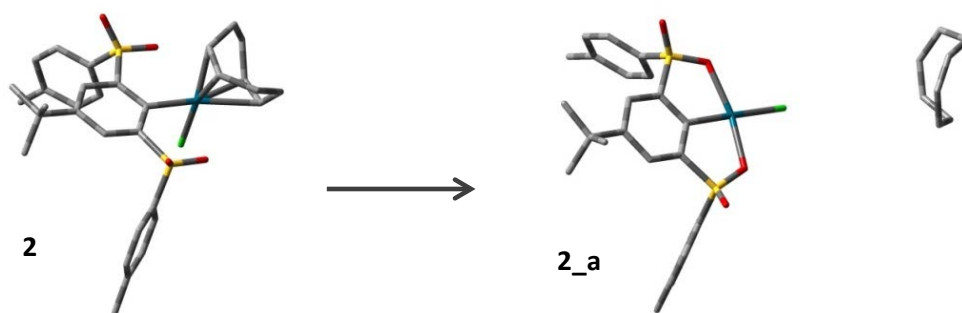


Figure 3. Potential chemical decomposition of complex **2** into a pincer-type palladium complex, **2_a**, and the cyclooctadiene group; hydrogen atoms were omitted for clarity.

The total energy corresponding to the O→Pd interactions in complex **2_a** (155.5 kcal/mol) is with 28 kcal/mol higher than the one calculated for the $\eta^2(\text{C}=\text{C})\rightarrow\text{Pd}$ ones within derivative **2** (127.5 kcal/mol). According to the calculated energies of the investigated species, the reaction presented in Figure 3 is not thermodynamically favorable. Thus, the calculated energy of complex **2** is with 38.8 kcal/mol lower than the sum of the computed energies of **2_a** and of the free cyclooctadiene group (zero-point energy – ZPE – corrections were included in all cases). However, this energy difference could be significantly overestimated due to possible basis set superposition error.

The ruthenium complex **3** was also investigated by using DFT analysis. The optimized structure of **3** indicates a *quasi*-octahedral arrangement around the ruthenium atom with strong Ru-P bonds with calculated lengths of 2.393 Å, for the Ru-bond displaced in *trans* with respect to the Ru-C chemical bonding, and 2.261 Å for the one placed in the *cis* position. Short bond length was also calculated for the Ru-C bond (2.005 Å) while the Ru-Cl one has a calculated length of around 2.533 Å. For the Ru-O contacts, distances of 2.212 - 2.214 Å were obtained.

CONCLUSIONS

New palladium and ruthenium complexes were obtained using a bis-sulfone ligand. Both complexes, **2** and **3**, were characterized by NMR spectroscopy in solution and complex **2** also by single crystal X-ray analysis. It was shown that the bis-sulfone ligand **1** is also suitable to obtain transition metal derivatives; these compounds are the first examples of complexes with this ligand, opening the road to a new class of derivatives supported by sulfone based ligands. NBO analysis brought further explanations to the formation of the obtained palladium derivative. Furthermore, DFT calculations also supported the formation of the ruthenium complex

EXPERIMENTAL PART

All manipulations were realized in a dry, oxygen-free argon atmosphere using Schlenk-line and glove-box techniques. All the solvents were purified with a MBRAUN SBS-800 apparatus. The NMR spectra were recorded with a Bruker Avance II 300 apparatus: ^1H (300.13 MHz), ^{13}C (75.48 MHz), ^{31}P (121.51 MHz, reference H_3PO_4) at 298 K. High-resolution mass spectrometry (HRMS) spectra were measured with a GCT Premier Waters in DCI mode (CH_4). The X-ray data were collected at 193(2) K on a Bruker - AXS APEX II Quazar diffractometer, equipped with a 30 W air-cooled microfocus source using MoK_α radiation (wavelength = 0.71073 Å). Phi- and omega- scans were used. The data were integrated with SAINT[41] and an empirical absorption correction with SADABS[42] was applied. The structures were solved by direct methods using SHELXS-97[43] and refined using a least-squares method on F^2 . All non-H atoms were refined with anisotropic displacement parameters. CCDC 1829298 (**2**) contains the supplementary crystallographic data for this paper. These data can be obtained free of charge from The Cambridge Crystallographic Data Centre via www.ccdc.cam.ac.uk/data_request/cif

Computational Chemistry calculations were performed within the Density Functional Theory (DFT) framework. The hybrid functional used was B3LYP[44,45] in conjunction with Grimme's D3 dispersion correction,[46] along with the triple-zeta Def2-TZVP basis set[47] and Stuttgart effective core potentials[47] for the relativistic core electrons of the Pd atom. Optimization criteria were set to tight, vibrational analysis being performed on the optimized structures. The integration grid used was of 99 radial shells and 950 angular points for each shell (99,950). All the calculations were carried out using the Gaussian 09 package.[48] Natural Bond Orbital (NBO)[49-51] *single-point* calculations were performed using the Gaussian implemented version of the NBO Program.[52]

Synthesis of (2,6-(para-tolylsulfonyl)-4-tert-butylphenyl)-palladium- η^2 -cyclooctadienyl chloride 2

To a solution of bis-sulfone **1** (150 mg, 0.34 mmol) in 6 mL toluene cooled to -40°C , *n*-butyl lithium (0.22 mL, 0.36 mmol, 1.6 M in hexane) was added dropwise. The deep red solution was stirred 20 minutes at this temperature then was added over a suspension of $\text{Cl}_2\text{Pd}(\text{COD})$ (97 mg, 0.34 mmol) in 2 mL toluene at -40°C . The dark red reaction mixture was stirred for 15 minutes at this temperature then allowed to warm slowly to room temperature and stirred for 18 hours, to become a black solution. After the evaporation of the volatiles, the compound was washed with Et_2O and obtained as a dark grey powder. (135 mg, yield=58%) Colourless crystals suitable for X-ray analysis were obtained by slow diffusion of pentane in CH_2Cl_2 solution.

$^1\text{H NMR}$ (CDCl_3) δ = 1.05 (s, 9H, *t*-Bu), 2.37 (s, 6H, Me), 2.95 and 3.12 (m, CH_2 COD) 5.54 (m, 2H, CH COD), 6.34 (m, 2H, CH COD), 7.26 (d, 4H, $^3J_{\text{HH}}$ = 7.98 Hz, *m*-CH Tol), 7.56 (s, 2H, *m*-CH Ph), 8.08 (d, 4H, $^3J_{\text{HH}}$ = 8.30 Hz, *o*-CH Tol).

$^1\text{H NMR}$ (C_6D_6) δ = 0.86 (s, 9H, *t*-Bu), 1.73 (s, 6H, Me), 2.48 and 2.81 (m, CH_2 COD) 5.44 (m, 2H, CH COD), 6.38 (m, 2H, CH COD), 6.75 (d, 4H, $^3J_{\text{HH}}$ = 7.96 Hz, *m*-CH Tol), 8.06 (s, 2H, *m*-CH Ph), 8.55 (d, 4H, $^3J_{\text{HH}}$ = 8.28 Hz, *o*-CH Tol).

$^{13}\text{C NMR}$ (C_6D_6) δ = 21.8 (Me), 30.8 (*t*-Bu), 34.4 (C *t*-Bu), 28.2 and 31.3 (CH_2 COD), 107.4 and 122.4 (CH COD), 128.8 (*o*-CH Tol), 129.8 (C3, C5), 131.8 (*m*-CH Tol), 139.0, 140.4, 144.1, 147.7, 149.7.

HR-MS (DCI CH_4): ($\text{C}_{32}\text{H}_{37}\text{O}_4\text{S}_2\text{PdCl}$) $[\text{M}-\text{Cl}]^+$ calcd: 655.1179, found: 655.1182.

Synthesis of (2,6-(para-tolylsulfonyl)-4-tert-butylphenyl)-ruthenium-bis(triphenylphosphine) chloride 3

To a solution of bis-sulfone **1** (150 mg, 0.34 mmol) in 6 mL toluene cooled to -40°C , *n*-butyl lithium (0.22 mL, 0.36 mmol, 1.6 M in hexane) was added dropwise. The deep red solution was stirred 20 minutes at this temperature then was added over a suspension of $(\text{PPh}_3)_3\text{RuCl}_2$ (325 mg, 0.34 mmol) in 1 mL toluene at -40°C . The dark red solution was allowed to warm slowly to room temperature and stirred for 18 hours. After the evaporation of the volatiles, the compound was washed with Et_2O and pentane to obtain it as a light brown powder. (110 mg, yield=30%).

$^1\text{H NMR}$ (C_6D_6) δ = 0.85 (s, 9H, *t*-Bu), 1.77 (s, 6H, Me), 6.71 (d, 4H, $^3J_{\text{HH}}$ = 8.09 Hz, *m*-CH Tol), 6.87-7.03 (m, PPh_3), 7.32 (d, 2H, J = 1.37 Hz, *m*-CH Ph), 7.55 (m, PPh_3), 7.85 (m, PPh_3), 8.61 (d, 4H, $^3J_{\text{HH}}$ = 8.38 Hz, *o*-CH Tol).

$^{13}\text{C NMR}$ (C_6D_6) δ = 21.2 (Me), 31.1 (*t*-Bu), 34.5 (C *t*-Bu), 130.5 (C8, C12), 127.1 (d, J = 2.28 Hz, C3, C5), 129.8 (C9, C11), 144.7 (C7), 145.8 (C2, C6),

136.8, (C10), 148.3 (d, $J = 1.87$ Hz, C4), 186.7 (dd, $J = 10.09$ and 76.09 Hz, C1), 127.3, 127.4, 127.6, 127.8, 129.6 (PPh₃), 134.2 (d, $^3J_{PC} = 9.33$ Hz, PPh₃), 135.4, 135.7 (PPh₃), 135.5 (d, $^3J_{PC} = 10.99$ Hz, *o,m*-CH PPh₃), 136.2 (d, $^3J_{PC} = 10.82$ Hz, *o,m*-CH PPh₃), 138.3 (d, $^1J_{PC} = 28.11$ Hz, *ipso*-PPh₃).

^{31}P NMR (C₆D₆) $\delta = 52.3$ (m), 25.4 (m)

$^{31}\text{P}\{\text{H}\}$ (C₆D₆) $\delta = 52.3$ (d, $^2J_{P-P} = 23.39$ Hz), 25.4 (d, $^2J_{P-P} = 23.45$ Hz)

IR (nujol) ν (cm⁻¹) = 1595, 1465, 1377, 1321, 1261, 1187, 1146, 1106, 1058, 1009, 814, 741, 695, 662, 586, 520

ACKNOWLEDGEMENTS

This work was supported by a grant of Ministry of Research and Innovation, CNCS – UEFISCDI, project number PN-III-P4-ID-PCE-2016-0351, within PNCDI III, by the Babeş-Bolyai University of Cluj-Napoca and by the Centre National de la Recherche Scientifique (CNRS) and the Université de Toulouse (UPS).

REFERENCES

1. N. Fey, A.G. Orpen and J. N. Harvey, *Coordination Chemistry Reviews*, **2009**, *253*, 704.
2. J.R. Khusnutdinova and D. Milstein, *Angewandte Chemie International Edition*, **2015**, *54*, 12236.
3. C. Gunanathan and D. Milstein, *Accounts of Chemical Research*, **2011**, *44*, 588.
4. G. van Koten, *Pure and Applied Chemistry*, **1989**, *61*, 1681.
5. E. Negishi, Ed., *Handbook of Organopalladium Chemistry for Organic Synthesis*, John Wiley & Sons, Inc., New York, USA, **2002**.
6. D. Morales-Morales and C. Jensen, Eds., *The Chemistry of Pincer Compounds*, Elsevier, **2007**.
7. P. Jia, R. Ouyang, P. Cao, X. Tong, X. Zhou, T. Lei, Y. Zhao, N. Guo, H. Chang, Y. Miao and S. Zhou, *Journal of Coordination Chemistry*, **2017**, *70*, 2175.
8. U. Schatzschneider, *European Journal of Inorganic Chemistry*, **2010**, *2010*, 1451.
9. M.Á. Martínez, M.P. Carranza, A. Massaguer, L. Santos, J.A. Organero, C. Aliende, R. de Llorens, I. Ng-Choi, L. Feliu, M. Planas, A.M. Rodríguez, B.R. Manzano, G. Espino and F.A. Jalón, *Inorganic Chemistry*, **2017**, *56*, 13679.
10. Y. Zhang, Q. Zhou, N. Tian, C. Li and X. Wang, *Inorganic Chemistry*, **2017**, *56*, 1865.
11. M. Albrecht and G. van Koten, *Angewandte Chemie International Edition*, **2001**, *40*, 3750.

12. E. Holder, B.M.W. Langeveld and U.S. Schubert, *Advanced Materials*, **2005**, *17*, 1109.
13. G. Van Koten and R.A. Gossage, *The Privileged Pincer-Metal Platform: Coordination Chemistry & Applications*, Springer International Publishing, Cham, **2016**, vol. 54.
14. G. van Koten and D. Milstein, Eds., *Organometallic Pincer Chemistry*, Springer Berlin Heidelberg, Berlin, Heidelberg, **2013**, vol. 40.
15. D. Zhang and Q. Wang, *Coordination Chemistry Reviews*, **2015**, *286*, 1.
16. G. Sipos, E.E. Drinkel and R. Dorta, *Chemical Society Reviews*, **2015**, *44*, 3834.
17. P. Das and W. Linert, *Coordination Chemistry Reviews*, **2016**, *311*, 1.
18. H.P. Dijkstra, M.Q. Slagt, A. McDonald, C.A. Kruithof, R. Kreiter, A.M. Mills, M. Lutz, A.L. Spek, W. Klopper, G.P.M. van Klink and G. van Koten, *European Journal of Inorganic Chemistry*, **2003**, *2003*, 830.
19. J. Vicente, A. Arcas, M.-A. Blasco, J. Lozano and M.C. Ramírez de Arellano, *Organometallics*, **1998**, *17*, 5374.
20. G.R. Fulmer, W. Kaminsky, R.A. Kemp and K.I. Goldberg, *Organometallics*, **2011**, *30*, 1627.
21. R. Septean, I.-T. Moraru, T.-G. Kocsor, N. Deak, N. Saffon-Merceron, A. Castel and G. Nemes, *Inorganica Chimica Acta*, **2018**, *475*, 112.
22. D. Matioszek, T.-G. Kocsor, A. Castel, G. Nemes, J. Escudié and N. Saffon, *Chemical Communication*, **2012**, *48*, 3629.
23. T.-G. Kocsor, G. Nemes, N. Saffon, S. Mallet-Ladeira, D. Madec, A. Castel and J. Escudié, *Dalton Transactions*, **2014**, *43*, 2718.
24. G. Carel, D. Madec, A. Saponar, N. Saffon, G. Nemes, G. Rima and A. Castel, *Journal of Organometallic Chemistry*, **2014**, *755*, 72.
25. S. Ech-Cherif El Kettani, J. Escudié, C. Couret, H. Ranaivonjatovo, M. Lazraq, M. Soufiaoui, H. Gornitzka and G. Cretiu Nemes, *Chemical Communication*, **2003**, *1*, 1662.
26. R. Septean, G. Nemes, J. Escudié, I. Silaghi-Dumitrescu, H. Ranaivonjatovo, P. Petrar, H. Gornitzka, L. Silaghi-Dumitrescu and N. Saffon, *European Journal of Inorganic Chemistry*, **2009**, *2009*, 628.
27. R. Septean, H. Ranaivonjatovo, G. Nemes, J. Escudié, I. Silaghi-Dumitrescu, H. Gornitzka, L. Silaghi-Dumitrescu and S. Massou, *European Journal of Inorganic Chemistry*, **2006**, *2006*, 4237.
28. P.M. Petrar, R. Şeptean, N. Deak, H. Gornitzka and G. Nemeş, *Journal of Organometallic Chemistry*, **2015**, *787*, 14.
29. L. Baiget, M. Bouslikhane, J. Escudie, G.C. Nemes, I. Silaghi-Dumitrescu and L. Silaghi-Dumitrescu, *Phosphorus Sulfur Silicon and Related Elements*, **2003**, *178*, 1949.
30. G.C. Nemes, L. Silaghi-Dumitrescu, I. Silaghi-Dumitrescu, J. Escudié, H. Ranaivonjatovo, K.C. Molloy, M.F. Mahon and J. Zukerman-Schpector, *Organometallics*, **2005**, *24*, 1134.
31. G. Nemes, J. Escudié, I. Silaghi-Dumitrescu, H. Ranaivonjatovo, L. Silaghi-Dumitrescu and H. Gornitzka, *Organometallics*, **2007**, *26*, 5136.
32. N. Deak, P.M. Petrar, S. Mallet-Ladeira, L. Silaghi-Dumitrescu, G. Nemeş and D. Madec, *Chemistry - a European Journal*, **2016**, *22*, 1349.

33. N. Deak, I.-T. Moraru, N. Saffon-Merceron, D. Madec and G. Nemes, *European Journal of Inorganic Chemistry*, **2017**, 2017, 4214.
34. J. Becker and V.H. Gessner, *Organometallics*, **2014**, 33, 1310.
35. D. Madec, F. Mingoia, C. Macovei, G. Maitro, G. Giambastiani and G. Poli, *European Journal of Organic Chemistry*, **2005**, 2005, 552.
36. A. Szadkowska, K. Żukowska, A.E. Pazio, K. Woźniak, R. Kadyrov and K. Grela, *Organometallics*, **2011**, 30, 1130.
37. T. Tuntulani, G. Musie, J.H. Reibenspies and M.Y. Darensbourg, *Inorganic Chemistry*, **1995**, 34, 6279.
38. B. Cordero, V. Gómez, A.E. Platero-Prats, M. Revés, J. Echeverría, E. Cremades, F. Barragán and S. Alvarez, *Dalton Transactions*, **2008**, 2832.
39. M. Mantina, A.C. Chamberlin, R. Valero, C.J. Cramer and D.G. Truhlar, *Journal of Physical Chemistry A*, **2009**, 113, 5806.
40. A. Bondi, *Journal of Physical Chemistry*, **1964**, 68, 441.
41. SAINT, Program for data reduction, Bruker-AXS.
42. SADABS, Program for data correction, Bruker-AXS.
43. SHELXS-97, SHELXL-14 Program for Crystal Structure refinement, G.M. Sheldrick, *Acta Crystallographica Section A* **2008**, 64, 112. SHELXL, G.M. Sheldrick, *Acta Crystallographica Section C*, **2015**, 71, 3.
44. C. Lee, W. Yang, R.G. Parr. *Physical Review B, Condensed Matter and Materials Physics*, **1988**, 37, 785.
45. A.D. Becke. *Journal of Chemical Physics*, **1993**, 98, 5648.
46. S. Grimme, J. Antony, S. Ehrlich, H. Krieg. *Journal of Chemical Physics*, **2010**, 132, 154104.
47. D. Rappoport, F. Furche. *Journal of Chemical Physics*, **2010**, 133, 134105.
48. M.J. Frisch, G.W. Trucks, H.B. Schlegel, G.E. Scuseria, M.A. Robb, J.R. Cheeseman, G. Scalmani, V. Barone, G.A. Petersson, H. Nakatsuji, X. Li, M. Caricato, A. Marenich, J. Bloino, B.G. Janesko, R. Gomperts, B. Mennucci, H.P. Hratchian, J.V. Ortiz, A.F. Izmaylov, J.L. Sonnenberg, D. Williams-Young, F. Ding, F. Lipparini, F. Egidi, J. Goings, B. Peng, A. Petrone, T. Henderson, D. Ranasinghe, V.G. Zakrzewski, J. Gao, N. Rega, G. Zheng, W. Liang, M. Hada, M. Ehara, K. Toyota, R. Fukuda, J. Hasegawa, M. Ishida, T. Nakajima, Y. Honda, O. Kitao, H. Nakai, T. Vreven, K. Throssell, J.A. Montgomery, Jr., J.E. Peralta, F. Ogliaro, M. Bearpark, J.J. Heyd, E. Brothers, K.N. Kudin, V.N. Staroverov, T. Keith, R. Kobayashi, J. Normand, K. Raghavachari, A. Rendell, J.C. Burant, S.S. Iyengar, J. Tomasi, M. Cossi, J.M. Millam, M. Klene, C. Adamo, R. Cammi, J.W. Ochterski, R.L. Martin, K. Morokuma, O. Farkas, J.B. Foresman, D.J. Fox, Gaussian 09, revision E.01; Gaussian, Inc.: Wallingford, CT, **2009**.
49. F. Weinhold, C.R. Landis, *Valency and Bonding: A Natural Bond Orbital Donor-Acceptor Perspective*; Cambridge Univ. Press: Cambridge, U.K., **2005**.
50. F. Weinhold, C.R. Landis, *Discovering Chemistry with Natural Bond Orbitals*; Wiley-Interscience: Hoboken, NJ., **2012**.
51. F. Weinhold, C.R. Landis, E.G. Glendening, *International Reviews in Physical Chemistry*, **2016**, 35, 399.
52. E.D. Glendening, A.E. Reed, J.E. Carpenter, F. Weinhold, NBO Version 3.1.

(PHENOTHIAZINYL)VINYL-INDOLIUM CATIONIC DYES

BALÁZS BRÉM^a, QUENTIN COLANGE^b, EMESE GAL^a, DAN PORUMB^a,
CASTELIA CRISTEA^{a*}, LUIZA GĂINĂ^a, TAMÁS LOVÁSZ
AND LUMINIȚA SILAGHI-DUMITRESCU^a

ABSTRACT. New 2-(2-(10*H*-phenothiazin-3yl)vinyl)-3*H*-indolium cationic dyes were successfully prepared by Knoevenagel condensation of 1,2,3,3-tetramethyl-3*H*-indolium iodide with 10-methyl-10*H*-phenothiazine-3-carbaldehyde and 10*H*-phenothiazine-3-carbaldehyde respectively. Their optical properties were emphasized by UV-Vis absorption spectroscopy. The position of their characteristic intramolecular charge transfer absorption maxima is situated in the visible range (550-630 nm), exhibiting solvatochromism induced by solvent polarity. Experimental evidences of linear optical properties were completed by a theoretical DFT computational study.

Key words: 10*H*-phenothiazine, indolium salts, cyanine dyes

INTRODUCTION

The tuneable optical properties of cyanine dyes supported the development of new organic functional dyes. The phenothiazine was selected in the design of several Donor- π -Acceptor type molecular structures characterized by intense optical absorption and emission properties, taking benefit of its electron rich heterocyclic core which recommends it as an excellent electron donor and its butterfly conformation which may hinder the molecular aggregation.

The Knoevenagel condensation of N-alkyl quaternary ammonium salts, described as a convenient reaction path for the preparation of dimethine cyanine dyes [1] was successfully applied in the preparation of cyanine dyes

^a Babes-Bolyai University, Faculty of Chemistry and Chemical Engineering, RO-400028, Cluj-Napoca, Romania

^b Université de Rouen, Institute Universitaire de Technologie, 76821 Mont Saint Aignan CEDEX, France

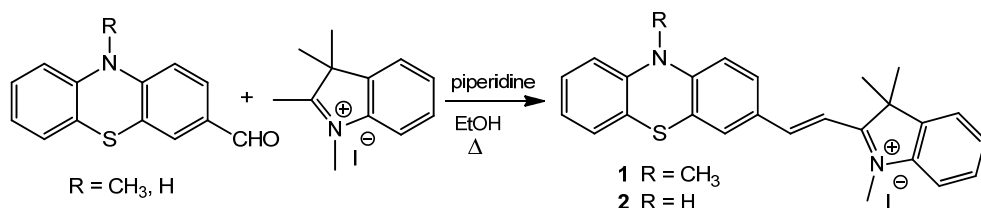
* Corresponding author: castelia@chem.ubbcluj.ro

containing phenothiazine as electron donor moiety and indolium quaternary salts as acceptors. Condensation of 10-alkyl-10*H*-phenothiazine-3-carbaldehyde derivatives with different 2, 3, 3-trimethyl-indolium quaternized salts such as: 5-carboxy-1-hexyl-2, 3, 3-trimethyl-indolium [2], 5-carboxy-2,3,3-trimethyl-1-octyl-3*H*-indolium [3] and 1-ethyl-2,3,3-trimethylindolenium respectively, [4] gave cyanine dyes characterized by intense intramolecular charge transfer (ICT) absorption bands situated in the visible region of the electromagnetic spectrum. Their linear optical properties appear modulated by solvatochromism and substitution of the heterocyclic units with auxochromic groups recommending them for potential applications in materials science.

Our previous results in the preparation and assessment of the optical properties of cationic dyes containing electron donor 10*H*-phenothiazine units and electron acceptor pyridinium units connected through a vinylene bridge [5] stimulated our interest in the field of cyanine dyes. In this work we describe the synthesis of new 2-((phenothiazin-3yl)vinyl)-indolium cationic dyes designed to enrich the series of dimethine cyanine dyes reported in the literature with the purpose of gathering more systematic information on their structure-optical properties relationship.

RESULTS AND DISCUSSIONS

Two new 2-(2-(10*H*-phenothiazin-3yl)vinyl)-3*H*-indolium (PVI) cationic dyes were successfully prepared by Knoevenagel condensation of 1,2,3,3-tetramethyl-3*H*-indolium iodide with 10-methyl-10*H*-phenothiazine-3-carbaldehyde (PVI **1**) and 10*H*-phenothiazine-3-carbaldehyde respectively (PVI **2**), as shown in scheme 1.



Scheme 1

The structural assignments of PVI **1** and **2** were based on spectroscopic data. MS spectra confirmed the molecular weight of the cationic dyes. In the ¹H-NMR spectra the key signals generated by the

protons belonging to the vinyl bridge appeared split in doublet with vicinal coupling constants of 16.2 Hz, thus suggesting the formation of the geometrical *trans*- isomer.

The optical properties of PVI **1** and **2** were emphasized by UV-Vis absorption spectroscopy. The position of their characteristic intramolecular charge transfer (ICT) $\pi \rightarrow \pi^*$ absorption maxima are situated in the visible range (550-630 nm), exhibiting solvatochromism induced by solvent polarity as depicted in figure 1. This behaviour was also observed in the case of similar cyanine dyes and explained by a better stabilization of the polar ground state upon increasing solvent polarity [4].

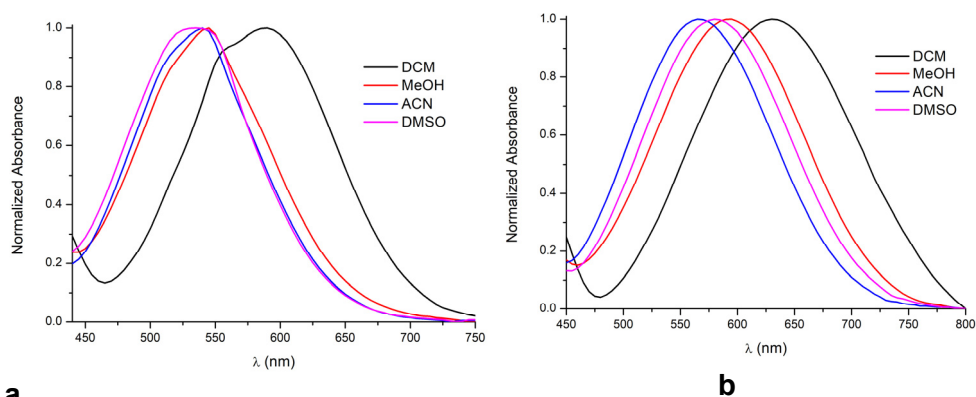
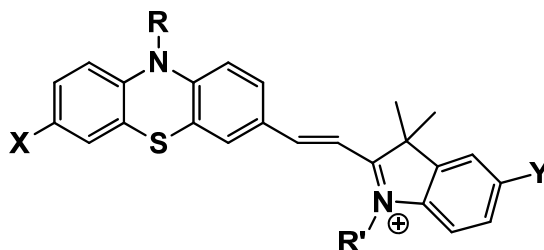


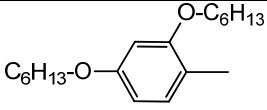
Figure 1. Electronic absorption spectra in different solvents for:
a) PVI **1**, b) PVI **2**

A large bathochromic shift can be observed in each case when dichloromethane (DCM) was used as a solvent. The position of the recorded absorption maxima shows an important red shift in the case of PVI **2** (λ_{\max} 630 nm) as compared to PVI **1** (λ_{\max} 585 nm) suggesting a superior electron donating ability of the unsubstituted phenothiazine unit.

In table 1 the electronic properties of PVI **1** and **2** were depicted together with those of previously reported similar cyanine dyes. The highest bathochromic shift was observed for the cyanine dye containing two auxochromic groups: one electron donor dialcoxiaryl substituent coupled to the phenothiazine unit and one electron withdrawing substituent (-COOH) attached to the indolium moiety (table 1). The length of the alkyl chain attached to the heterocyclic N atom slightly influenced the position of the absorption maxima.

Table 1. Position of the characteristic intramolecular charge transfer $\pi \rightarrow \pi^*$ absorption maxima for 2-((*N*-alkyl-10*H*-phenothiazin-3yl)vinyl)-3,3-dimethyl-1-alkyl-3*H*-indolium dyes in dichloromethane solvent.



R	R'	X	Y	λ_{abs}	Ref.
<i>n</i> -C ₈ H ₁₇	C ₂ H ₅	H	H	591 nm	[4]
<i>n</i> -C ₆ H ₁₃	<i>n</i> -C ₈ H ₁₇		-COOH	679 nm	[2]
CH ₃	CH ₃	H	H	585 nm	PVI 1
H	CH ₃	H	H	630 nm	PVI 2

The steric effect induced by a bulky alkyl substituent attached to the phenothiazine N atom may render less effective the participation of the lone pair of electrons to the extended conjugated system. The optimized geometries of PVI 1 and 2 suggested an equatorial position of the substituent attached to the phenothiazine N atom, thus enabling the participation of the lone pair of electrons to the extended conjugated system.

An inspection of the electron distribution in the molecular orbitals of each PVI 1 and 2 indicated that the frontier filled orbitals HOMO appear located predominantly on the electron donor phenothiazine unit, whereas the unoccupied molecular orbitals LUMO are located predominantly on the indolium core. In figure 2 plots of the frontier molecular orbitals are depicted together with the computed energies resulted by DFT geometry optimizations on PVI 1 and 2. The separation of computed energy levels of the frontier molecular orbitals appeared slightly larger for PVI 1.

(PHENOTHIAZINYL)VINYL-INDOLIUM CATIONIC DYES

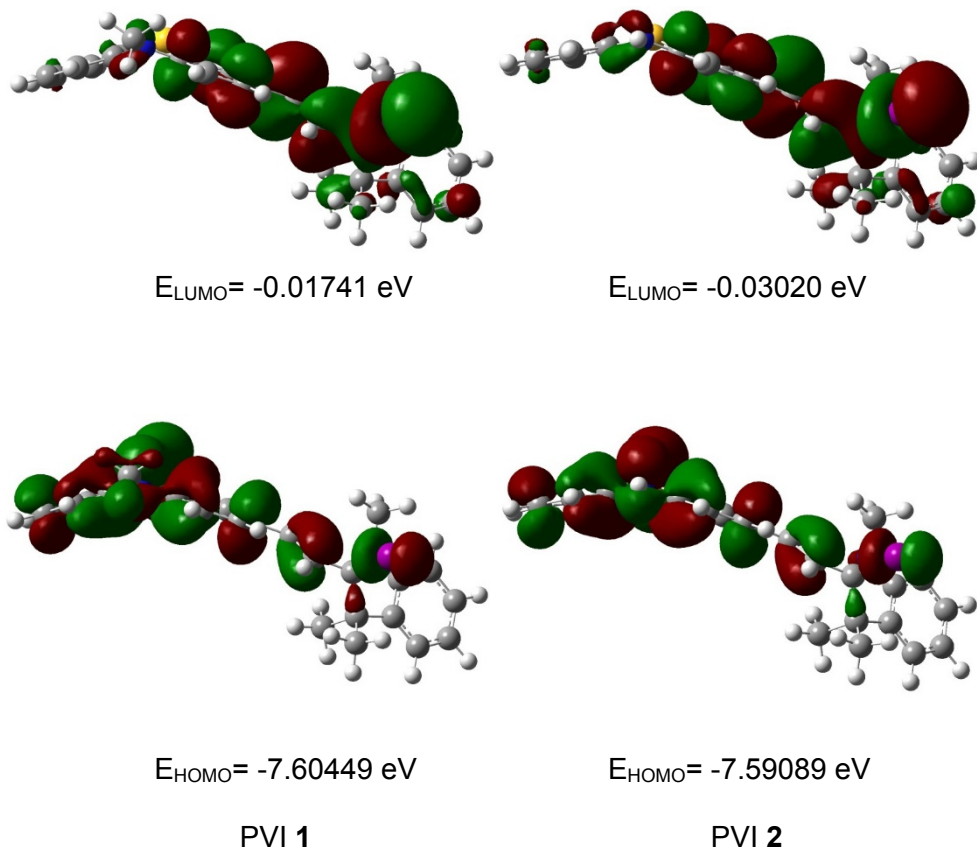


Figure 2. Plots of frontier molecular orbitals of PVI 1 and 2 and their corresponding values of computed energies resulted by DFT geometry optimizations and computation at B3LYP/6-31(d,p) level using the Gaussian 09W program package.

CONCLUSIONS

The new 2-(2-(10*H*-phenothiazin-3yl)vinyl)-3*H*-indolium cationic dyes described in this work broadened the series of cyanine dyes containing phenothiazine as electron donor and indolium quaternary salts as electron withdrawing unit. Their optical properties experimentally observed by UV-Vis absorption spectroscopy indicate a superior electron donating ability of the unsubstituted phenothiazine unit, in comparison to the *N*-alkyl derivatives.

EXPERIMENTAL SECTION

HRMS spectra were recorded using Thermo LTQ *Orbitrap XL* mass spectrometer.

NMR spectra were recorded at room temperature on 600 MHz Bruker Avance instrument. Chemical shifts are expressed in δ (ppm) relative to standard tetramethylsilane (TMS).

UV-Vis absorption spectra were recorded in various solvents with a Perkin Elmer Lambda 35 spectrometer DFT calculations:

Geometries constructed with Gaussview [6] have been optimized with the Gaussian software package [7] using the 6-31G(d,p) basis set. Frequency analysis has been performed in order to ensure that the optimized geometries are genuine minima.

Phenothiazine carbaldehydes were prepared according to our previously reported procedures. [8]

1,2,3,3-Tetramethyindolium iodide was prepared according to literature reported procedure [1].

General procedure for the synthesis of 2-(2-(10H-phenothiazin-3yl)vinyl)-3H-indolium cationic dyes

1,2,3,3-tetramethyindolium iodide (1.5g, 5.0 mmol), phenothiazin-3-yl carbaldehyde (4.5 mmol) and piperidine (1.0 ml) were added to 50 ml ethanol. The reaction mixture was stirred for 12 h under reflux. The precipitate was filtered and the solvent was evaporated to dryness. The solid was purified by column chromatography on silica gel solid support using dichloromethane as mobile phase.

2-(2-(10-methyl-10H-phenothiazin-3yl)vinyl)-3H-indolium iodide 1.

Purification by column chromatography, gave 0.6 g, yield 35%, dark purple powder.

HRMS: found 397.17410, $C_{26}H_{25}N_2S^+$ requires 397.17330

1H RMN (600 MHz, DMSO), δ (ppm)= 1.78 (s, 6H); 3.45 (s, 3H); 4.11 (s, 3H); 7.06 (m, 2H); 7.13 (d, 1H, $^3J= 8.4$ Hz); 7.22 (dd, 1H, $^3J=7.8$ Hz, $^4J= 1.8$ Hz); 7.28 (td, 1H, $^3J=7.8$ Hz, $^4J= 1.2$ Hz); 7.54 (d, 1H, 16.2 Hz); 7.61 (m, 2H); 7.85 (d, 1H, $^3J=7.8$ Hz); 8.08 (dd, 1H, $^3J=9.0$ Hz, $^4J= 1.8$ Hz); 8.12 (d, 1H, $^4J= 1.2$ Hz); 8.32 (d, 1H, 16.2 Hz)

^{13}C RMN (150 MHz, DMSO), δ (ppm)= 152.4; 150.1; 143.8; 142.3; 133.0; 129.4; 129.3; 128.6; 128.2; 127.4; 124.2; 123.2; 123.0; 121.4; 116.1; 115.3; 115.2; 110.8; 55.4; 52.2; 44.1; 36.3; 34.6; 26.0; 22.6;

2-(2-(10H-phenothiazin-3yl)vinyl)-3H-indolium iodide 2.

Purification by column chromatography, gave 0.1g, 25% as dark powder.

HRMS: found 383.15877, C₂₅H₂₃N₂S⁺ requires 383.15765.

¹H RMN (600 MHz, DMSO), δ(ppm)= 1.75 (s, 6H); 4.05 (s, 3H); 6.63 (dd, 1H, ³J= 7.8 Hz), 6.72 (m, 2H); 6.84 (t, 1H); 6.95 (d, 1H, ³J=7.0); 7.03 (t, 1H, ³J= 7.8 Hz); 7.37 (d, 1H, ³J=16.2 Hz); 7.58 (m, 2H); 7.83 (m, 4H); 8.18 (d, 1H, ³J= 16.2 Hz)

¹³C RMN (150 MHz, DMSO), δ(ppm)= 152.4; 146.7; 143.5; 142.3; 139.0; 129.3; 129.2; 128.9; 128.8; 128.7; 128.4; 126.7; 123.9; 123.5; 123.2; 117.6; 116.3; 115.9; 114.8; 114.7; 109.1; 34.2; 26.2; 22.6; 22.0

REFERENCES

1. A.C. Pardal, S.S. Ramos, P.F. Santos, L.V. Reis, P. Almeida, *Molecules*, **2002**, 7, 320.
2. M. Cheng, X. Yang, C. Chen, J. Zhao, Q.Tan, L. Sun, *Physical Chemistry Chemical Physics*, **2013**, 15, 17452.
3. M.R. Jung, Y.S. Han, D.Y. Jung, H.S. Yang a, J.H. Kim, D.K. Lee, *Molecular Crystals and Liquid Crystals*, **2013**, 586, 111.
4. R.M. El-Shishtawy, F.A.M. Al-Zahrani, S.M. Afzal, M.A.N. Razvi, ZM. Al-amshany, A.H. Bakry, AM. Asiria, *RSC Advances*, **2016**, 6, 91546.
5. L. Găină, I. Torje, E. Gal, A. Lupan, C. Bischin, R. Silaghi-Dumitrescu, G. Damian, P. Lönnecke, C. Cristea, L. Silaghi-Dumitrescu, **2014** *Dyes and Pigments*, 102, 315.
6. GaussView, Version 5, Dennington R, Keith T, Millam J, Semichem Inc., Shawnee Mission KS, 2009.
7. Gaussian 09, Revision A.02, Frisch MJ, Trucks GW, Schlegel HB, Scuseria GE, Robb MA, Cheeseman JR, et al, Gaussian, Inc., Wallingford CT, 2009.
8. L. Găină, D. Porumb D, I. Silaghi-Dumitrescu, C. Cristea, L. Silaghi- Dumitrescu, *Canadian Journal of Chemistry* **2010**, 88, 42.

VOLATILE COMPOSITION OF SOME RED WINES FROM ROMANIA ASSESSED BY GC-MS

MIHAIL MANOLACHE^a, TIBERIA IOANA POP^a,
ANCA CRISTINA BABEȘ^a, IULIA-ALEXANDRA FARCAȘ^a,
MARIA LAURA MUNCACIU^a, ANAMARIA CĂLUGĂR^{a*}, EMESE GAL^{b*}

ABSTRACT. Four varietal wines Fetească Neagră, Merlot, Cabernet Sauvignon and Pinot Noir from Romania were submitted to a liquid-liquid extraction with dichloromethane and analysed by gas chromatography-mass spectrometry (GC–MS). A total of 29 volatile compounds were identified and quantified over two periods of ageing. Wines were differentiated by a number of compounds, such as esters, higher alcohols, and lactones. During wine ageing, all chemicals changed in the volatile composition. Most of alcohols and acids (hexanoic and octanoic acids) increased during ageing, while the esters, except ethyl lactate and diethyl succinate, were found in lower concentrations as ageing time increased. Considering all the volatile compounds detected, esters and higher alcohols are the main contributors for Romanian red wines.

Keywords: GC-MS, volatile compounds, red wine, liquid-liquid extraction

INTRODUCTION

Volatile compounds (VOCs) have an important role in contributing to wine aromatic attributes, beverage flavor and its quality [1]. Aroma and flavor compounds are found and released in three distinct categories: 1) they originate from the grapes where they are synthesized; 2) most of them are formed during the process of grape must fermentation, and 3) they result from aging and storage [2, 3]. About 600 to 800 volatile compounds such as alcohols, esters organic acids, aldehydes, ethers, ketones, and terpenes, etc.,

^a University of Agricultural Sciences and Veterinary Medicine Cluj-Napoca, Faculty of Horticulture, 3-5 Calea Mănăștur str, RO-400372, Cluj-Napoca, Romania

^b Babeș-Bolyai University, Faculty of Chemistry and Chemical Engineering, 11 Arany Janos str., RO-400028, Cluj-Napoca, Romania

* Corresponding authors: anamariacalugar1981@gmail.com, emese@chem.ubbcluj.ro

have been identified in wines [4], though the knowledge of the aroma of wines is not a simple task for researchers. Although several hundreds of chemical compounds were identified in grapes and wines, only a few compounds contribute to the organoleptic perception of wine [5]. The groups of volatile compounds have different chemical and physical properties, like polarity and volatility, and their concentrations may vary from few ng/L to more than 100 mg/L [6]. Higher alcohols, acids, and esters are found in large quantities and are important for the sensory properties and quality of wine [7]. Small amounts of higher alcohols are contributing positively to wine quality, while excessive amounts may detract from quality [2]. Higher alcohols are important as precursors for ester formation during aging (bottle or barrel aging). Esters comprise an important family of aroma compounds in wine. Ethyl esters are found in the largest quantities, while acetates, found in a less quantity, contribute to the intensity and quality of wine aroma [8]. These esters identified in wine are found in the grape, but their main origin is from the secondary metabolism of yeasts during fermentation [9]. The ethyl esters of the majority of acids in wine are made during the ageing process [10]. The release of aroma precursors can occur during wine aging, under mild acidic conditions [11]. Fatty acids have been reported to be able to affect the aromatic equilibrium of wines because they are opposed to the hydrolysis of the corresponding esters. Those compounds strengthens wine flavor at low concentration, but at high levels, conferred wine sour and thin tasting [12]. Esters based on ethanol and saturated fatty acids, such as hexanoic and octanoic acids, generally contribute to the 'fruity' or 'wine-like' aroma of wine, their presence even at sub-threshold levels having a possible additive effect [13]. The flavor-active metabolites that have an impact on wine perception are derived from the grapes and from microorganisms during fermentation, as well as from chemical processes during production and maturation [14]. During wine ageing under different conditions, the volatile composition could be changed due to the appearance of some volatiles that could decline the wine aroma quality [15, 16]. Therefore, the final aroma of aged wines is really complex [17].

Aroma of a wine can be influenced by several factors: grape varietal characteristics [7, 18, 19], light intensity, temperature [12], soil, climate [20, 21], degree of maturation, cultivation practices [22-24]. The winemaking technologies applied (pressing, fermentation temperature, maceration, yeast strain, SO₂, wine ageing, and storage) affect the final aroma compounds of wines [25-27]. Moreover, the personality of each wine is due to the infinitely varied combinations and concentrations of the various volatile compounds [28].

Qualitative and quantitative characterizations of volatile compounds in wine are performed by GC-MS, as one of the most sensitive techniques for the analysis of volatile compounds in wine [29, 30]. Since wine is a complex matrix, GC-MS is suitable for quantification purposes, using the polar column for separation of the components, due to the fact that is more sensitive for analysis of components present in a low concentration [31]. The volatile compounds are usually extracted by different methods, such as solid-phase extraction [32], solid-phase micro-extraction [33], stir bar sorptive extraction [34], or liquid-liquid extraction methods using organic solvents [35] before the gas chromatographic analysis. There are few data available for the volatile compounds of the international grape varieties grown in Romania and wines, but also for Romanian grape varieties and wines [36-38]. Fetească Neagră is one of the most widespread and economically important cultivars grown in Romania [39]. Previous research has been performed on the volatile composition of the Fetească Neagră wines by Miclean et al., 2010, Antocea, 2012, Palade et al., 2016 [40-42]. Therefore, the aim of the present work was to characterize the main volatile component for the first time of the autochthonous red wine Fetească Neagră grown in two wine regions in Romania and Cabernet Sauvignon, Merlot, and Pinot Noir wines, produced from grape varieties grown in the north-east and south-east regions of Romania.

RESULTS AND DISCUSSION

The basic composition of the wine was analyzed according to the methods proposed by OIV 2013 and the results are revealed in Table 1.

The ethanol content of the red wine decreased during the 6 months of aging with losses of about 0.3-0.5%, in accordance with other studies [43].

As shown in Table 1, there was an increase in volatile acidity during barrel ageing, which could be primarily due to the extraction of volatile acids from the oak [44] and to ethanol oxidation. Barrels are the same in coopering methods and are provided by the same tonnellerie, so the barrel type had no influence in volatile acidity. Titratable acidity (Table 1) presented an increase due to the rise in volatile acidity, during the 6 months of ageing this rise, indicating the extraction of carboxylic, phenolic and volatile acids from wood, as suggested by Canas, 2017 [45]. In all wine samples, free and total SO₂ content decreased with storage time. The losses of total SO₂ during ageing may be attributed to measurable oxygen permeability of oak staves of barrels. The free SO₂ and total SO₂ values for all wine samples were less or equal with specific limit existing for red wines to 35 ml/L, respectively 200 mg/L, proposed by EU [46]. These parameters were determined in duplicates.

Table 1. Evolution of the enological parameters of red wines with two periods of ageing (6 and 12 months)

Wine oenological parameters	Cabernet Sauvignon Dobra (Satu Mare)		Fetească Neagră Rătești (Satu Mare)		Pinot Noir Rătești (Satu Mare)		Merlot Aliman (Constanța)		Fetească Neagră Aliman (Constanța)	
	6	12	6	12	6	12	6	12	6	12
%alcohol content ethanol	112.04	112.00	113.07	13.04	113.48	113.45	14.17	14.10	13.96	112.89
pH	3.89	3.64	3.96	3.56	3.55	3.32	3.68	3.36	3.65	3.24
Total acidity (g/l acid tartaric)	5.40	5.43	5.93	5.97	6.00	6.02	5.22	5.27	5.39	5.43
Volatile acidity (g/l acid acetic)	0.45	0.48	0.54	0.59	0.51	0.54	0.62	0.68	0.70	0.75
Dry extract (g/l)	33.10	31.32	33.50	29.78	35.40	32.24	33.60	31.89	34.20	30.23
Non - reducing dry extract (g/l)	30.14	28.98	29.00	27.67	31.12	29.43	32.78	30.12	31.25	29.72
Free SO ₂ (mg/l)	14.89	12.56	25.00	22.76	27.50	23.69	16.64	12.45	25.05	21.76
Total SO ₂ (mg/l)	25.00	19.98	60.00	55.65	60.00	54.67	67.84	61.23	111.3	98.43

The 29 volatile compounds grouped according to their chemical structure, include 10 alcohols, 11 esters, 5 fatty acids, 1 lactone and 2 other compounds - acetovanilona, ethyl vanillate, were identified and quantified in red wine samples (Table 2 and Table 3). The sub-total concentration of particular classes and their percentage of the total content of volatile compounds were calculated to verify whether the examined wines differentiated in proportions of aroma compounds classes.

Wine volatile compounds, such as esters, acids, and alcohols, are transformed during wine ageing, leading to changes in wine aroma [47].

Interesting similarities were observed in the evolutionary trends of volatile compounds during 6 and 12 months of the aging period. It was noted that volatile compounds possessed different evolution patterns during aging. Some volatiles decreased in the concentration along with the aging period. The majority of esters, alcohols, and acids followed an evolution pattern where an increase in the concentration was observed in 12 months (Table 3) of aging compared with 6 months period (Table 2).

Alcohols

Overall, 10 alcohols have been identified in the analyzed red wines (Table 2 and Table 3) for the two periods of ageing. The composition of alcohols differed both qualitatively and quantitatively among the wines. The total concentration of the alcohols ranged from 6405.16 µg/L (Merlot from the south-east region) to 9637.64 µg/L (Cabernet Sauvignon from the north-west region) for the wines aged for 6 months, being 10.91% and 36.06%, respectively, of the total volatile compounds detected at this stage (Table 2). The content of higher alcohols of wines aged for 12 months was ranged from 6878.20 µg/L (Fetească Neagră from the south-east region) to 22515.33 µg/L (from Cabernet Sauvignon from the north-west region) being 9.74% and 32.66% respectively, for volatiles detected at this stage (Table 3). The concentrations of alcohols of the total volatile compounds in wines from our study were much lower compared with those reported in French wines 44.98 - 74.52%, in Italian wines 51.15 - 66.61%, in Spanish wines 46.02 - 57.86%, and in Polish wines 42.85 - 67.73% [48].

This volatile fraction was mainly composed of isopentyl alcohol (bitter; harsh), isobutanol – (medicinal, wine-like), 2-phenyl-ethanol (roses, pollen, flowery) and 1-hexanol (floral, green, grass cut; herbaceous, fatty, resinous) as the major components in the overall volatile content of the wines. Our results are in accordance with those obtained in Italy [49], [50] which reported also higher amounts of 2-phenylethanol and isopentyl alcohol in aroma compound classes in Negroamaro and Primitivo wines.

2,3 - butanediol cannot be expected to appreciably affect sensory qualities of wine, because of its slightly bitter taste, but it may contribute to the body of a wine because of its viscosity and its high content [51]. The amounts of 2,3 – butanediol in wines from our study (1336.68 - 6895.2 µg/L) may be due to the malolactic fermentation or by aeration through barrels staves used for the first time. Similar amounts of 2,3-butanediol were found in Vilana wines in Greece [52]. In contrast with our results, others detected much lower amount of this compound in French, Polish, Italian and Spanish wines [48].

Higher alcohols amounts changed with ageing, for majority an increase could be observed (Table 3), perhaps as a result of hydrolysis of the esters or evaporation during wood maturation [53].

Esters

Because the wine contains a large number of different alcohols and acids, a wide variety of esters could be formed. In our study, 11 esters were detected in the analyzed wines (Table 2 and Table 3). The total concentration of esters ranged from 11116.14 µg/L (Cabernet Sauvignon from the north-west

region) to 41165.43 $\mu\text{g/L}$ (Merlot from the south-east region) for the wines aged for 6 months, being 42.43% and 70.43%, respectively, of the total VOCs detected at this stage (Table 2). The content of ester of wines aged for 12 months was ranged from 19220.83 $\mu\text{g/L}$ (Fetească Neagră from the south-east region) to 52467.93 $\mu\text{g/L}$ (Merlot from the south-east region) being 28.31% and 76.62% respectively, for volatiles detected at this stage (Table 3).

Wine samples show low concentrations of acetate esters and only two were detected (Table 2 and Table 3). They were isoamyl acetate (fresh, banana) and octyl acetate (fruity, candy, pineapple, pear, floral) and they may produce synergistic effects on the overall flavor of wine, as they provide pleasant fruity notes.

Wines from the two regions showed differences in the concentrations of acetate esters. Increases in acetate esters in wine samples have been observed during the ageing of wines or remained stable, these findings being in agreement with other studies [54, 55]. Among ethyl esters, the most abundant compounds in wines samples were ethyl hexanoate, ethyl decanoate, and ethyl lactate, the same findings were reported for Italian wines, Spanish wines, Polish wines and French wines [48].

The ethyl hexanoate (green apple; fruity; strawberries, anise note) is a volatile ester produced during fermentation process by yeasts, varied from a minimum of 86.44 $\mu\text{g/L}$ in the samples of Fetească Neagră from south-east of Romania to a maximum of 434.53 $\mu\text{g/L}$ for the same sample after 12 months of barrel aging. For all wine samples, this volatile compound registered an increase in concentration during ageing.

An interesting variability in the analyzed samples was for ethyl decanoate (fruity, grape notes) an ester specific for the alcoholic beverages. The highest quantity was identified in the samples aged for 6 months but decreased over time as wine ages due to spontaneous hydrolysis [16]. Except this trend was for Fetească Neagră wines from the north-west region, ethyl decanoate was not detected in wines aged for 6 months, but found in small amounts in wines aged for 12 months (9.64 $\mu\text{g/L}$) as shown in Table 3. Also, Merlot wines from the south-east region aged for 12 months (Table 3) contained a higher quantity of ethyl decanoate compared with the samples aged for 6 months (Table 2). The presence of esters in higher concentrations in wines from the south-east region compared to those from the north-west region might be explained by the different environmental conditions [38].

Ethyl lactate (lactic, medicinal, raspberry and strawberry) is formed mainly during the malolactic fermentation, in red wines the concentration is higher, the large variation between the wines can be explained by the achievement of this compound during malolactic fermentation [56]. This compound varied from several to almost 24 mg /L in wine samples (Table 3), the results are comparable with those found in Malbec wines [57].

Table 2. Concentrations of free volatile compounds ($\mu\text{g/L}$) in red wines aged 6 months from Satu Mare and Constanța County (n=2)

Wine location Volatile compounds	Cabernet sauvignon Dobra (Satu Mare)	Fetească neagră Rătești (Satu Mare)	Pinot noir Rătești (Satu Mare)	Fetească neagră Aliman (Constanta)	Merlot Aliman (Constanta)
Alcohols^a					
Isopentyl alcohol	1282.6 \pm 41.29	2347.3 \pm 18.58	2997.20 \pm 25.36	1562.57 \pm 14.4	1092.89 \pm 15.2
Isobutanol	1490.89 \pm 34.34	1579.53 \pm 32.97	948.86 \pm 31.6	115.23 \pm 2.84	104.96 \pm 3.10
Butanol	-	10.04 \pm 0.21	7.28 \pm 0.07	3.70 \pm 0.15	2.88 \pm 0.10
1-Hexanol	529.77 \pm 0.39	232.83 \pm 1.46	394.25 \pm 7.89	246.57 \pm 0.07	139.04 \pm 3.25
1-Heptanol	44.66 \pm 0.19	23.84 \pm 0.23	20.24 \pm 0.07	23.91 \pm 0.09	12.55 \pm 0.63
2-Nonanol	45.02 \pm 0.37	10.80 \pm 0.12	30.03 \pm 0.23	30.89 \pm 0.05	17.17 \pm 0.27
2,3-butandiol	3899.17 \pm 9.54	1535.62 \pm 26.9	1455.77 \pm 3.72	4827.00 \pm 1.3	3021.22 \pm 30.4
3-(Methylthio)-1-propanol	109.08 \pm 0.16	24.62 \pm 1.68	-	65.99 \pm 0.5	25.29 \pm 0.28
Phenylmethanol	85.45 \pm 0.32	116.83 \pm 2.65	243.56 \pm 0.18	53.28 \pm 3.10	101.96 \pm 3.54
2-Phenylethanol	2151 \pm 0.18	1279.5 \pm 6.48	2936.5 \pm 35.0	2021.5 \pm 0.50	1887.2 \pm 3.54
Total alcohols ($\mu\text{g/L}$)	9637.64 \pm 86.7	7160.91 \pm 91.4	9033.69 \pm 104.1	8950.64 \pm 23.1	6405.16 \pm 60.3
% of total VOC concentration	36.06	15.46	18.62	19.36	10.91
Esters^b					
isoamyl acetate	-	63.86 \pm 1.33	64.41 \pm 0.10	41.46 \pm 0.02	34.94 \pm 0.31
Ethyl caproate	164.10 \pm 1.92	87.03 \pm 1.48	94.75 \pm 0.50	86.44 \pm 5.38	92.07 \pm 8.85
Ethyl lactate	6016.48 \pm 5.28	19080.00 \pm 145.5	19039.2 \pm 71.6	-	21130.48 \pm 172.4
Ethyl-3-hydroxybutanoate	270.94 \pm 9.01	174.08 \pm 3.33	69.89 \pm 1.44	48.38 \pm 0.46	28.67 \pm 0.44
Octyl acetate	370.40 \pm 5.35	-	184.88 \pm 0.11	571.69 \pm 36.1	245.17 \pm 7.3
Ethyldecanoate	136.00 \pm 1.69	-	9.58 \pm 0.33	43.07 \pm 0.31	69.08 \pm 1.68
Ethylhydrogen succinate	1198.30 \pm 2.69	2468.44 \pm 14.5	1369.44 \pm 1.41	7120.44 \pm 0.1	11656.29 \pm 164.7
N-phenyl acetamide	85.01 \pm 0.94	31.47 \pm 0.21	29.00 \pm 0.07	10.50 \pm 0.11	-
Diethyl malate	422.70 \pm 5.69	291.00 \pm 12.04	301.65 \pm 1.87	1204.82 \pm 18.1	359.73 \pm 18.43
Diethyl succinate	696.23 \pm 0.78	917.08 \pm 101.6	998.36 \pm 2.26	11323.03 \pm 35.28	7435.61 \pm 174.64
Methyl-4-hydroxybutanoate	1799.98 \pm 1.75	1315.57 \pm 18.97	2611.97 \pm 86.35	517.05 \pm 17.29	113.39 \pm 0.81
Total esters ($\mu\text{g/L}$)	11160.14 \pm 35.1	24428.53 \pm 298.9	24773.13 \pm 166.1	20966.88 \pm 113.08	41165.43 \pm 549.58
% of total VOC concentration	42.34	52.75	51.26	45.92	70.43

Table 2 continued

Fatty acids ^a					
Butyric acid	74.02±0.19	164.84±0.22	200.99±1.83	246.90±0.88	-
Hexanoic acid	329.55±0.16	865.39±18.05	1083.72±2.40	235.51±3.01	104.15 ±3.08
Octanoic acid	167.18±6.26	218.68±3.34	182.53±0.10	175.12±1.78	63.85 ±2.99
Pidolic acid	-	100.99±1.66	58.03±0.27	76.11±0.25	101.43±3.13
5-oxotetrahydrofuran-2-carboxylic acid	25.68±0.64	420.88±1.94	304.35±0.28	176.03±2.47	249.99±3.42
Total fatty acids (µg/L)	596.43±7.25	1770.78±25.2	1829.62±4.88	909.67±8.39	519.42±12.6
% of total VOC concentration	2.23	3.82	3.77	1.97	0.89
Lactones					
Butyrolactone	4963±0.13	12921±0.36	12643.5±0.35	14775±0.24	10356.21±48.56
% of total VOC concentration	18.57	27.90	26.06	31.96	17.65
Other compounds					
Ethyl vanilate	-	13.47±0.70	23.65±0.06	28.30±0.05	-
Acetovanillone	-	19.51±0.41	27.64±0.04	25.11±0.14	-
Total other compounds (µg/L)	-	32.98±1.11	51.29±0.10	53.41±0.19	-
% of total VOC concentration	0.00	0.07	0.11	0.12	0.00
Total volatiles (µg/L)	26357.21±129.26	46314.20±417.04	48331.23±275.49	45655.60±144.92	58446.22±671.11
% of total VOC concentration	100	100	100	100	100

^a Expressed in equivalents of phenyl ethanol

^b Expressed in equivalents of ethyl decanoate

Concentration in microgram per liter ±RSD (relative standard deviation (%))

The ethyl esters are among the key compounds in the fruity flavors and they make a general positive contribution to the general quality of wines. Besides the acetate and ethyl esters, some other fatty acid esters of higher alcohols were also identified, including diethyl succinate and diethyl malate (fruity). Diethyl succinate (wine, fruity, caramel) is an ester usually present in the fermented beverages that have been aged for several months.

Our results revealed that the majority of esters, except for ethyl lactate and diethyl succinate, were found in lower concentration as ageing time increased. Ethyl lactate and diethyl succinate showed constant concentration increases that could be caused by chemical esterification during the course of ageing.

Fatty acids

The production of fatty acids is dependent on the composition of the must and fermentation conditions [9]. Five fatty acids were identified in all wine samples. The total concentration of those volatile compounds ranged from 519.42 µg/L (Merlot from the south-east region) to 1829.62 µg/L (Pinot Noir from the north-west region) for the wines aged for 6 months, being 0.89% and 3.77%, respectively, of the total volatile compounds detected at this stage (Table 2). The content of fatty acids of wines aged for 12 months ranged from 793.26 µg/L (Cabernet Sauvignon from the north-west region) to 5838.57 µg/L (Fetească Neagră from the south-east region) being 1.15% and 8.27%, respectively, for volatiles detected at this stage (Table 3).

Volatile components belonging to the group of fatty acids, such as octanoic (rancidity, candy, cheese, animal, spicy, unpleasant) and hexanoic (cheese, greasy) acids, were detected and quantified in the wines and our results are supported by previous findings [58, 59]. Hexanoic acid and octanoic acid were found in all wine samples. In our study, fatty acids might have a positive impact on the aroma of the wines examined since their levels were all far below 20 mg/L [60].

Table 3 show a differentiated behaviour of fatty acid during ageing. For all wines, it was observed a small increase in medium- and long-chain fatty acids, such as hexanoic and octanoic acids, during ageing. The only except was for Fetească neagră from south-east region, whose concentration in hexanoic and octanoic acids changed slightly when comparing between wines with 6 and 12 months. Short-chain fatty acids, such as butanoic acid, increased his contents during wine ageing.

The level of the dissolved oxygen in wines decreased during ageing and then remained at a low level. This could explain why some volatile alcohols declined, but some aldehydes, acids, and esters were accumulated in the concentration within 6–12 months barrel aging.

Lactones

A considerable amount of butyrolactone (fruity, coconut-like notes) was found in all red wine samples, due to the fact that all wines were aged for 6-12 months in oak barrels. The presence of butyrolactone in wines could be an indication of a wine's oak ageing.

Other compounds

Acetovanillone arises from thermal degradation of lignin from oak barrels, although their extraction into wine occurs via different means [45]. Garde-Cerdan et al., 2002 [61] state that acetovanillone was extracted from the wine up to 10 months of ageing and afterward its concentration diminished

slightly. This finding may be compared with our results, acetovanillona (vanilla) and ethyl vanillate (vanilla, honey), showed an increase during 12 months of ageing, for all wine samples. Moreover, for Cabernet Sauvignon wines from the north-east region and for Fetească Neagră wines from the south east region aged for 6 months, acetovanillone and ethyl vanillate were not detected.

Table 3. Concentrations of free volatile compounds ($\mu\text{g/L}$) in red wines aged 12 months from Satu Mare and Constanța County (n=2)

Wine location Volatile compounds	Cabernet Sauvignon Dobra (Satu Mare)	Fetească Neagră Rătești (Satu Mare)	Pinot Noir Rătești (Satu Mare)	Fetească Neagră Aliman (Constanta)	Merlot Aliman (Constanta)
Alcohols^a					
Iso pentyl alcohol	4384.1 \pm 52.4	2779.46 \pm 21.70	3587.80 \pm 12.36	2312.2 \pm 32.4	2143.25 \pm 18.65
Iso butanol	3906.97 \pm 31.71	1607.67 \pm 5.26	2023.71 \pm 10.46	118.24 \pm 1.55	458.97 \pm 0.17
Butanol	24.08 \pm 1.29	16.19 \pm 0.58	12.99 \pm 0.04	5.26 \pm 0.04	9.10 \pm 0.02
1-Hexanol	570.89 \pm 8.04	250.48 \pm 2.02	431.79 \pm 0.06	462.93 \pm 9.03	183.79 \pm 0.22
1-Heptanol	38.29 \pm 0.93	26.05 \pm 0.63	18.76 \pm 0.04	48.15 \pm 0.34	15.80 \pm 0.34
2-Nonanol	62.14 \pm 0.62	29.82 \pm 0.29	26.61 \pm 0.19	-	28.93 \pm 0.63
2,3-butandiol	6895.2 \pm 10.73	4961.83 \pm 323.11	1336.68 \pm 9.60	-	2993.63 \pm 1.39
3-(Methylthio)-1-propanol	114.03 \pm 0.27	32.85 \pm 0.32	64.91 \pm 0.46	90.90 \pm 3.14	53.47 \pm 6.38
Phenylmethanol	237.63 \pm 3.36	62.92 \pm 0.26	77.55 \pm 1.50	178.02 \pm 0.16	235.02 \pm 2.87
2-Phenyl ethanol	6282 \pm 0.11	1266.5 \pm 9.68	2398 \pm 0.12	3662.5 \pm 0.45	2431 \pm 5.79
Total alcohols ($\mu\text{g/L}$)	22515.33 \pm 109.4	11033.77 \pm 363.8	9978.80 \pm 34.8	6878.20 \pm 47.1	8552.96 \pm 36.4
% of total VOC concentration	32.56	17.30	16.73	9.74	12.46
Esters^b					
N-amyl acetate	170.91 \pm 1.73	49.44 \pm 1.69	64.70 \pm 0.57	156.25 \pm 0.46	53.45 \pm 1.87
Ethyl caproate	340.79 \pm 12.91	124.30 \pm 3.47	231.13 \pm 0.65	434.53 \pm 6.82	202.34 \pm 0.12
Ethyl lactate	6417.48 \pm 8.35	19400.39 \pm 177.23	24418.60 \pm 6.66	-	24164.77 \pm 357.78
Ethyl-3-hydroxy butanoate	737.37 \pm 8.35	31.76 \pm 0.67	62.40 \pm 0.44	126.4 \pm 1.06	43.67 \pm 0.11
Octyl acetate	239.12 \pm 1.78	85.50 \pm 5.19	26.36 \pm 0.53	2714.50 \pm 5.91	139.36 \pm 0.17
Ethyldecanoate	10.77 \pm 0.21	9.64 \pm 0.32	0.82 \pm 0.03	24.39 \pm 0.31	199.92 \pm 2.66
Ethyl hydrogen succinate	12698.45 \pm 15.83	5468.00 \pm 54.93	3618.67 \pm 0.58	8142.23 \pm 16.26	6125.20 \pm 45.91
N-phenyl acetamide	130 \pm 0.76	9.61 \pm 0.20	13.72 \pm 0.01	-	1912.25 \pm 2.34
Diethyl malate	1075.85 \pm 16.53	444.08 \pm 27.84	730.07 \pm 0.44	3223.95 \pm 15.10	1912.25 \pm 2.34
Diethyl succinate	14292.21 \pm 162.94	8457.77 \pm 129.04	2873.12 \pm 0.26	3496.21 \pm 3.78	17506.49 \pm 185.7

Table 3 continued

Methyl-4 hydroxy-butanoate	4983.96±8.06	1389.70±19.53	493.78±12.75	902.37±4.42	208.23±1.15
Total esters (µg/L)	41096.91±237.4	35470.19±420.1	32533.37±22.9	19220.83±54.1	52467.9±600.1
% of total VOC concentration	59.63	55.68	54.57	28.31	76.62
Fatty acids^a					
Butyric acid	73.62±1.25	334.66±1.90	333.02±0.04	490.88±1.47	43.51±0.52
Hexanoic acid	338.36±1.42	862.86±60.55	1500.29±5.64	736.24±1.31	284.23±0.11
Octanoic acid	241.75±0.71	135.87±2.19	235.08±0.59	904.19±4.28	383.19±12.06
Pidolic acid	71.52±3.11	118.08±1.59	-	618.51±0.55	323.41±2.43
5-oxotetra hydrofuran-2-carboxylic acid	68.01±3.90	743.64±14.76	1218.87±0.51	3088.75±2.72	1685.65±6.61
Table 3 continued					
Total fatty acids (µg/L)	793.26±10.4	2195.11±80.9	3287.26±6.8	5838.57±10.3	2719.99±21.7
% of total VOC concentration	1.15	3.44	5.51	8.27	3.96
Lactones					
Butyrolactone	4409±2.70	14933±0.08	13800±0.14	35791±120.17	4624.42±31.23
% of total VOC concentration	6.38	23.41	23.14	50.69	6.74
Other compounds					
Ethyl vanilate	74.28±3.19	46.95±1.59	-	97.01±0.1	72.15±1.16
Acetovanillone	31.55±0.90	29.68±0.30	21.72±0.05	66.98±0.14	43.62±0.62
Total other compounds (µg/L)	105.83±4.09	76.63±1.89	21.72±0.05	163.99±0.24	115.77±1.78
% of total VOC concentration	0.15	0.12	0.04	0.23	0.17
Total volatiles (µg/L)	68920.3±364.0	63708.7±866.9	59647.5±65.3	67892.6±231.9	68481.1±691.3
% of total VOC concentration	100	100	100	100	100

^a Expressed in equivalents of phenyl ethanol

^b Expressed in equivalents of ethyl decanoate

Concentration in microgram per liter ±RSD (relative standard deviation (%))

During aging, the level of the dissolved oxygen in wines decreased and stays at a low level and this could explain why some volatile alcohols declined, but some acids and esters were accumulated in the concentration within 6-12 months barrel aging.

Of the chemical groups found in the volatile fraction of the red wines sample analyzed, esters were present in the highest number (11), followed by alcohols (10), acids (5), lactone (1). The predominance of volatile compounds belonging to this class of esters, alcohols, and acids has been previously observed by Welke et al., 2012 [62] and Jiang et al., 2013 [12], Ivanova et al., 2013 [3], Arcaria et al., 2017 [63], in different varietal red wines.

CONCLUSIONS

A total of 29 volatile compounds were determined by GC-MS in red wines produced in Romania. Considering all the detected volatiles, esters and alcohols were the main contributors to the overall volatile composition of the wines, which made up to 30–70% and 10–35% of the total level of volatiles, respectively. Wines aged for 12 months contained a higher amount of volatile compounds compared to the wines aged for 6 months. The Romanian red wines were characterized by higher level of esters, alcohols, and lactones. The volatile compounds in red wines aged for two periods of time are strongly marked by a decrease in the concentration of esters as the ageing time gets longer, with only ethyl lactate and diethyl succinate showing an increase. Higher alcohols amounts increased with ageing maybe as a result of hydrolysis of the esters or evaporation. The high amount of butyrolactone in all sampled wines is an indication of the ageing of these wines in oak barrels.

Considering all volatiles detected, esters and higher alcohols are the main aromatic contributor for Romanian wines in both oenological regions.

EXPERIMENTAL SECTION

Vineyard

Grapes were collected during the 2016 season, at commercial harvest, in the wine producing areas Dobra and Rătești both located in Satu Mare County (north-west region of Romania) and Aliman, located in the Constanța County, south-east of Romania.

Table 4 shows climatic conditions from the two regions and latitude, longitude and altitude of the areas were determined with the global positioning system GPS apparatus.

In an effort to identify volatile compounds related to grape variety and wine characteristics rather than growing conditions, wine samples were sourced from three commercial vineyards located in the mentioned regions.

Table 4. Climatic conditions and geographic coordinates of *Vitis vinifera* L. grapes from Romania investigated in this study

Location	<i>Vitis vinifera</i> L. grape variety	Latitude	Longitude	Altitude (m)	Annual mean temperature (°C)	Mean relative humidity (%)	Annual mean rainfall (mm)	Vineyard exposure
Dobra Satu Mare County	Cabernet Sauvignon	47°29'41"N	22°49'39"E	130-160	10.1	50-60	623	S, S-W
Rătești Satu Mare County	Fetească Neagră, Pinot Noir	47°34'55"N	22°52'45"E	160-200	10.1	50-60	623	S, S-E, S-W
Aliman Constanța County	Merlot, Fetească Neagră	44°11'30"N	27°48'51"E	100-120	11.7	40-50	440	S, S-E, S-W

Wine samples

The wine samples consisted in five red wines from two wine regions: Cabernet Sauvignon, Fetească Neagră and Pinot Noir (from Satu Mare - north-west of Romania) and Fetească Neagră and Merlot (from Constanța – south-east of Romania) were kindly donated by wineries. All the wine samples were from the same vintage, 2016.

All wine samples were fermented in stainless steel fermenters at 20–32°C and the malolactic fermentation was performed ten days after the alcohol fermentation. Wines were aged in the same type of oak barrel provided by the same tonnellerie, for 6 months and 12 months. The oaks from species *Q. robur* were grown in the forests of Arad County. The oak barrels were medium toast (2.5 hours, toast temperature - 120-160°C).

All samples were kept at 4°C before the analysis.

Oenological parameters were analyzed for two reasons: first, some of them are directly connected with wine quality (volatile acidity and ethanol content), with wine stability (pH, titrable acidity, levels of tartaric acid, levels of sulphur dioxide); second, they are closely correlated with the extractive capacity of wines.

All the wines were elaborated and aged in the winery and cellars of Dobra Wine (situated in Dobra - Satu Mare County), Rătești Wine (situated in Rătești - Satu Mare County) and Alira Wine (situated in Aliman - Constanța County).

Chemicals and Reagents

The reference standards, 2-phenyl ethanol, ethyl decanoate, butyrolactone, isoamyl alcohol and 1-octanol (used as internal standard, IS) were supplied from Fluka. Dichloromethane, used for extraction of volatiles, was purchased from VWR. The standard stock solutions were prepared by dissolving 10 mg of each reference compound in 10 ml of dichloromethane.

Liquid-liquid extraction

The protocol used by Andujar-Ortiz et al., 2009 [64], was adapted and used for isolation of the volatile compounds from the wine samples. To 50 ml of wine spiked with 1-octanol (614 $\mu\text{g/L}$ concentration) internal standard was added 20 mL of dichloromethane and placed in Erlenmeyer flask equipped with a ground stopper. The extraction was carried out under continuous stirring in an ice bath for 30 minutes. Then the mixture was kept for 15 minutes in an ultrasonic bath at the same temperature, to avoid possible formation of an emulsion. After separation, the organic layer was dried on Na_2SO_4 , evaporated under a nitrogen stream to approximately 200 μL volume of the extract. From this solution, 1 μL was injected into the GC-MS system. All extractions were carried out in triplicate.

GC-MS analysis

Analysis of wine volatile compounds was carried out using a Shimadzu QP 2010 PLUS Mass Spectrometer coupled with Gas Chromatograph (Shimadzu) equipped with a Carbowax type column from Agilent, with a dimension 30 m x 0.32 mm ID and 0.50 μm film thicknesses. The carrier gas was He (6.0) with a flow rate 1.7 mL/min. The working parameters were: injector temperature 250°C, the ion source temperature 220°C, and the interface temperature 250°C. The column temperature program was conducted as follows: 40°C was the initial temperature for 5 min, increasing at a rate of 4°C/min to 220°C, and holding 220°C for 15. The electron impact (EI) was set at 70 eV. A mass range of 35–500 m/z was recorded at one scan per second.

Calibration curves

For quantification, five-point calibration curves were constructed for the following standard compounds: isoamyl alcohol (31-63000 $\mu\text{g/L}$), butyrolactone (30-62000 $\mu\text{g/L}$), ethyl-decanoate (48-15000 $\mu\text{g/L}$) and 2-phenyl ethanol (64-12900 $\mu\text{g/L}$), containing the internal standard (1-octanol). The linearity data

of the analytical method are presented in Table 5. As can be seen from Table 5, the linearity is satisfactory in all cases with correlation coefficients (R^2) ranging from 0.9954 (ethyl decanoate) to 0.9991 (butyrolactone).

Table 5. Linear regression data

Compound	Intercept	Slope	R^2	Range ($\mu\text{g/L}$)
Butyrolactone	-0.8469	-0.0152	0.9991	30- 62000
2-Phenyl ethanol	-0.2280	-0.0320	0.9972	64- 12900
Ethyl decanoate	-0.2282	-0.0015	0.9954	48- 15000
Isoamyl alcohol	0.0388	0.00038	0.9971	31-63000

ACKNOWLEDGMENTS

Authors are grateful to Mr. Kallos Francisc (Dobra Wine), to Mr. Ionuț Gozar (Rătești Wine) and Mr. Marian Ivănescu (Alira Wine) for providing wine samples, and to Mr. Sorin Botoș (Transylvania Bois Tonnellerie) for providing oak barrels in this research.

REFERENCES

1. E.S. Palomo, E.G. García-Carpintero, M.A.G. Viñas, *South African Journal for Enology & Viticulture*, **2015**, 36, 117.
2. A. Rapp, H. Mandery, *Experientia*, **1986**, 42, 873.
3. V. Ivanova, M. Stefova, B. Vojnoski, T. Stafilov, I. Bíró, A. Bufa, A. Felinger, F. Kilár, *Food Bioprocess Technology*, **2013**, 6, 1609.
4. M.P. Marti, M. Mestres, C. Sala, O. Busto, J. Guasch, *Journal of Agricultural and Food Chemistry*, **2003**, 51, 7861.
5. P. Polásková, J. Herszage, S.E. Ebeler, *Chemical Society Reviews*, **2008**, 37 (11), 2478.
6. S. Ebeler, *Food Reviews International*, **2001**, 17, 45.
7. J. Bao, Z. Zhang, *Molecules*, **2010**, 15, 9184.
8. C.A. van der Merwe, C.J. van Wyk, *American Journal of Enology and Viticulture*, **1981**, 32, 41.
9. P. Schreir, *Critical Reviews in Food Science and Nutrition*, **1979**, 12, 49.
10. R.S. Jackson, "Wine Science: Principles and Applications", Academic Press, San Diego, CA, **1994**, chapter 11.
11. A. Bisotto, A. Julien, P. Rigou, R. Schneider, J.M. Salmon, *Australian Journal of Grape & Wine Research*, **2015**, 21, 194.

12. B. Jiang, X. Zhumei, L. Meijuan, Z. Zhang, *Food Research International*, **2013**, 51 (2), 482.
13. M.A. Amerine, E.B. Roessler, "Wines. Their sensory evaluation", Freeman San Francisco, **1976**.
14. S.C. Fairbairn, A.Y. Smit, D. Jacobson, B.A. Prior, F.F. Bauer, *South African Journal for Enology & Viticulture*, **2014**, 35 (2), 168.
15. L.J. Perez-Prieto, J.M. Lopez-Roca, E. Gomez-Plaza, *Journal of Food Composition and Analysis*, **2003**, 16, 697.
16. D. Liu, R.-R. Xing, Z. Li, D.-M. Yang, Q.-H. Pan, *European Food Research and Technology*, **2016**, 242, 1937.
17. G. Styger, B. Prior, F.F. Bauer, *Journal of Industrial Microbiology & Biotechnology*, **2011**, 38 (9), 1145.
18. I. Lukić, I. Horvat, *Food Technology and Biotechnology*, **2017**, 55 (1), 95.
19. D. Dimitrov, V. Haygarov, T. Yoncheva, D. Nedelkovski, *Journal of Mountain Agriculture on the Balkans*, **2017**, 20 (3), 187.
20. S.P. Imre, P.A. Kilmartin, T. Rutan, J.L. Mauk, L. Nicolau, *Journal of Food Agriculture and Environment*, **2012**, 10 (2), 280.
21. A. Slegers, P. Angers, K. Pedneault, *Journal of Food Chemistry and Nanotechnology*, **2017**, 3 (1), 8.
22. M. Vilanova, M.P. Diago, Z. Genisheva, J.M. Oliveira, J. Tardaguila, *Journal of The Science of Food and Agriculture*, **2012**, 92, 935.
23. J.M. Meyers, G.L. Sacks, J.E. Vanden Heuvel, *HortTechnology*, **2013**, 23 (5), 581.
24. M. Vilanova, Z. Genisheva, M. Tubio, K. Álvarez, J.R. Lissarrague, J.M. Oliveira, *Molecules*, **2017**, 22, 1500.
25. J.M. Gambetta, S.E.P. Bastian, D. Cozzolino, D.W. Jefferies, *Journal of Agricultural and Food Chemistry*, **2014**, 62, 6512.
26. J.J. Rodríguez-Bencomo, M. Ortega-Heras, S. Pérez-Magariño, González-Huerta, *Journal of Agricultural and Food Chemistry*, **2009**, 57, 6383.
27. L. Rolle, V. Englezos, F. Torchio, F. Cravero, S. Rio Segade, K. Rantsiou, S. Giacosa, A. Gambuti, V. Gerbi, L. Coccolin, *Australian Journal of Grape and Wine Research*, **2018**, 24, 62.
28. P. Ribéreau-Gayon, Y. Glories, A. Maujean, D. Dubourdieu, "Handbook of enology. Vol 2: The chemistry of wine: Stabilization and treatments", 2nd Ed. Chichester, Wiley, **2006**.
29. P. Polaskova, J. Herszage, S.E. Ebeler, *Chemical Society Reviews*, **2008**, 37, 2478.
30. R. Bleiziffer, S. Suvar, P. Podea, C. Mesaros, M. Culea, *STUDIA UBB CHEMIA*, **2017**, LXII, 3, 123.
31. L. Castro-Vázquez, M.E. Alañón, E. Calvo, M.J. Cejudo, M.C. DíazMaroto, M.S. Pérez-Coello, *Journal of Chromatography A*, **2011**, 1218, 4910.
32. R. López, M. Aznar, J. Cacho, V. Ferreira, *Journal of Chromatography A*, **2002**, 966 (1-2), 167.
33. L. Cai, S. Rice, J.A. Koziel, M. Dharmadhikari, *Separations*, **2017**, 4, 24.
34. D. Caven-Quantrill, A.J. Buglass, *Beverages*, **2017**, 3, 62.

35. H.S. Canbay, *International Journal of Analytical Chemistry*, **2017**, Article ID 4870671.
36. V. Avram, C.G. Floare, A. Hosu, C. Cimpoiu, C. Măruțoiu, Z. Moldovan, *Analytical Letters*, **2015**, *48*, 1099.
37. M. Palade, M.-E. Popa, *Scientific Bulletin, Series F. Biotechnologies*, **2015**, *XIX*, 174.
38. A.-M. Moroșanu, V.V. Cotea, C.E. Luchian, M. Niculau, C. Colibaba, A.C. Tarțian, *BIO Web of Conferences*, 39th World Congress of Vine and Wine, **2016**, *7*.
39. F.D. Bora, A. Donici, A. Ciubucă, E. Postolache, G. Tabaranu, V. Enache, N. Bîrliga, N. Pop, C. Bunea, *Bulletin UASVM Horticulture*, **2016**, *73* (2), 116-125.
40. M. Miclean, A. Naghiu, P. Badea, L.R. Fotescu, *Agricultura – Știință și practică*, **2010**, 1-2 (73-74), 68.
41. A.O. Antoce, *Revista de chimie*, **2012**, *63*, 9, 859.
42. L.M. Palade, D. Duta, C. Popescu, C. Croitoru, M.E. Popa, *Romanian Biotechnological Letters*, **2016**, *22* (6), 12005.
43. M. Pomar, L.A. Gonzalez-Mendoza, *Journal International des Sciences de la Vigne et du Vin*, **2001**, *35* (1), 41.
44. N. Vivas, A. Lonvaud, Y. Glories, *Journal des sciences et techniques de la tonnellerie*, **1995**, *1*, 81.
45. S. Canas, *Beverages*, **2017**, *3* (55), 1.
46. ***, EC Commission Regulation (EC) No. 606/2009 of 10 July 2009 laying down certain detailed rules for implementing Council Regulation (EC) No. 479/2008 as regards the categories of grapevine products, oenological practices and the applicable restriction, Official Journal of the European Union, L 193 (**2009**), pp. 1-59. EC No 606/2009, Annex I B.
47. R.S. Jackson, "Wine science, principles and applications", 3rd ed., Academic Press-Elsevier, Burlington, USA, **2008**.
48. A. Stój, T. Czernecki, D. Domagała, Z. Targoński, *International Journal of Food Properties*, **2017**, *20* (1), 830.
49. M. Tufariello, S. Capone, P. Siciliano, *Food Chemistry*, **2012**, *132*, 2155.
50. S. Capone, M. Tufariello, L. Francioso, G. Montagna, F. Casino, A. Leone, P. Siciliano, *Sensors and Actuators B*, **2013**, *179*, 259.
51. P. Romano, G. Suzzi, V. Brandolini, E. Menziani, P. Domizio, *Letters in Applied Microbiology*, **1996**, *22*, 299.
52. M. Revi, A. Badeka, S. Kontakos, M.G. Kontominas, *Food Chemistry*, **2014**, *152*, 331.
53. C. Bayonove, R. Baumes, J. Crouzet, Z. Gunata, *Enologia. Fundamentos científicos y tecnológicos*, **2000**, 147.
54. J.M. Oliveira, P. Oliveira, R.L. Baumes, O. Maia, *Journal of Food Composition and Analysis*, **2008**, *21*, 695.
55. M. Patrianakou, I.G. Roussis, *South African Journal of Enology and Viticulture*, **2013**, *34* (2), 241.
56. M. Gil, J.M. Cabellos, T. Arroyo, M. Prodanov, *Analytica Chimica Acta*, **2006**, *563*, 145.

57. E. Sanchez-Palomo, M. Trujillo, A. García Ruiz, M.A. González Viñas, *Food Research International*, **2017**, *100*, 201.
58. R. Perestrelo, A. Fernandes, F.F. Albuquerque, J.C. Marques, J.S. Camara, *Analytica Chimica Acta*, **2006**, *563*, 154.
59. C. Coetzee, W.J. du Toit, *Food Research International*, **2012**, *45* (1), 287.
60. S. Lafon-Lafourcade, C. Geneix, P. Ribéreau-Gayon, *Applied and Environmental Microbiology*, **1984**, *47*, 1246.
61. T. Garde-Cerdan, D. Torrea-Goni, C. Ancin-Azpilicueta, *Australian Journal of Grape and Wine Research*, **2002**, *8* (2), 140.
62. J.E. Welke, V. Manfroi, M. Zanus, M. Lazarotto, C.A. Zini, *Journal of Chromatography A*, **2012**, *1226*, 124.
63. S.G. Arcaria, V. Caliaric, M. Sganzerla, H.T. Godoya, *Talanta*, **2017**, *174*, 752.
64. I. Andujar-Ortiz, M.V. Moreno-Arribas, P.J. Martín-Álvarez, M.A. Pozo-Bayón, *Journal of Chromatography A*, **2009**, *1216*, 7351.

CHROMATOGRAPHIC ANALYSIS OF CAROTENOIDS AND ANTHOCYANINS IN SWEET CHERRY AUTUMN LEAVES USED IN ORNAMENTAL LANDSCAPES

TABITA-TEODORA LISANDRU^a, ANDREA BUNEA^b, ADRIAN FÜSTÖS^a,
ADELINA DUMITRAȘ^c, CLAUDIU-IOAN BUNEA^a,
VALENTIN SEBASTIAN DAN^a, EMESE GÁL^d, VIOREL MITRE^{a*}

ABSTRACT. The pigments composition of sweet cherry leaves (*Prunus avium* L.) were identified for the first time under condition of Cluj-Napoca city. Five cherry tree varieties (Merchant, Early Red, Lapins, Burlat, Kordia) have been selected in autumn of 2016 in order to identify and quantify the major pigments in these types of leaves. Five carotenoids (lutein, β -carotene, zeaxanthin, cis- β -caroten, α -carotene) and one major anthocyanin (cyanidin-3-glucoside) were found in cherry leaves. The main carotenoids identified in all cultivars were lutein (340.55 $\mu\text{g/g}$), followed by β -carotene (147.06 $\mu\text{g/g}$). Early Red cultivar had the highest content of cyanidin-3-glucoside (17.96 mg/100g), followed by Kordia variety (11.46 mg/100g). Cyanidin-3-glucoside is responsible for red coloration of the leaves, meanwhile lutein, β -carotene, zeaxanthin, cis- β -carotene and α -carotene are providing yellow to orange colours of the leaves. The coloration of sweet cherry leaves, given by the accumulation of anthocyanin and carotenoids in autumn, makes this species suitable for ornamental use in urban design.

Keywords: anthocyanin, carotenoids, HPLC

^a Department of Horticulture and Landscape Architecture, University of Agricultural Sciences and Veterinary Medicine, Calea Mănăștur 3-5, 400372, Cluj-Napoca, Romania

^b Department of Biochemistry, University of Agricultural Sciences and Veterinary Medicine, Calea Mănăștur 3-5, 400372, Cluj-Napoca, Romania

^c Department of Forestry, University of Agricultural Sciences and Veterinary Medicine, Calea Mănăștur 3-5, 400372, Cluj-Napoca, Romania

^d Babeș-Bolyai University, Faculty of Chemistry and Chemical Engineering, 11 Arany János str., RO-400028, Cluj-Napoca, Romania,

* Corresponding author: viorel.mitre@usamvcluj.ro

INTRODUCTION

Recently, leaves colour change of the deciduous tree in autumn gained a lot of interest when this remarkable phenomenon was observed from an ecological perspective [1]. To explain the significance of autumnal colours of the leaves a few hypotheses appeared [2, 3, 4, 5] but even so the dominant explanation is based on plant physiology: autumn bright colours are the result of leaf senescence, while physiological functions of leaves are related to pigments [6, 7]. What it was not discussed yet, is how this phenomenon can be used with ornamental purpose by integrating some species into urban design because of their beautiful autumnal colours of the leaves. The colour change of the leaves remodels every year the landscape into a spectacular mosaic of yellow, orange and red [8]. Nevertheless, there are some deciduous tree species which lose their leaves without changing their colour. Just ~10% of the trees from temperate climate present red autumn colours while ~15% of the trees present yellow leaves colour [9, 8]. Originally from Caspian and Black Seas, and currently spread in all continents [10] sweet cherry (*Prunus avium* L.) is one of the tree species which is changing the colour of the leaves from green to bright colours of yellow and red in autumn, creating wondrous landscapes and having a great ornamental potential. The cause of leaves colour change of cherry tree in autumn months is due to the accumulation of anthocyanin and carotenoids in the leaves.

Anthocyanins belong to flavonoids (plant secondary metabolites) and are water-soluble pigments responsible for the attractive colours of flowers, fruits and leaves [11, 12]. They provide red, blue and purple colours and are important phenolic component in colour traits of ornamental species. Red leaves are an important element in ornamental landscape use [13] which adds warmth to the landscape. Plants with colourful foliage have been always appreciated in landscape design because of the beautiful perspectives created by their presence and because they allow you to alter mood or perception of the urban space (e.g. make small spaces seem larger; focus attention to a particular area).

Anthocyanins are not the only pigments answerable for autumn colours; carotenoids pigments are contributing also to the autumn bright colours. Carotenoids are the second major group of pigments which accumulates in the plastids of leaves and provide red, orange and yellow pigments [14, 15]. Unlike anthocyanin, carotenoids are synthesized all along growing season in order to enable or protect photosynthetic light capture [16].

The magnificent appearance of autumn senescence is the result of the degradation of the chlorophyll which allows the red and yellow hues of anthocyanins and carotenoids to be visible [17, 9].

Sweet cherry tree (*Prunus avium* L.) may be considered an ornamental species not just because of the beautiful flowers that provide in spring time but also for autumnal colours of the leaves that creates brilliant landscapes at the end of the vegetation period. Fruit trees were used with ornamental purpose since ancient time but over time their usage had just one purpose: fruit production. Nowadays, beside their fruit production and fruit nutritional values, fruit trees have begun to be part of landscape design being recognized for their ornamental values. Fruit trees are planted every year in urban greenery while the existing fruit trees are groomed and nurtured [18]. They are used in landscape either for fruits, either for the shade provided by the crown of the trees [19]. The shape of the crown, the vibrant colours of the leaves integrates fruit trees in urban design alongside ornamental plants creating attractive perspectives in urban cities.

In this work, we chose five varieties of sweet cherry tree (*Prunus avium* L.) with the purpose to identify the pigments that provide autumnal colors of leaves species. The selected cultivars are usually used in intensive and super intensive orchards but the leaves color change make these varieties suitable for landscape design use. This study was inspired by the colourful landscapes given by the leaves appearance of the sweet cherry tree (*Prunus avium* L.) in autumn months.

RESULTS AND DISSCUSION

Carotenoid composition in leaves

Five carotenoids answerable for yellow-orange colour were separated from *Prunus avium* L. leaves cultivars and have been identified according to their chromatographic and spectroscopic properties (UV-VIS spectra).

The average values of major carotenoids show significant differences between all five cultivars. The sweet cherry cultivar with the highest level of carotenoids was 'Merchant' (220.06 $\mu\text{g/g}$) followed by 'Burlat' (114.04 $\mu\text{g/g}$) and 'Kordia' (112.3 $\mu\text{g/g}$). The accumulation of pigments in 'Early Red' and 'Lapins' varieties is about three times lower than 'Merchant'. HPLC chromatogram of 'Lapins' cultivar obtained from pigments leaf extracts shows five carotenoid peaks corresponding to the retention time and spectra absorption to lutein, zeaxanthin, α -carotene, β -carotene and cis- β -carotene (Figure 1).

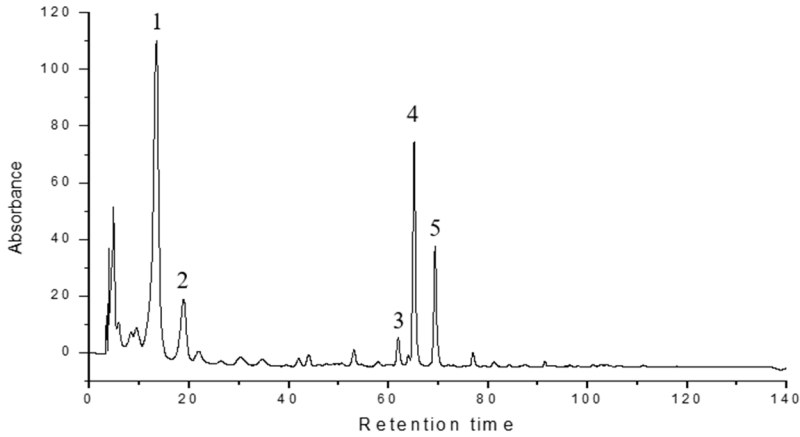


Figure 1. HPLC chromatogram obtained from carotenoid extracts from ‘Lapins’ cultivar leaves. 1 - Lutein; 2- Zeaxanthin, 3- α -carotene; 4- β -carotene; 5- cis- β -carotene

The main carotenoid found in all varieties of cherry leaves is represented by lutein, followed by β -carotene (Table 1). Previous studies results showed also lutein as major carotenoid in *Moringa oleifera* leaves, with a per cent of 53.6 and 52.0 % of total carotenoids [20]. The content of lutein, for leaves of ‘Burlat’ variety was 87.84 $\mu\text{g/g}$.

Table 1. Carotenoid composition ($\mu\text{g}\pm\text{SD/g}$) of leaves of *Prunus avium* cultivars.

Identified carotenoids	Concentration of carotenoids ($\mu\text{g}\pm\text{SD/g}$) in leaves				
	Merchant	Early Red	Lapins	Burlat	Kordia
Lutein	81.2 \pm 1.03 ^b	50.11 \pm 0.87 ^d	43.3 \pm 0.69 ^e	87.84 \pm 0.92 ^a	78.1 \pm 1.02 ^c
Zeaxanthin	13.81 \pm 0.7 ^a	10.06 \pm 0.07 ^b	7.98 \pm 0.06 ^c	4 \pm 0.02 ^e	6.7 \pm 0.05 ^d
β -carotene	87.9 \pm 1.65 ^a	7.28 \pm 0.02 ^e	14.43 \pm 0.2 ^d	17.55 \pm 0.2 ^c	19.9 \pm 0.5 ^b
cis- β -carotene	37.15 \pm 0.9 ^a	3.34 \pm 0.02 ^e	8.07 \pm 0.06 ^b	4.65 \pm 0.08 ^d	7.63 \pm 0.06 ^c
Total of carotenoids	220.06 A	70.79 E	74.39 D	114.04 B	112.33 C

Different letters indicate statistical differences between *Prunus avium* varieties regarding the carotenoid composition in leaves ($\text{DS}_{5\%} = 0.20\text{-}0.23$).

The statistical analysis from Table 1 was preformed between identified carotenoids from each cultivar.

The leaves of 'Merchant' variety had a lutein content of 81.2 $\mu\text{g/g}$, followed by 'Kordia' variety with lutein content of 78.1 $\mu\text{g/g}$. Leaves of 'Early Red' and 'Lapins' varieties showed lutein content of 50.11 $\mu\text{g/g}$ for 'Early Red' and 43.3 $\mu\text{g/g}$ for 'Lapins'.

The results showed that there is a significant difference ($P < 0.05$) between levels of lutein content for these five cultivars of *Prunus avium*. The β -carotene levels found in cherry leaves also showed significant difference ($P < 0.05$) between all sweet cherry varieties.

'Merchant' leaves showed the highest level of β -carotene (87.9 $\mu\text{g/g}$), followed by 'Kordia' with a concentration of 19.9 $\mu\text{g/g}$, 'Burlat' (17.55 $\mu\text{g/g}$), 'Lapins' (14.43 $\mu\text{g/g}$) and 'Early Red' (7.28 $\mu\text{g/g}$). Also, zeaxanthin and cis- β -carotene were found in leaves of cherry tree. The levels of these two carotenoids showed significant differences between all cultivars studied ($P < 0.05$). Another identified carotenoid was α -carotene which was found just in leaves of 'Lapins' variety with a concentration of 0.61 $\mu\text{g/g}$.

Pigments differences between *Prunus avium* cultivars have been interpreted by using principal component analysis (PCA). PCA multivariate statistical analysis shows the pigments concentrations differences between all five varieties of *Prunus avium*, with a sample variance of 99.9 % defined by the first two components. Multivariate analysis shows a clear and significant separation of the 'Merchant' variety (from quadrant I) to the 'Early Red' cultivar and to the other three cultivars similar to each other (Figure 2). The carotenoid pigment responsible for the difference is lutein.

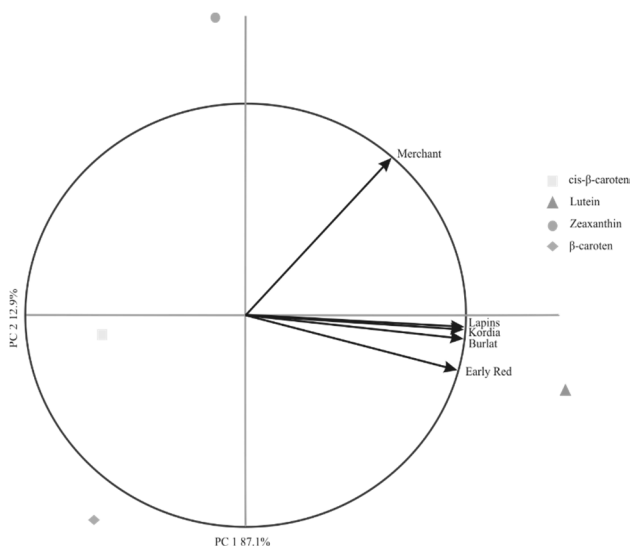


Figure 2. Principal component analysis. Correlation biplot 99.9%

The results confirm the presence of five major carotenoid pigments in the leaves of cherry studied cultivars. The concentration of identified pigments is significantly different for each cultivar and all five varieties contained the same pigments, except 'Lapins' cultivar which contain also a small concentration of α -carotene.

Anthocyanin composition in leaves. The anthocyanin pigments responsible for red and blue colour of plants were found in the leaves of *Prunus avium* studied cultivars. HPLC analysis showed one major anthocyanin peak, corresponding to the retention time and spectra absorption to cyanidin-3-glucoside (Figure 3).

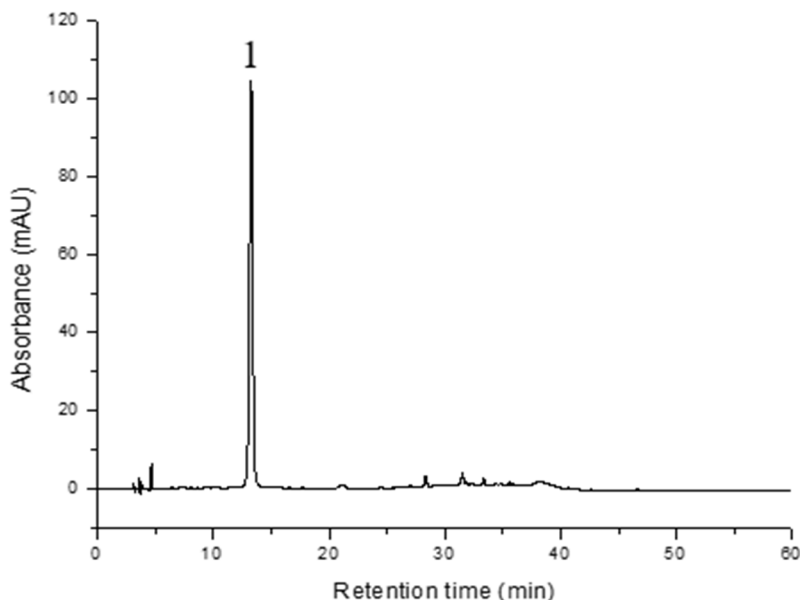


Figure 3. HPLC chromatogram obtained from anthocyanin extracts from 'Kordia' variety (*P. avium* L.) leaves. Only one peak (1) was detected corresponding to cyanidin-3-glucoside

'Early Red' cultivar had the highest level of cyanidin-3-glucoside (17.96 mg/100g), followed by 'Kordia' (11.46 mg/100g), while 'Burlat' and 'Kordia' had similar content of anthocyanin pigment (Table 2).

Table 2. The concentration of cyanidin-3-glucoside in sweet cherry leaves.

Sweet cherry varieties	Cyanidin-3-glucoside (mg/100g)	±d	Mean difference
Merchant (Mt)	9.85±1.23	0.00	-
Kordia	11.46±2.68	-1.61	-
Early Red	17.96±3.24	-8.11	***
Lapins	5.77±0.78	4.08	**
Burlat	5.71±0.67	4.14	**

Different symbols indicate statistical difference between *Prunus avium* L. cultivars (DL_{5%}=2.2; DL_{1%}=3.2; DL_{0.1%}=4.81)

The results of HPLC analysis showed that there was a significant difference ($d \geq DL 0.1\%$) between sweet cherry cultivars regarding the leaves content in cyanidin-3-glucoside. Although, ‘Lapins’ and ‘Burlat’ showed a similar concentration of anthocyanin pigments, which means that there is not a significant difference between these two cultivars.

Following the results, we observed that the anthocyanin composition of cherry leaves is generally inversely proportional to carotenoid content (Figure 4), which means that the ornamental value of this species in fall season is mostly given by carotenoids pigments. Yellow-orange pigments of cherry leaves are predominant and became visible earlier than anthocyanin pigments, but together they make this species suitable for landscape design use by giving it a great ornamental potential.

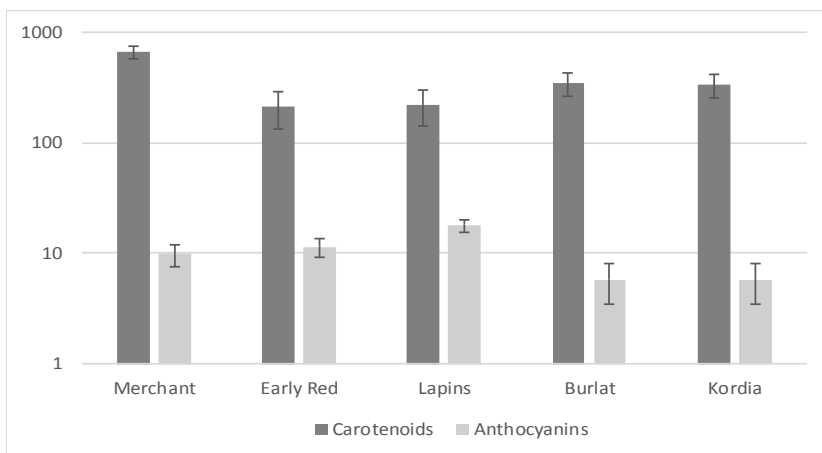


Figure 4. Differences among carotenoids and anthocyanin content in *Prunus avium* L. cultivars leaves

The researches regarding the carotenoids and anthocyanin content in leaves of some sweet cherry cultivars has not been reported before, preceding studies been focused more on flowers, antioxidant efficiency and fruits quality of cherry tree. B.J. Glover consider that the research regarding plant leaves colour are limited recorded due to slight colour variation in comparison with flower colour [21].

In this research, the HPLC-PDA method was used to determine the pigments of cherry leaves and to establish the ornamental value of cherry tree given by leaves colour in autumn. Five carotenoids (lutein, β -carotene, zeaxanthin, cis- β -carotene, α -carotene) and one anthocyanin (cyanidin-3-glucoside) were found in composition of cherry leaves.

The red colour of the sweet cherry varieties leaves is provided by the presence of the anthocyanin pigments. Anthocyanin pigments are the most abundant polyphenols which can be found in all parts of the plant being responsible for red, violet and blue colours [22]. The coloration of the leaves in most species is the result of the accumulation of anthocyanin pigments in the vacuoles of (sub)epidermal cells, principally in flower, fruits and vegetables but also in leaves [23, 24]. The colour of anthocyanin may change because of the acidity of the vacuole providing red colour in acidic environment and blue colour in neutral or weak acidic conditions [25].

Along sweet cherry leaves, in available literature there were reported different leaves species and cultivars which contained cyanidin-3-glucoside as major anthocyanin. For instance, the existence of cyanidin-3-glucoside pigment was showed in grape leaves in proportion of 43% [26]. Different sweet potato varieties leave had also a high content of cyanidin pigment indicating that the anthocyanin leaves composition may be cyaniding type [27]. Studies on crab-apple determined that cyanidin pigment was also the major anthocyanin, which was responsible for the various red colours of the leaves species [23]. The anthocyanin content of purple basil leaves was expressed as cyanidin-3-glucoside also [11].

The yellow-to-red colour of the leaves is provided by the accumulation of lipid-soluble compounds, carotenoids, in chloroplasts [28]. Carotenoids can be found as crystals, lipid-dissolved or lipid-crystalline forms in the chromoplast structure [29]. They protect the photosynthetic apparatus and appear as a result of leaf senescence in autumn, when chlorophyll is degraded and grants carotenoids to be visible [30, 9].

Studies regarding the content of carotenoids in leaves were made before and there were reported similar content of β -carotene in leaves of *Pereskia* species (13.8-47.0 $\mu\text{g/g}$) as in 'Lapins', 'Burlat' and 'Kordia' cultivars [31]. Also, zeaxanthin levels found in cherry leaves were much higher than zeaxanthin values reported in spinach, endive or lettuce leaves (0.1-0.07 $\mu\text{g/g}$) [32].

The existence of pigments in different species leaves was recorded during the time and it was the object of many studies in last decade. The colours change of the leaves of the species during the autumn months has triggered curiosity of scientists and ecologists which understood the importance of autumn phenology [33].

The autumnal landscapes have various intensity in every part of the world and bring millions of visitors to admire the spectacular perspectives created by the colourful leaves of the species [4], [34]. According to [35] and [36] red autumn leaves are dominating in some parts of the world like North America and East Asia, while yellow autumn leaves are dominating in Finland and temperate Northern Europe [37]. Anthocyanins and carotenoids pigments are repeatedly present in the same organs increasing in this way the colour variety and in the same time the ornamental value of the species [22].

On the other hand, colours are an important element in natural scenes that contributes to the visual recognition of the landscape [38], but also is a challenging subject to be studied [39]. Old literature and even modern one have not described properly the landscape importance of the colours of the leaves [40, 41] and [42] consider that the most problematic interpretation of visual world is colour [43].

CONCLUSIONS

The starting point of this study was to determine for the first time the anthocyanins and carotenoids from some sweet cherry cultivars (*Prunus avium* L.) leave composition in order to identify the pigments which transform the leaves into a mosaic of colours in autumn months. Our results showed that cyanidin and carotenoids pigments are present in leaves composition of sweet cherry tree. According to these results and with the fact that anthocyanins and carotenoids are responsible for the autumnal colour of the leaves, sweet cherry trees can be used for ornamental purpose and in association with ornamental plants in landscape design. The colourful leaves of this species make it suitable for landscape design by giving a great effect on the visual perception of the space.

EXPERIMENTAL SECTION

Plant material and sample preparation. Five varieties of sweet cherry tree were selected to be studied: Merchant, Early Red, Lapins, Burlat, Kordia. Leaves were collected in autumn of 2016 from Steluta Farm Ltd.

orchard located in Cluj-Napoca, Romania. All five varieties were cultivated under full sun. The colour transformation of the leaves was observed during one month and the samples were collected in two steps: when the leaves turned on in yellow and after the leaves became red. In this way, the ornamental value of the cherry tree which is given by the leaves colour can be highlight. In order to identify the pigments content of the leaves, extraction and quantification of the carotenoids and anthocyanins were performed.

Chemicals. Methanol, ethyl acetate, petroleum ether, diethyl ether, sodium chloride, anhydrous sodium sulphate was purchased from Merck, Germany. Lutein, zeaxanthin and β -carotene standards were provided by LGC Standards. Methanol and tert-butyl methyl ether (TBME) (HPLC grade) were purchased from Merck.

Extraction of carotenoid pigments. Carotenoids were extracted from 5 g leaves using the procedure described by [44]. The leaves were homogenized and extracted three times with a mixture of methanol/ethyl acetate/petroleum ether (1:1:1, v/v/v). The combined extracts were partitioned in a separatory funnel with water, diethyl ether and saline solution, the ether phase was evaporated to dryness. The extract rich in carotenoids was further diluted with TBME, filtered (PTFE, 0.45 μm) and subjected to high-performance liquid chromatography-photodiode array detector (HPLC-PDA) analysis.

HPLC Determination of carotenoid pigments. HPLC-PDA was performed using a Shimadzu system LC20 AT with a SPD-M20A diode array detector and YMC C30 column (24 cm x 4.6 mm; particle size 5 μm) was used. The mobile phase used was a mixture of two solvents: solvent A: methanol/tert-butyl methyl ether/water (81:15:4, v/v/v) and solvent B: tert-butyl methyl ether/methanol/water (90:7:3, v/v/v). The gradient started with 1% B at min 0 and increased to 100% B at min 160 according to the method described by [45]. The flow-rate was adjusted to 0.8 ml min⁻¹. The carotenoids identification in leaves was carried out by comparison of the UV-VIS spectra and retention time of sample peaks with those of the standards [46]. The carotenoids concentration was calculated using calibration curves of carotenoid standards (lutein, zeaxanthin and beta-carotene).

Extraction of anthocyanin pigments. Anthocyanins were extracted from the leaves with acidified methanol (0.3 % HCl) using a homogenizer (Micra D-9 KT Digitronic, Bergheim, Germany). Re-extraction was done until the residue was colourless, the final extraction was done overnight, at 4°C in the dark. The colored extract was filtered then concentrated under vacuum to remove methanol. After adding 1 ml of methanol, filtered through 0.45 μm the samples were analysed using HPLC-DAD.

HPLC Determination of anthocyanin pigments. Analyses were performed on a Shimadzu HPLC system equipped with a binary pump delivery system LC-20 AT (Prominence), a degasser DGU-20 A3 (Prominence), diode-array SPD-M20 A UV-VIS detector and a Luna Phenomenex C-18 column (5µm, 25 cm x 4.6 mm) was used. The mobile phase consisted in: solvent A-formic acid (4.5%) in bidistilled water and solvent B - acetonitrile. The gradient elution system was: 10% B, 0-9 min; 12% B, 9-17 min; 25% B 17-30 min; 90% B, 30-50 min; 10% B, 50-55 min. The flow rate was 0.8 ml/min and the analyses were performed at 35°C. The chromatograms were monitored at 520 nm. The compounds identification and peak assignments were done based on their retention times, UV-VIS spectra and also comparing with standards (cyaniding-3O-glucoside) and published data. The anthocyanin quantification was performed by using cyanidin-3-O-galactoside as pure standard and the calculation were made using calibration curve.

Statistical analysis. The extraction was made in triplicate from each leaves analysed. Values of each cultivar were averaged and standard deviations were calculated. Data obtained were statistically evaluated using analyse of variance (ANOVA) with Duncan test in order to compare means among groups and to determine significant differences among concentration of pigments in leaves. The level of significance used was $p < 0.05$. Principal component analysis (PCA) was used to determine the correlations between pigments contain and *Prunus avium* L. studied cultivars.

REFERENCES

1. K. Yamazaki, *Naturwissenschaften*, **2008**, 95, 671.
2. M. Archetti, *Journal of Theoretical Biology*, **2000**, 205, 625.
3. W.D. Hamilton, S.P. Brown, *Proc Roy Soc Lond B*, **2001**, 268, 1489.
4. D.W. Lee, K.S. Gould, *Amer Sci*, **2002**, 90, 524.
5. Y. Manetas, *Flora*, **2006**, 201, 163.
6. D.A. Sims, J.A. Gamon, *Remote Sensing of Environment*, **2002**, 81, 337.
7. P. Matile, *Exp Gerontol*, **2000**, 35, 145.
8. M. Archetti, T.F. Doring, S.B. Hagen, N.M. Hughes, S.R. Leather, D.W. Lee, S. Lev-Yadun, Y. Manetas, H.J. Ougham, P.G. Schaberg, T. Howard, *Trends in Ecology and Evolution*, **2009**, 24, 3.
9. M. Archetti, S.P. Brown, *The Royal Society, Proc. R. Soc. Lond. B*, 2004, 271, 1219.

10. A.D. Webster, *Crop physiology, production and uses*, CAB International, Wallingford, Oxon, UK, **1996**.
11. U. Szymanowska, U. Złotek, M. Karas, B. Baraniak, *Food Chemistry*, **2015**, 172, 71.
12. L. Hai-Peng, D. Wei-Dong, T. Jun-Feng, G. Li, Z. Yin, L. Zhi, *Journal of Functional Foods*, **2015**, 17, 449.
13. Y. Zhang, J. Zhang, T. Song, J. Li, J. Tian, K. Jin, *PLoS ONE*, **2014**, 9, 6.
14. G.A. Blackburn, *J. Exp. Bot.*, **2007**, 58, 855.
15. S.C. Chae, S.W. Lee, J.K. Kim, W.T. Park, M.R. Uddin, H.H. Kim, S.U. Park, *Asian Journal of Chemistry*, **2013**, 25, 8.
16. L. Taiz, E. Zeiger, *Plant Physiology*. Sinauer Associates Inc., **2002**, Sunderland.
17. J. Keskitalo, G. Bergquist, P. Gardeström, S. Jansson, *Plant Physiology*, **2005**, 139, 4.
18. R.J. McLain, M.R. Poe, P.T. Hurley, J. LeCompte, M.R. Emery, *Urban Forestry & Urban Greening*, **2012**, 11, 2.
19. E.D.G. Fraser, A.W. Kenney, *Journal of Arboriculture*, **2000**, 26, 2.
20. S.R. Kumar, S.N. Prasad, P. Giridhar, *Eur Food Res Technol*, **2014**, 238,971.
21. B.J. Glover, *International Journal of Design & Nature and Ecodynamics*, **2009**, 4, 3.
22. Y. Tanaka, N. Sasaki, A. Ohmiya, *The Plant Journal: For Cell and Molecular Biology*, **2008**, 54, 4.
23. H. Zhang, M. Jordheimb, D.H. Lewisa, S. Arathoona, M.A. Øyvind, K.M. Davies, *Scientia Horticulturae*, **2014**, 165, 29.
24. T. Goto, T. Kondo T, *Angewandte Chemie International Edition*, **1991**, 30,1.
25. N.M. Karaaslan, M. Yaman, *Eur Food Res Technol*, **2015**, doi: 10.1007/s00217-015-2524-9.
26. N. Rim, S. Achour, M. Jourdes, P.L. Teissedre, A.N. Helal, B. Ezzili, *J. Int. Sci. Vigne Vin*, **2013**, 47, 4.
27. S. Islam, M. Yoshimoto, N. Terahara, O. Yamakawa, *Biosci. Biotechnol. Biochem.*, **2002**, 66, 11, 2483.
28. C. Carrillo, C. Buvé, A. Panozzo, T. Grauwet, M. Hendrickx, *Food Chemistry*, **2017**, 227, 271.
29. I. Sensoy, *Critical Reviews in Food Science and Nutrition*, **2014**, 54, 7, 902.
30. B. Llorente, J.F. Martinez-Garcia, C. Stange, M. Rodriguez-Concepcion, *Plant Biology*, **2017**, 37, 49.
31. T.S. Agostini-Costa, G.K.A. Pêsoa, D.B. Silva, I.S. Gomes, J.P. Silva, *Journal of functional foods*, **2014**, 11, 178.
32. E. Murillo, A. Melendez-Martinez, F. Portugal, *Food Chemistry*, **2010**, 122, 1, 167.
33. A.S. Gallinat, R.B. Primack, D.L. Wagner, *Trends in Ecology & Evolution*, **2015**, 30, 3.
34. G.A.E. Hendry, *New Scientist*, **1988**, 1637, 38.
35. W.A. Hoch, E.L. Zeldin, B.H. McCown, *Tree Physiology*, **2001**. 21, 1–8.
36. D.W. Lee, J. O'Keefe, N.M. Holbrook, T.S. Field, *Ecological Research*, **2003**, 18, 677.

37. J.K. Holopainen, P. Peltonen, *Oikos*, **2002**, 99, 184.
38. T.C.W. Nijboer, R. Kanai, E.H.F De Haan. M.J. Van der Smagt, *Consciousness and Cognition*, **2007**, 17, 741.
39. J. Gage," Colour and Culture: Practice and Meaning from Antiquity to Abstraction", *Thames and Hudson*, **1993**, London.
40. M.J. Grose, *Journal of the Royal Society of Western Australia*, **2007**, 90, 179.
41. G. Monge, *Annales deChimie*, **1789**, 3, 131.
42. M. Lancaster," Colourscape", *Academy Ed. London*, **1996**.
43. M.J. Grose, *Landscape and Urban Planning*, **2016**, 146, 20.
44. J. Schlatterer, D.E. Breithaupt, *J. Agr. Food Chem.*, **2006**, 54, 2267.
45. D. Giuffrida, A. Pintea, P. Dugo, G. Torre, R.M. Pop, Mondello L., *Phytochem Analysis*, **2012**, 23, 267.
46. G. Britton, S. Liaaen-Jensen, H. Pfander," Carotenoids", *Birkhäuser, Basel*, **1996**, Vol.1B.

INVESTIGATION OF THERMAL BEHAVIOR OF *NIGELLAE SATIVAE SEMEN* FROM DIFFERENT TYPES OF EXTRACTS

CLAUDIA-CRINA TOMA^{a**}, BOGDAN TITA^{a#},
NELI-KINGA OLAH^{a,b}, GIANCARLO STATTI^c

ABSTRACT. Thermal methods have an important applicability in the pharmaceutical field, such as raw material control, purity determination, thermal stability determination, substance compatibility, qualitative and quantitative analysis of drugs, etc. Data on substance stability are obtained from the analysis of thermal decomposition determinations that occur both under isothermal conditions and under non-isothermal conditions. Thermogravimetry and derived thermogravimetry (TG / DTG) and differential scanning calorimetry (DSC) that are used to study the compatibility of the active substances and excipients have become increasingly important, because identify possible interactions between these components of the drugs. These thermoanalytic techniques have been used to study the behavior of a *Nigella sativa semen* glycerin macerate. To obtain tinctures and glycerin macerates, the European Pharmacopoeia methodology was followed. The thermoanalytic curves were recorded in a dynamic atmosphere of nitrogen and air (20 ml / min). The sample heating rate was 10 ° C / min. Thermal TG / DTG and DSC methods were applied in the temperature range of 25-1000 ° C.

Keywords: *Nigella sativa semen*, thermogravimetry, differential scanning calorimetry

^a VasileGoldis Western University of Arad, Faculty of Pharmacy, 86 L. Rebreanu str., RO-310414, Arad, Romania

^b SC PlantExtrakt SRL, 407059-Rădaia, Jud. Cluj, Romania

^c Department of Pharmacy, Health and Nutritional Sciences University of Calabria, Arcavacata di Rende, 87030, Italy

equal contribution

*Correspondent author: claudiatoma2004@yahoo.com,

INTRODUCTION

An important plant from the ethnobotanical tradition of Northern Afrika is *Nigella sativa*, *Ranunculaceae* family, named also black cumin. It is considered one of the most used spice of the muslims, cited in the Coran because of its seeds. Seeds are the vegetal product used by *Nigella* genus in traditional medicine. The seeds are small, black, with a lot of therapeutic indications but also with toxicological activity [1].

The use of extracts, instead of isolated active principles, makes it possible to exploit the synergies of action between the multiple compounds from phytocomplex. This, however, requires the assessment of thermal stability, also in relation to possible interactions between the present compounds.

One of the frequently used analytical method in pharmaceutical research is the thermal analysis, meaning the study of thermal stability and the substances' decomposition. This method is used for the thermal characterization of all solid and semi-solid substances that are used in the pharmaceutical industry[2,3].

It is very important to determine the temperature range in which the pharmaceutical substance is thermally stable. If are stored at these temperature, the substances will maintain their chemical structure and implicit their pharmaceutical actions. The technological transformations must take place at these temperatures in order to obtain the good quality pharmaceutical products [4,5].

The study of the thermal stability of pharmaceutical products takes place by analyzing the decomposition of the substances under isothermal and non-isothermal conditions. Drug decomposition occurs through the loss of irreversible mass. Reactions to drug decomposition are of theoretical and practical importance. From high-temperature research, when the processes are accelerated, the data obtained provides the rate of degradation of drugs at marketing temperatures [6,7].

The analytical methods have been used to characterize compounds also from herbal medicine. Thermal analysis, infrared spectroscopy, and X-ray diffraction are examples of methods used for characterizing drugs and herbal medicines [6].

Thermogravimetric method is a reproducible method that has a high sensitivity and provides a rapid response regarding the mass variations that occur. The results obtained from thermogravimetry are related to the thermal stability and composition of the sample [8].

Differential scanning calorimetry is used in pharmaceutical research as a very important analytical method for identifying and determining the purity of active substances, but especially for obtaining information on compatibility of substances and how are they affected by thermal processes [6,8].

Such techniques have attracted a particular interest of researchers because they can also be used to characterize medicinal products of both natural and synthetic origin, but also food, polymers or cosmetics [9].

In other articles we have presented the usefulness and importance of thermal analysis in determining the thermal stability and the compatibility of different pharmaceuticals by thermal behavior. [10,11].

In this article we intend to characterize *Nigella sativa semen* by thermal methods, thus obtaining information that will be used to obtain natural products used for medicinal purposes. This study proposed investigations in the field of thermal stability of *Nigellae sativae semen* extracts, from vegetal material harvested from Tunisia, in 2015.

RESULTS AND DISCUSSIONS

The thermal behavior of tincture in the two working atmospheres, air and nitrogen is virtually the same. This was to be expected and the thermoanalytic curves of Figs. 1 and 2 show this.

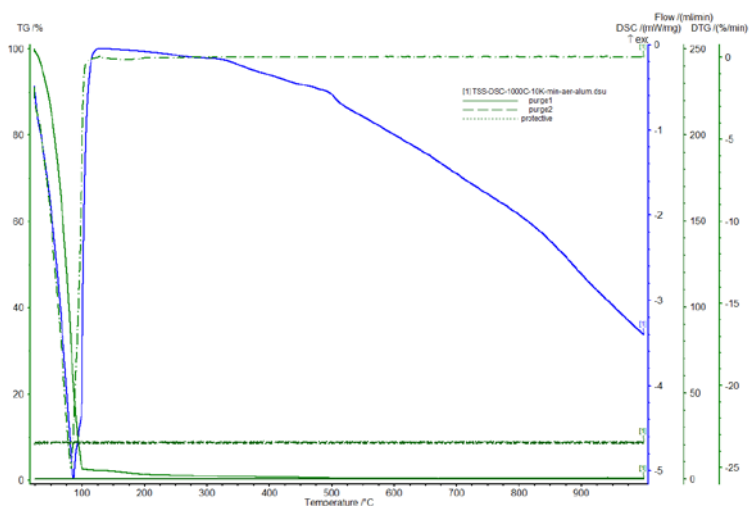


Figure 1. Thermoanalytical curves of the *Nigella sativa semen* tincture (air atmosphere)

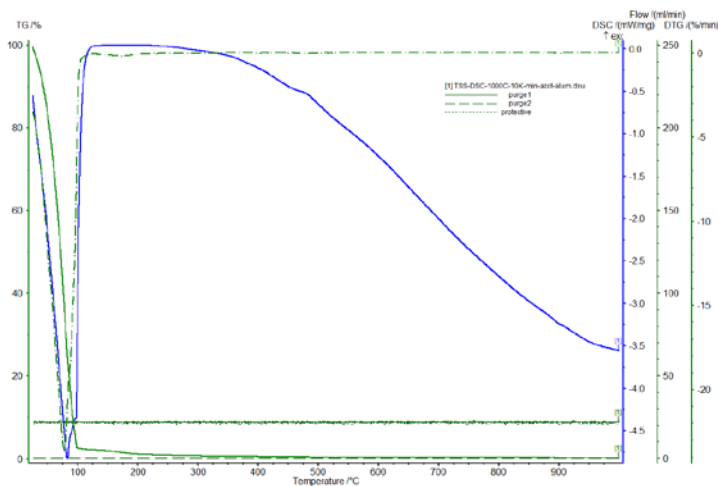


Figure 2. Thermoanalytical curves of the *Nigella sativa semen* tincture (nitrogen atmosphere)

The TG / DTG curves show a single decomposition step, which is well-defined and it takes part 25 – 125.0°C respectively 125.0°C in nitrogen atmosphere with a mass loss of 97.8%. Then there is a very slow mass loss (2.20%), so at 450.0°C the residual mass is zero and $T_{\text{peak DTG}}$ is 84.2°C respectively 84.6°C (in nitrogen atmosphere).

The DSC curves showed that thermal processes occur between the mentioned temperatures. The presence of one endothermic event at 85.8 °C respectively 85.2°C was observed, which is related to the loss of volatile constituents of the sample.

As for the glycerin macerates of *Nigellae sativae semen*, their thermal behavior in air and nitrogen is partly different. This is especially evident on the DSC curves presented in Figures 3 and 4.

The temperature range at which the decomposition takes place in the air is 25.0 – 269.0°C with two successive stages. These stages are very difficult to delimit. The temperature range for the first stage is 25 – 156°C with $T_{\text{peak DTG}}$ at 84.6°C. The loss of mass for this first stage is 30.0% and the thermal process is accompanied by an endothermic effect on the DSC curve, with $T_{\text{peak DSC}}$ at 92.3 °C. The thermal effect corresponds to the loss of the volatile constituents of the sample. The second thermal process, the main one, corresponds to the temperature range 156.2 – 269 °C, with $T_{\text{peak DTG}}$ at 264.6 °C and $\Delta m = 68.9\%$, so at ≈ 350 °C the residual mass is zero. For this process, a component volatilization, the DSC curve presents a sharp endothermic peak, with $T_{\text{peak DSC}}$ at 263.8 °C.

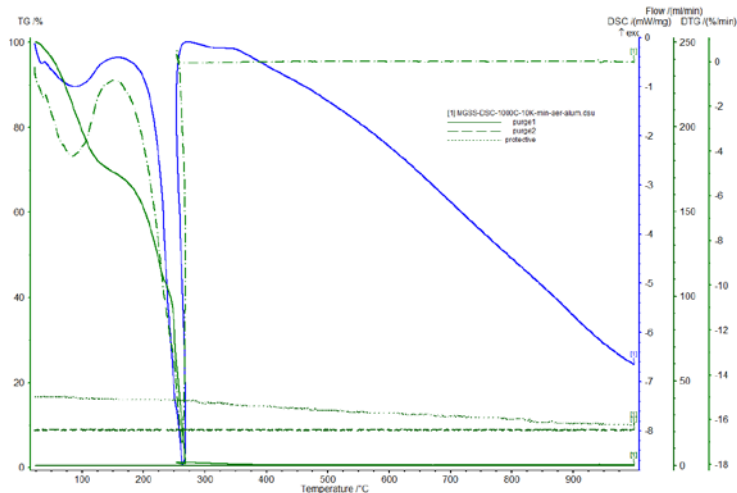


Figure 3. Thermoanalytical curves of the *Nigella sativa semen* glycerin macerate (air atmosphere)

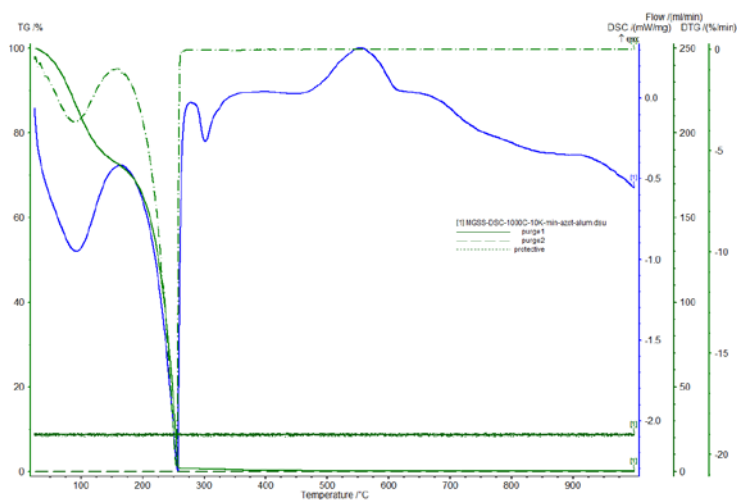


Figure 4. Thermoanalytical curves of the *Nigella sativa semen* glycerin macerate (nitrogen atmosphere)

Regarding nitrogen decomposition, the differences are insignificant for the actual air decomposition part (the first two thermal processes), e.g.: 159.2°C instead of 156.2 °C; 269.2 °C instead of 269 °C; 257.7 °C instead of 264.6 °C and 263.8 °C; $\Delta m_1 = 27.9\%$ instead of 30%; $\Delta m_2 = 70.9\%$ instead of 68.9%.

Moreover, the thermal decomposition occurs with formation of several endothermic ($T_{\text{peak DSC}} = 300 \text{ }^{\circ}\text{C}$) and exothermic ($T_{\text{peak DSC}} = 553.8 \text{ }^{\circ}\text{C}$) peaks. This decomposition may be associated with a wide variety of secondary metabolites, principally phenolics, present in the extract.

CONCLUSIONS

The pharmaceutical industry disposes of valuable tools used for quality control of products and raw materials. These tools can be used for products of plant origin, which also require characterization. Because *Nigellae sativae* semen is conditioned in dietary supplements, with huge importance for different types of therapies, the quality of the products is very important.

This work showed the application of thermal analysis on a vegetal-derived raw material, obtaining results which provide important information about its stability, standardization, composition, crystalline conformation, etc. This information can be used to establish parameters on the development of phytotherapeutic products, helping to insure its quality and, therefore, its safety and efficacy.

The main conclusion of this study is that the glycerin macerates show higher stability compared to tincture.

In addition to the kinetic study applications for the assessment of drug stability, including the determination of time and storage conditions, another practical application is the determination of drug stability time(s). It is known that with the classic stability test it takes months or even years, whereas with thermal analysis this is solved in a very short time. Thus, we can determine: lifetime under certain environmental conditions (the time period for which a drug keeps its activity); half-life time; shelf-life time (the amount of time that isothermal decomposition of a small amount of product is preset).

The determination of the above-mentioned times is done by heating the sample and speeding up the decomposition process so that their values should be interpreted with caution at room temperature.

Among the various methods of active substance-excipient compatibility studies, the DSC method is increasingly regarded as an important tool at the beginning of the preformulation study of any solid dosage form to obtain rapid information on possible interactions between the formulation components.

Possible interactions between components are obtained or deduced from the DSC curves by the occurrence, modification or disappearance of DSC peaks, especially the DSC melt peak, and/or variations in the assumed enthalpy values (ΔH). Interaction results in a decrease or increase in ΔH in the case of overlapping is a more complex process.

EXPERIMENTAL PART

Materials and methods

The *Nigellae sativae semen* was harvested from Tunisia, in June 2015, identified in the laboratory of the Pharmacognosy- "VasileGoldis" Western University of Arad, Faculty of Pharmacy. One voucher specimen was maintained in the herbarium of the laboratory.

The tincture was prepared using one part of raw material (*Nigellae sativae semen*) for ten parts of alcohol 70v/v macerated for 7 days, then pressed and filtered. For obtaining the hydro-glycero-alcoholic extract one part of the raw material must be macerated 21 days in twenty parts of solvent (1:1 alcohol 96 v/v and glycerine). *Nigellae sativae semen* must be minced in order to extend the surface of the raw material for a good extraction.

Thermogravimetry consists in recording the sample mass by temperature or time ($m = f(T)$; $m = f(t)$) as the sample temperature increases linearly over time. Graphical representation of mass or mass percentage by temperature or time is the thermogravimetric (TG) or thermogram curve.

Therefore, in TG, the mass of the sample is continuously measured in a crucible, heated in an oven, in a programmed temperature, in an atmosphere that can be controlled or set by the introduction of a gas. Mass measurements are made using an analytical balance included in a thermogravimetric analyser.

The principle of the DSC method during heating or cooling is to measure the enthalpy or heat flux difference between the test sample and the reference substance during heat treatment.

The TG/DTG and DSC curves were made with a Netzch-STA 449 TG/DTA apparatus manufactured by Netzch Geratebau GMBH, Germany, under the following conditions:

- temperature range 25-1000°C - heating rate (β): 10°C/min;
- platinum crucible;
- sample mass: \approx 22 mg;
- atmosphere: Nitrogen stream with a flow rate of 20mL/min

REFERENCES

1. J. Bellakhdar, *La Pharmacopee marocaine traditionnelle*, Ibis Press, **1997**, 457.
2. B. Tita, C. Morgovan, D. Tița, T. A. Neag, *Revista de Chimie*, **2016**, *67(1)*, 38.
3. F.H.A. Hernandez, C.P. Santana, R.L. Santos, L.P. Correia, R.O. Macedo, *Journal of Thermal Analysis and Calorimetry* **2013**, *113*, 443.
4. B. Tita, E. Marian, G. Rusu, G. Bandur, D. Tita, *Revista de Chimie. Bucharest*, **2013**, *64 (12)*, 1390.
5. R.S. da Costa, Ch.A.B. Negrao S.R.P. Camelo, W.L.R. Barbosa, J.O.L. Silva Junior, *Journal of Thermal Analysis and Calorimetry*, **2013**, *111*, 1959.
6. B. Tita, T. Jurca, G. Rusu, G. Bandur, D. Tita, *Revista de Chimie Bucharest*, **2013**, *64(10)*, 1089.
7. L.P. Correia, C.P. Santana, A.C.D. Medeiros, R.O. Macedo, *Journal of Thermal Analysis and Calorimetry*, **2015**, *123(2)*, 993.
8. L.P. Correia, C.P. Santana, M.F. Pinto, A.F.O. Santos, R.O. Macedo, *Journal of Thermal Analysis and Calorimetry*, **2015**, *122(1)*, 207.
9. N. Chirani, H. Yahia, L. Gritsch, F.L. Motta, S. Chirani, S. Fare, *Journal of Biomedical Science*, **2015**, *4*, 2.
10. E. Marian, N. Duteanu, L. Vicas, B. Tita, P. Sfirloaga, T. Jurca, *Revista de Chimie Bucharest* **2017**, *68(7)*, 1435.
11. C.C. Toma, T.A. Neag, B. Tita, *Revista de Chimie. Bucharest*, **2017**, *68(5)*, 1007.

COMPLEXATION OF DNA WITH CATIONIC POLYMERS

ALEXANDRA FARCAȘ^{a,b*}, TITUS A. BEU^a

ABSTRACT. Polyethylenimine (PEI) represents the most extensively used non-viral vector for gene delivery. The complexation between nucleic acids and PEI chains is intimately related to electrostatic interactions of the positively charged amine groups with the negatively charged phosphate groups. All-atom molecular dynamics simulations of alternatively protonated PEI chains, DNA and, respectively, polyplexes thereof in solution were performed. Our results reveal an increase in gyration radius of solvated PEI chains in the presence of DNA. In order to understand the major changes in DNA properties, the impact of PEI chains on the ionic environment of DNA is described in detail. In addition, the amine-phosphate contact analysis provides valuable insight into the formation mechanism of PEI/DNA complexes.

Keywords: polyethylenimine, cationic polymers, molecular dynamics simulations, PEI/DNA polyplexes, gene delivery systems.

INTRODUCTION

Gene therapy is designed to introduce nucleic acids into cells for the treatment of cancer or other genetic diseases and the development of effective delivery vectors is one of the central challenges. Current gene delivery vectors are divided into two major types, viral and non-viral, with the latter ones being less immunogenic and toxic [1-3]. The use of cationic polymers as non-viral systems to condense nucleic acids into polyplexes represents a promising therapeutic strategy, and, polyethylenimine (PEI) is one of the most versatile carrier system of this class [4]. In spite of major recent advances in the development PEI-based delivery systems, there still persist numerous open questions concerning the formation of PEI/DNA polyplexes.

^a Babeș-Bolyai University, Faculty of Physics, Mihail Kogălniceanu Street 1, Cluj-Napoca 400084, Romania

^b National Institute for Research and Development of Isotopic and Molecular Technologies 65-103 Donath Street, Cluj-Napoca 400084, Romania

* Corresponding author: farcasalex@yahoo.com

Complex all-atom molecular-dynamics (MD) simulations have been employed in the last decade to elucidate the structure and properties of PEI/DNA complexes. Essentially, it was shown ([5]-[6]) that the DNA-PEI complexation is controlled by the attractive electrostatic interaction between the protonated amine groups of PEI and the phosphate groups of DNA. Ziebarth et al. [7] studied the structural differences between DNA and siRNA, and their role in the stability of PEI/DNA complexes. It should be noted, however, that the general AMBER force field [8] they have used in the simulations does not provide specific parameters for PEI.

RESULTS AND DISCUSSION

In order to study the complexation dynamics of DNA with PEI polymers, the initial structure of DNA was constructed using the Nucleic Acid Builder [9] via server <http://structure.usc.edu/make-na/server.html>. Specifically, a DNA strand composed of 42 bases was built in the canonical B form. In the simulations, we considered alternatively protonated linear PEI chains composed of 20 monomers. We performed three types of simulations, respectively, (a) solvated DNA strands, (b) solvated PEI chains, and (c) solvated DNA-PEI mixtures. The initial configurations for these simulations respectively comprise (a) a DNA 42-mer with the base structure described in Table 1, (b) six linear PEI chains with the mass centers forming a hexagon, and (c) a DNA strand with the center of mass placed at the PEI hexagon center and aligned parallel with the PEI chains.

Table 1. Simulated configurations

PEI			DNA		Solvation		
Size/ Prot.Frac	No. of chains	No. of atoms	Sequence	Helix type	Water molec	Na ⁺	Cl ⁻
20-mer 1/2	6	186 each PEI chain			31206	88	148
			CGCGAATTCGCGATATCCCGG CCGGGATATCGCGAATTCGCG	B	31489	129	89
20-mer 1/2	6	186 each PEI chain	CGCGAATTCGCGATATCCCGG CCGGGATATCGCGAATTCGCG	B	30562	86	106

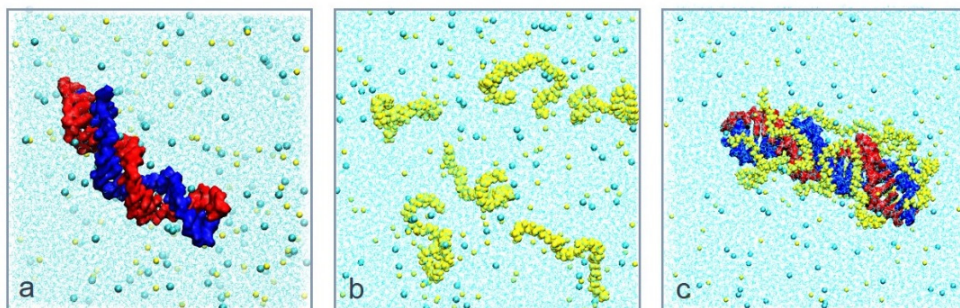


Figure 1. Intermediate configurations of a typical trajectory for: a) DNA, b) 6 alternatively protonated PEI chains, c) PEI/DNA complex.

The systems were solvated into a rectangular water box of size $100 \times 100 \times 100 \text{ \AA}^3$, which results in a total of approximately 30000 water molecules in each system. The exact number of water molecules and neutralizing counterions are summarized in Table 1.

Isothermal-Isobaric (NPT) runs of 20 ns were performed to study the DNA behavior in solution (see Fig. 1a) and 30 ns to characterize the solvated PEI chains (Fig. 1b) and the PEI/DNA complex (Fig. 1c). All the snapshots from the simulations have been extracted using the VMD package [10]. The basic data for each simulated system are presented in Table 2.

Table 2. Details of molecular dynamics simulations

System description	No. of trajectories	Simulation length (ns)	PEI chains
PEI	4	30	6 PEI 20-mers (protonation 1/2)
DNA	3	20	
PEI/DNA complex	4	30	6 PEI 20-mers (protonation 1/2)

Figure 2 presents the time dependence of the gyration radius (R_g) for alternatively protonated PEI 20-mers in interaction with DNA. The initial linear PEI chains condense into random structures and bind to DNA. In calculating the average values of R_g , we discarded the first 5 ns of each run to allow for the complex to be formed. The average R_g of PEI chains interacting with DNA in solution is 12.65 \AA , very similar with the average value of bare PEI chains (12.55 \AA).

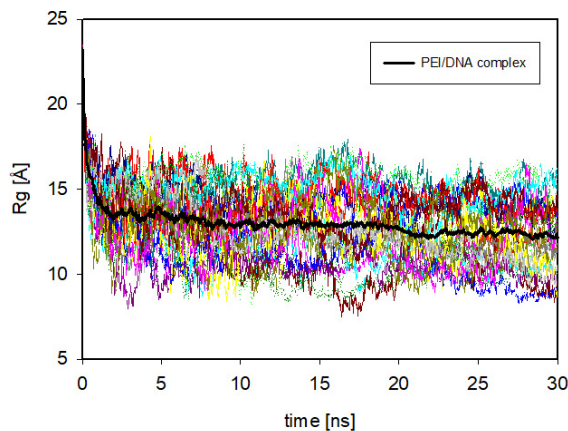


Figure 2. Time evolution of the gyration radius for 6 alternatively protonated PEI 20-mers interacting with DNA in 4 independent trajectories (black – average).

To suggest the average spatial extent of solvated PEI chains, both bare and interacting with DNA (PEI/DNA complex), probability distributions of the time-averaged gyration radius are comparatively presented in Fig. 3. Bare PEI (black curve) shows a single peak corresponding to a random folded conformation. The profile for PEI chains interacting with DNA (red curve) displays an additional peak at about 14 Å, which corresponds to PEI chains that bind to DNA (PEI/DNA complexes).

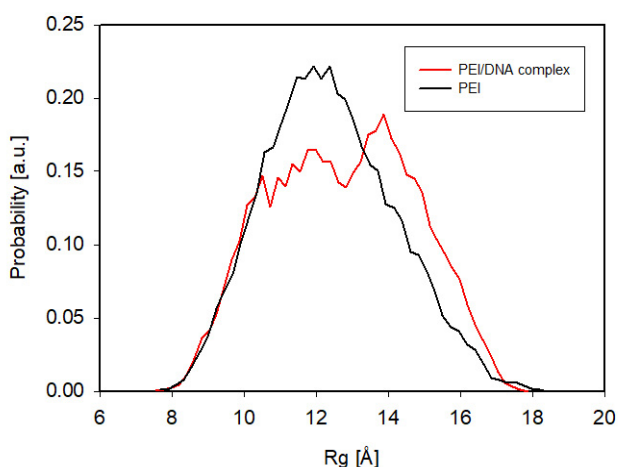


Figure 3. Probability distributions of radius of gyration for alternatively protonated PEI 20-mers (black – PEI chains in solution, red – PEI chains interacting with DNA in solution).

The binding patterns of the unprotonated vs. protonated nitrogen atoms of the PEI chains are depicted in Fig. 4. It is apparent that the number of protonated nitrogen atoms which are in direct interaction with DNA (within 4 Å), is double as compared to the number of unprotonated nitrogen atoms.

In order to characterize the electrostatics around solvated DNA, cumulative charge distributions of the solution counterions (Na^+ and Cl^-) are presented in Fig. 5, showing the amount of charge situated within a given distance from DNA. As expected, more Na^+ ions reside around bare DNA than around DNA complexed with protonated PEI chains. Conversely, the screening of the negatively charged phosphate groups by the protonated amine groups, enables complexed DNA to attract more Cl^- ions than in uncomplexed state.

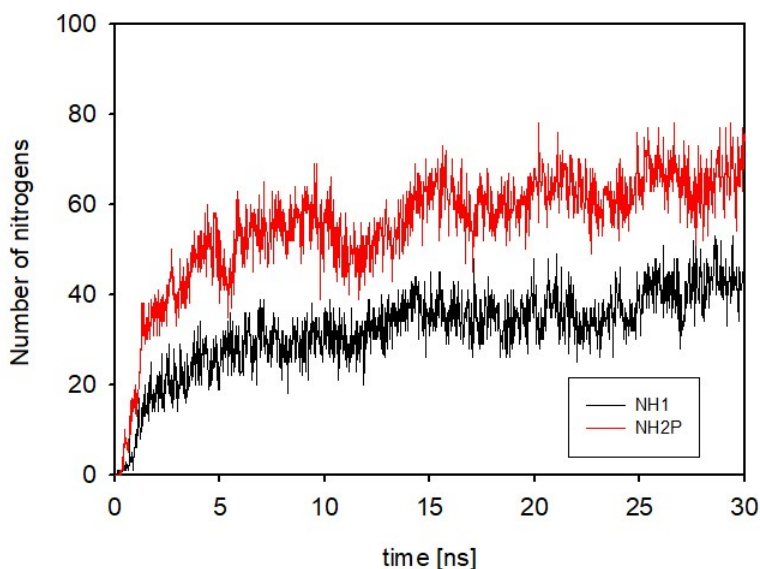


Figure 4. Time dependence of the ensemble-averaged number of unprotonated/protonated nitrogen atoms of PEI chains within 4 Å of any phosphorus atom of DNA.

Figure 6 presents the evolution in time of the ensemble-averaged number of Na^+ (orange) and Cl^- (cyan) ions situated within 4 Å of any atom of DNA (solvated DNA-PEI mixtures). A clear decrease in the number of Na^+ evidenced the screening effect of PEI chains on the negatively charged phosphate groups of DNA.

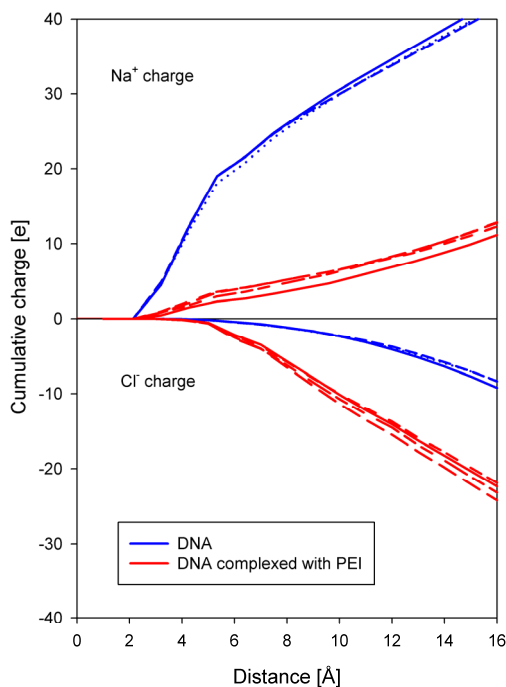


Figure 5. The cumulative charge distributions of the counterions in the vicinity of DNA (blue – bare DNA strands, red – DNA complexed with PEI chains). The curves correspond to the different trajectories.

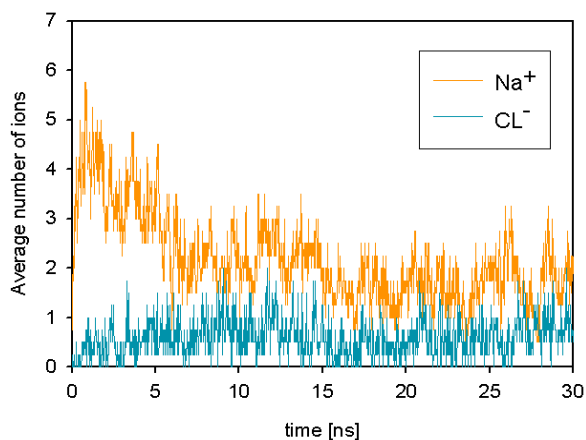


Figure 6. Time dependence of the ensemble-averaged number of counterions within 4 Å of an atom of DNA (solvated DNA-PEI mixtures).

CONCLUSIONS

In this work we performed molecular dynamics simulations of alternatively protonated PEI chains, DNA strands and DNA/PEI polyplexes in solution. The results reveal a complex behavior of solvated PEI chains in the vicinity of DNA strands. Alternatively protonated PEI chains closely package solvated DNA strands, showing a considerably higher radius of gyration than in uncomplexed state.

The protonated amine groups of PEI strongly bind to the phosphate groups of DNA, roughly outnumbering the unprotonated amine groups residing on average in the vicinity of DNA by a factor of 2.

The screening effect of the protonated PEI chains on the phosphate groups of DNA is reflected by a clear decrease in the number of attracted sodium counterions.

EXPERIMENTAL SECTION

All molecular dynamics simulations were performed with the NAMD package [11] using the CHARMM36 Nucleic Acid force field [12], [13] in conjunction with the CHARMM force field that we have recently developed for protonated PEI chains [14] [18].

In all simulations we used a time step of 2 fs combined with the SHAKE algorithm [15], [16] to constrain covalent bonds involving hydrogen atoms to fixed lengths. A cutoff distance of 12 Å was used to treat the short-ranged Lennard-Jones interactions. The particle mesh Ewald method [17] was used to treat the long-range electrostatic interactions, using a discrete mesh with a spacing of 1 Å. The temperature was kept at 310K using a Langevin thermostat with a damping coefficient of 1 ps^{-1} , while the pressure was fixed at 1 atm using a Langevin piston.

ACKNOWLEDGMENTS

This work was supported by a grant of the Romanian Ministry of Research and Innovation, CNCS-UEFISCDI, project number PN-III-P4-ID-PCE-2016-0474.

REFERENCES

1. S. Y. Wong, J. M. Pelet, and D. Putnam, *Progress in Polymer Science*, **2007**, *32*, 799.
2. C. P. Lollo, M. G. Banaszczyk, and H. C. Chiou, *Current opinion in molecular therapeutics*, **2000**, *2*, 136.
3. Y. Zhang, A. Satterlee, and L. Huang, *Molecular Therapy*, **2012**, *20*, 1298.
4. K. Utsuno, H. Uludag, *Biophysical Journal*, **2010**, *99*, 201.
5. J. D. Ziebarth, Y. Wang, *Biomacromolecules*, **2010**, *11*, 29.
6. C. B. Sun, T. Tang, H. Uludag, and J. E. Cuervo, *Biophysical Journal*, **2011**, *100*, 2754.
7. J. D. Ziebarth, D. Kennetz, N. J. Walker, Y. Wang, *The Journal of Physical Chemistry B*, **2017**, *121*(8), 1941.
8. J. Wang, P. Cieplak, P. A. Kollman, *Journal of Computational Chemistry*, **2000**, *25*, 1049.
9. D. A. Case, J. T. Berryman, R. M. Betz, D. S. Cerutti, T. E. Cheatham III, T.A. Darden, R.E. Duke, T.J. Giese, H. Gohlke, A.W. Goetz, N. Homeyer, S. Izadi, P. Janowski, J. Kaus, A. Kovalenko, T. S. Lee, S. LeGrand, P. Li, T. Luchko, R. Luo, B. Madej, K. M. Merz, G. Monard, P. Needham, H. Nguyen, H. T. Nguyen, I. Omelyan, A. Onufriev, D. R. Roe, A. Roitberg, R. Salomon-Ferrer, C. L. Simmerling, W. Smith, J. Swails, R. C. Walker, J. Wang, R. M. Wolf, X. Wu, D. M. York, and P. A. Kollman, *AMBER 2015*, University of California, San Francisco, **2015**.
10. W. Humphrey, A. Dalke, and K. Schulten, *Journal of Molecular Graphics*, **1996**, *14*, 33.
11. J. C. Phillips, R. Braun, W. Wang, J. Gumbart, E. Tajkhorshid, E. Villa, C. Chipot, R. D. Skeel, L. Kale, and K. Schulten, *Journal of Computational Chemistry*, **2005**, *26*, 1781.
12. Foloppe N., MacKerell A. D., *Journal of Computational Chemistry*, **2000**, *21*, 86.
13. Denning E. J., Priyakumar U. D., Nilsson L., Mackerell A. D., *Journal of Computational Chemistry*, **2011**, *32*, 1929.
14. T. A. Beu, A. Farcaș, *Journal of Computational Chemistry*, **2017**, *38*(27), 2335.
15. J. P. Ryckaert, G. Ciccotti, H. J. C. Berendsen., *Journal of Computational Physics*, **1977**, *23*, 327.
16. S. Miyamoto, P. A. Kollman, *Journal of Computational Chemistry*, **1992**, *13*, 952.
17. U. Essmann, L. Perera, M. L. Berkowitz, T. Darden, H. Lee, and L. G. Pedersen, *The Journal of Chemical Physics*, **1995**, *103*, 8577.
18. T.A. Beu, A. Farcaș, *AIP Conference Proceedings*, **2017**, 1916, UNSP 020001.